

UNIVERSITY OF CALIFORNIA, SAN DIEGO

A Performance Comparison of Condition Based Monitoring Damage Features Used in
Rotating Machines under Variable Conditions

A Thesis submitted in partial satisfaction of the
requirements for the degree Master of Science

in

Structural Engineering: Specialization in Health Monitoring, Prognosis and Validated
Simulations

by

Luke Thomas Robinson

Committee in charge:

Professor Michael Todd, Chair
Professor Chuck Farrar
Professor Bill Hodgkiss

2013

Copyright

Luke Thomas Robinson, 2013

All rights reserved.

The Thesis of Luke Thomas Robinson is approved, and it is acceptable
in quality and form for publication on microfilm and electronically:

Chair

University of California, San Diego

2013

TABLE OF CONTENTS

Signature Page	iii
Table of Contents.....	iv
List of Abbreviations	vi
List of Figures.....	vii
List of Tables	xii
Acknowledgements	xiii
Vita	xiv
Abstract.....	xv
Chapter 1 Introduction to Structural Health Monitoring and Condition Based Monitoring of Rotating Machines.....	1
1.1. Introduction.....	1
1.2. Structural Health Monitoring Process.....	2
1.2.1. Operational Evaluation	4
1.2.2. Data Acquisition	5
1.2.3. Feature Selection	6
1.2.4. Statistical Model Development.....	7
1.3. Condition Based Monitoring of Rotating Machines.....	9
1.3.1. Operational Evaluation	9
1.3.2. Data Acquisition	10
1.3.3. Feature Selection	11
1.3.4. Statistical Model Development.....	12
1.4. Scope of Thesis.....	13
Chapter 2 Technical Background	15
2.1. Introduction.....	15
2.2. Digital Signal Processing Techniques	15
2.2.1. Fourier Transform & Power Spectral Density	16
2.2.2. Time-Frequency Analysis.....	18
2.2.3. Signal Envelope and the Hilbert Transform	20
2.3. Condition Based Monitoring Feature Extraction.....	20
2.3.1. Angular Resampling	21
2.3.2. Time Synchronous Averaging	23
2.3.3. Discrete Random Separation	24
2.3.4. The Difference, Residual and Band-pass Mesh Signal.....	25

2.3.5.	Traditional Damage Features.....	26
2.3.6.	Hölder Exponent and the FMH Feature.....	29
Chapter 3	Experimental Setup & Feature Extraction Results.....	33
3.1.	Damage Types and Descriptions	33
3.2.	Experimental Setup.....	33
3.2.1.	Testbed Description and Evaluation.....	33
3.2.2.	Data Acquisition	37
3.2.3.	Description of System States	41
3.2.4.	Testing Procedures.....	49
3.2.5.	Sources of Variability.....	52
3.3.	Statistical Modeling and Detection Performance	53
3.3.1.	Hypothesis Testing & Receiver Operating Characteristic Curves.....	53
3.4.	Testing Results.....	59
3.4.1.	Worn Tooth Gearbox Damage Preliminary Results	61
3.4.2.	Main Shaft Ball Bearing Damage Preliminary Results	72
3.4.3.	Bearing Damage Detection and Varying Belt Tension	82
3.4.4.	Worn tooth Damage and Varying Torsional Load	91
Chapter 4	Conclusion & Future Work.....	98
4.1.	Conclusion	98
4.2.	Recommendations for Future Work	99
References	101

LIST OF ABBREVIATIONS

AR	Autoregressive
ARS	Angular Resampled Signal
CBM	Condition Based Monitoring
CWT	Continuous Wavelet Transform
DAQ	Data Acquisition
DRS	Discrete/Random Separation
DSP	Digital Signal Processing
DVWD	Discrete Wigner-Ville Distribution
FIR	Finite Impulse Response
FFT	Fast Fourier Transform
LPC	Linear Predictive Coding
NDE	Non Destructive Evaluation
PFA	Probability of False Alarm
PD	Probability of Detection
PSD	Power Spectral Density
ROC	Receiver Operating Characteristic
RMS	Root Mean Square
SHM	Structural Health Monitoring
SNR	Signal to Noise Ratio
STFT	Short Time Fourier Transform
TSA	Time Synchronous Average

LIST OF FIGURES

Figure 1: Angular Resampling Schematic [45].	22
Figure 2: Example of Short Delayed Window Structure for use in determining the DRS filter transfer function [51].	24
Figure 3: Residual Difference and Band Pass Mesh Power Spectral Densities for Baseline\Worn tooth Damage @ 1000 RPM Resampled to 2048 Samples per Revolution with 20 revolutions.	26
Figure 4: CWT scalogram and Hölder exponent series for a baseline condition gearbox signal.	30
Figure 5: CWT scalogram and Hölder exponent series for a worn tooth condition gearbox signal.	31
Figure 6: Power Spectral Densities of Hölder exponent series for undamaged and worn tooth damaged gearbox signals.	32
Figure 7: Machinery Fault Simulator (Top View).....	35
Figure 8: Machinery Fault Simulator Controller (Left Side).....	35
Figure 9: Gear Box Belt Drive (Side View)	36
Figure 10: Machinery Fault Simulator Gear Box (Top View)	36
Figure 11: Data Acquisition Card and Sensor	38
Figure 12: Tachometer Sensor Location (Channel 0).....	39
Figure 13: Gear Box Sensor Location (Channel 1)	40
Figure 14: Bearing Sensor Location (Channels 2-3)	40
Figure 15: Example of hypothesis for damage feature mean greater than baseline feature mean.	54
Figure 16: Example of hypothesis for damage feature mean less than baseline feature mean.	54
Figure 17: Example ROC curves for Gaussian Distributions with increasing separation of means.	56
Figure 18: Hypothetical bi-modal (top) and changing variance (bottom) damage distributions.	57

Figure 19: ROC curves of bi-modal damaged distribution (Feature 1) and changing variance damaged distributions (Feature 2).	58
Figure 20: Trial Power Spectrums for Worn Tooth Damage @ 1000RPM, 2048 Samples per Revolution, Channel 1	62
Figure 21: Damage Feature Distributions for Worn Tooth Damage @ 1000RPM, 2048 Samples per Revolution, 20 Revolutions, Channel 1	63
Figure 22: Damage Feature Statistical Performance for Worn Tooth Damage Detection @ 1000 RPM, 2048 Samples per Revolution, 20 Revolutions, Channel 1	64
Figure 23: Damage Feature Distributions for Worn Tooth Damage @ 1000RPM, 2048 Samples per Revolution, 4 Revolutions, Channel 1	64
Figure 24: Damage Feature Statistical Performance for Worn Tooth Damage Detection @ 1000 RPM, 2048 Samples per Revolution, 4 Revolutions, Channel 1	65
Figure 25: Worn Tooth Damage Power Spectrum @ 1000RPM, 512 Samples per Revolution, Channel 1	66
Figure 26: Damage Feature Distributions for Worn Tooth Damage @ 1000RPM, 512 Samples per Revolution, 20 Revolutions, Channel 1	66
Figure 27: Damage Feature Statistical Performance for Worn tooth Damage Detection @ 1000 RPM, 512 Samples per Revolution, 20 Revolutions, Channel 1	67
Figure 28: Damage Feature Distributions for Worn Tooth Damage @ 1000RPM, 512 Samples per Revolution, 4 Revolutions, Channel 1	68
Figure 29: Damage Feature Statistical Performance for Worn Tooth Damage Detection @ 1000 RPM, 512 Samples per Revolution, 4 Revolutions, Channel 1	68
Figure 30: Trial Power Spectrums for Worn Tooth Damage @ 2000RPM, 2048 Samples per Revolution, Channel 1	70
Figure 31: Damage Feature Distributions for Worn Tooth Gearbox Damage @ 2000RPM, 2048 Samples per Revolution, 40 Revolutions, Channel 1	71
Figure 32: Damage Feature Statistical Performance for Worn Tooth Gear Box Damage Detection @ 2000 RPM, 2048 Samples per Revolution, 40 Revolutions, Channel 1	71
Figure 33: Trial Power Spectra for Main Shaft Bearing Ball Fault Damage @ 1000RPM, 2048 Samples per Revolution, Channel 3	73
Figure 34: Damage Feature Distributions for Main Shaft Bearing Ball Fault Damage @ 1000RPM, 2048 Samples per Revolution, 20 Revolutions, Channel 3	74

Figure 35: Damage Feature Statistical Performance for Main Shaft Bearing Ball Fault Damage Detection @ 1000 RPM, 2048 Samples per Revolution, 20 Revolutions, Channel 3	74
Figure 36: Trial Power Spectrums for Main Shaft Bearing Ball Fault Damage under High Belt Tension @ 1000RPM, 2048 Samples per Revolution, Channel 3	75
Figure 37: Damage Feature Distributions for Main Shaft Bearing Ball Fault Damage Under High Belt Tension @ 1000RPM, 2048 Samples per Revolution, 20 Revolutions, Channel 3	76
Figure 38: Damage Feature Statistical Performance for Main Shaft Bearing Ball Fault Under High Belt Tension Damage Detection @ 1000 RPM, 2048 Samples per Revolution, 20 Revolutions, Channel 3.....	76
Figure 39: Trial Power Spectrums for Main Shaft Bearing Outer Race Fault Damage @ 1000RPM, 2048 Samples per Revolution, Channel 3	78
Figure 40: Damage Feature Distributions for Main Shaft Bearing Outer Race Fault Damage @ 1000RPM, 2048 Samples per Revolution, 20 Revolutions, Channel 3.....	79
Figure 41: Damage Feature Statistical Performance for Main Shaft Bearing Outer Race Fault Damage Detection @ 1000 RPM, 2048 Samples per Revolution, 20 Revolutions, Channel 3	79
Figure 42: Trial Power Spectrums for Main Shaft Bearing Outer Race Fault Damage w/ Varying Fault Position @ 1000RPM, 2048 Samples per Revolution, Channel 3.....	81
Figure 43: Damage Feature Distributions for Main Shaft Bearing Outer Race Fault Damage w/ Varying Fault Position @ 1000RPM, 2048 Samples per Revolution, 20 Revolutions, Channel 3.....	81
Figure 44: Damage Feature Statistical Performance for Main Shaft Bearing Outer Race Fault Damage Detection w/ Varying Fault Position @ 1000 RPM, 2048 Samples per Revolution, 20 Revolutions, Channel 3	82
Figure 45: Trial Power Spectrums for Main Shaft Bearing Ball Fault Damage w/ Varying Belt Tension @ 1000RPM, 2048 Samples per Revolution, Channel 3.....	84
Figure 46: Damage Feature Distributions for Main Shaft Bearing Ball Fault Damage w/ Varying Belt Tension @ 1000RPM, 2048 Samples per Revolution, 20 Revolutions, Channel 3	85

Figure 47: Damage Feature Statistical Performance for Main Shaft Bearing Ball Fault Damage Detection w/ Varying Belt Tension @ 1000 RPM, 2048 Samples per Revolution, 20 Revolutions, Channel 3.....	85
Figure 48: Trial Power Spectrums for Main Shaft Bearing Inner Race Fault Damage w/ Varying Belt Tension @ 1000RPM, 2048 Samples per Revolution, Channel 3.....	87
Figure 49: Damage Feature Distributions for Main Shaft Bearing Inner Race Fault Damage w/ Varying Belt Tension @ 1000RPM, 2048 Samples per Revolution, 40 Revolutions, Channel 3.....	87
Figure 50: Damage Feature Statistical Performance for Main Shaft Bearing Inner Race Fault Damage Detection w/ Varying Belt Tension @ 1000 RPM, 2048 Samples per Revolution, 40 Revolutions, Channel 3.....	88
Figure 51: Trial Power Spectrums for Main Shaft Bearing Outer Race Fault Damage w/ Varying Belt Tension @ 1000RPM, 2048 Samples per Revolution, Channel 3.....	89
Figure 52: Damage Feature Distributions for Main Shaft Bearing Outer Race Fault Damage w/ Varying Belt Tension @ 1000RPM, 2048 Samples per Revolution, 40 Revolutions, Channel 3.....	90
Figure 53: Damage Feature Statistical Performance for Main Shaft Bearing Outer Race Fault Damage w/ Varying Belt Tension @ 1000 RPM, 2048 Samples per Revolution, 40 Revolutions, Channel 3.....	90
Figure 54: Trial Power Spectrums for Worn Tooth Damage w/ Varying Torsional Load @ 1000RPM, 2048 Samples per Revolution, Channel 1.....	93
Figure 55: Damage Feature Distributions for Worn Tooth Damage w/ Varying Torsional Load @ 1000RPM, 2048 Samples per Revolution, 40 Revolutions, Channel 1.....	94
Figure 56: Damage Feature Statistical Performance for Worn Tooth Damage w/ Varying Torsional Load @ 1000 RPM, 2048 Samples per Revolution, 40 Revolutions, Channel 1.....	94
Figure 57: Trial Power Spectrums for Worn Tooth Damage w/ Varying Torsional Load @ 1000RPM, 2048 Samples per Revolution, Channel 3.....	95
Figure 58: Damage Feature Distributions for Worn Tooth Damage w/ Varying Torsional Load @ 1000RPM, 2048 Samples per Revolution, 40 Revolutions, Channel 3.....	96

Figure 59: Damage Feature Statistical Performance for Worn Tooth Damage w/
Varying Torsional Load @ 1000 RPM, 2048 Samples per Revolution, 40
Revolutions, Channel 3 97

LIST OF TABLES

Table 1: Traditional Damage Features [4], [12], [22], [23].....	28
Table 2: Gear Box Specifications.....	37
Table 3: PCB 352-C33 Accelerometer Specifications	38
Table 4: NI 9234 DAQ Card Secifications.....	39
Table 5: System States for Data Sets.....	42

ACKNOWLEDGEMENTS

I acknowledge and thank my advisor Michael Todd for all his advice, insight, and discussion over the past two years that has led to the completion of the work provided in this thesis. Special thanks to Chuck Farrar and the Los Alamos National Laboratory as well for providing the funding and fellowship. I would like to thank Dustin Harvey for his support in the acquisition of the data used in this thesis as well as the development in the condition based maintenance module for SHM tools. I would like to thank Zhu Mao for his assistance and conversations on various aspects of statistical analysis. Additional thanks to Colin Haynes, Scott Oullette, Richard Do, and Eric Kjolsing for their guidance and knowledge they have shared over my career as a graduate student researcher at UCSD.

VITA

2008 A.A. University Studies: Pre-Engineering
2010 Engineer-In-Training Certified
2011 B.S Structural Engineering
2013 Master of Science, University of California, San Diego

ABSTRACT OF THE THESIS

A Performance Comparison of Condition Based Monitoring Damage Features Used in Rotating Machines under Variable Conditions

by

Luke Thomas Robinson

Master of Science in Structural Engineering

University of California, San Diego, 2013

Professor Michael Todd, Chair

Condition based monitoring (CBM) is a subset of structural health monitoring (SHM) that is focused on monitoring vibration signals generated by rotating machines in situ and processing the data by various techniques designed to extract damage-sensitive features as a means of performing damage (e.g., bearing and gear failure) presence, location, or extent. To date, a wide variety of CBM techniques have been documented in the literature and are well accepted in the CBM community. The literature provides current technical means for extracting damage features and in some cases the trending of features in run-to-failure experiments under constant mechanical

parameters such as load and rotational speed, but it lacks any statistical analysis on the effects that varying parameters of the mechanical systems for binary damage states have on detectability. Specifications on data acquisition and choice of algorithm parameters used in extracting the damage-sensitive features remain somewhat vague. This thesis attempts to provide a better global understanding of how variability in the damage detection problem affects the features as a precursor for future work in pattern recognition and optimal detection of damage to rotating machines. This thesis compares the various features under varying conditions and computational parameters in a statistically rigorous way using receiver operating characteristic curves, which compare the probability of detection vs. the probability of false alarms as a means to improve detectability for future use in embedded systems. This thesis also introduces a new damage feature which demonstrates superior detection performance when compared to traditional damage features for use in detecting worn tooth gear box damage.

Chapter 1

Introduction to Structural Health Monitoring and Condition Based Monitoring of Rotating Machines

1.1. Introduction

Monitoring the health of a system is a multi-faceted problem but, at its most fundamental level, it seeks to answer the question of, “Is the structure damaged?” (a form of binary hypothesis test). Structural health monitoring (SHM) is the study of developing a monitoring system specific to a structures unique characteristics and seeks to answer this seemingly basic question. SHM is not isolated to any one field of industry but instead many different fields of study in the pursuit to provide damage detection capabilities, diagnostic information, and even prognostic information for any given structure.

Many different application domains have sought SHM solutions. One example of value to the civil engineering field would be to provide information on the health of infrastructure after a natural (e.g., earthquake) or human-caused terrorist attack; the civil engineering community has considered vibration-based monitoring since the early 1980s [1]. The aerospace industry can benefit from structural health monitoring systems

by monitoring the health of various aspects of a air and space substructures from wings to flight systems to engine components; the aerospace community began to study the use of vibration-based monitoring during the late 1970s and early 1980s [1].

Mechanical engineering applications stand to benefit from the study of SHM as well, from monitoring machines that are part of an assembly line to engines and braking systems in vehicles. Even the electrical engineering field has adopted SHM techniques in monitoring vibration-based damage applied to hard drives disk readers in order to detect potential writing errors of data and monitor electrical conductivity paths during chip fabrication. Amongst the different applications there have been varying degrees of success in the use of SHM. One of the most successful is the study of vibration-based monitoring of rotating machines known as condition-based monitoring (CBM), which has been repeatedly applied with success to a variety of machinery elements [2].

Regardless of the SHM application, however, the overall process adopted to accomplish SHM goals remains essentially the same, as will be described subsequently.

1.2. Structural Health Monitoring Process

The SHM process can be broken down into a four-step statistical pattern recognition paradigm that provides the foundation for any general SHM application. This four step process has been outlined in [1][2][3] and is summarized in the list below along with some of the major considerations involved with each step.

1. Operational Evaluation Process
 - a. Define cost justifications for SHM implementation.
 - b. Define system-specific damage types that are to be detected.

- c. Define operational and environmental conditions under which the system is to be operated.
 - d. Define constraints on the data acquisition system or implementation process under operational conditions.
2. Data Acquisition and Cleansing Process
- a. Define the type of data to be acquired and how often it should be collected.
 - b. Define the data to be used in the feature selection process.
 - c. Define requirements for sensor and hardware involved in data acquisition.
 - d. Define sensor placement locations.
 - e. Define sources of variability and normalization procedures to reduce this variability.
3. Feature Selection Process
- a. Define which features of the data are best for damage detection (sensitivity, robustness)
 - b. What are the statistical distributions of the extracted damage features?
 - c. What type of data condensation can be utilized?
 - d. Define sources of variability that may affect specific features.
4. Statistical Model Development Process
- a. Is data available from undamaged and damaged system (supervised learning) or only available from undamaged system (unsupervised learning)?

- b. Damage Classification
 - i. Is the system damaged or undamaged?
 - ii. Where is the damage located?
 - iii. What type of damage is present?
 - iv. What is the extent of the damage?
- c. Damage Prognostics
 - i. What is the remaining useful life of the structure?
 - ii. What is the probability of a correct diagnosis or prognosis?

The process outlined above may not always be developed in full for any particular SHM problem, dependent upon constraints, cost, or specific objective(s) defined. In general, the development of SHM systems are most often driven by cost justifications.

1.2.1. Operational Evaluation

In the operational evaluation phase of developing a SHM application the first consideration will be cost. For development to begin the economic benefits of detecting damage (and subsequently making the right decisions about maintenance, operation, etc.) must outweigh the cost of development and deployment. Some such things to consider are the savings that detecting damage would have on maintenance by reducing down time and, in extreme cases, the benefit that detecting damage would have on life safety. When defining the system-specific damage types to be detected, cost again is the driving factor. Structural elements having little effect on its overall performance or for which the cost of failure is relatively inexpensive may eliminate some failure modes (or

monitoring regions) from consideration, whereas even low-probability damage that may lead to catastrophic failure and cost might drive those decisions. The consideration of operational and environmental conditions need to be made such that appropriate damage-sensitive features and system hardware can be selected and still maintain an adequate level of performance under the given conditions. Lastly in assessing the limitations and challenges of the data acquisition, one must consider things like the size of the structure, what part of the structure is accessible for sensor placement, how will the data or features will be transmitted through the sensor network, and how will the sensors be powered. Overall the operational evaluation phase involves planning and development to solve the problems and costs associated with developing the SHM system.

1.2.2. Data Acquisition

The data acquisition process involves defining and acquiring the raw data types needed for the application at hand. Common kinematic data types for many structural applications include temperature, strain, vibrations, or displacements. The type of data that is to be acquired subsequently drives sensor selection. Infrared sensors or thermocouples may be used to detect the systems temperature, electrical resistant strain gauges or fiber optic strain gauges may be used to monitor strain, various accelerometers can be used for vibration-based monitoring and proximity probes or laser displacement sensors would be used for detecting displacements.

Data size, sampling frequency, and duty cycle will define what sort of hardware is needed. In addition to the period associated with data collection, the sampling rate will also affect what type of hardware that is selected. In the case of monitoring vibrations, for example, if the hardware and sensor(s) used are only capable of

collecting data at 10 kHz, only frequencies of 5 kHz or lower can be resolved using a Fourier Transform based on the Nyquist sampling criteria. If it is known that high frequency content is a feature of interest then DAQ hardware capable of sampling at the appropriate rate must be used. High sampling rates also may require specialized storage capability or read/write speed, as such all these factors must be considered in the data acquisition phase of the SHM paradigm.

Fundamental to sensor selection type is where to place them and how many are required. The common solution to the former question is to place the sensor(s) as close to the expected damage areas as possible. This location is certainly not always known a priori, although many applications—particularly in applications such as engine monitoring, rotating machinery, etc.—“hot spot” knowledge is known, to some degree. Sensor placement can be determined from physics based models, experimentation, or experience, but it is not a consideration in this thesis.

1.2.3. Feature Selection

In the feature extraction process it is desirable to pick features that will give the best performance for the system specific damage to be determined during the operational evaluation process. In the case of damage classification, ideally a feature with value(s) that will change for the specific damage type it was designed to detect but for no other damage or environmental changes is desired. The statistical distributions of the damage features are also important for detection performance. It is desirable to select features that have low variability under the operational and environmental conditions expected from the system and the best possible distinction or separation of the expected values between damaged and undamaged states. Another desirable trait of good damage features is reduced dimensionality, the lower the dimensionality of the

damage feature the easier it is to store and monitor reducing hardware costs. If using multiple sensors, data fusion is a tech unique used that combines the data from multiple sensors in a way that lead to improved detectability of the damage feature. Another technique used is known as data compression which reduced the dimensionality of the data collected into a reduced dimensional form that retains the damage specific information but excludes the non-damage specific qualities of the data collected.

1.2.4. Statistical Model Development

In the statistical model development process of the SHM paradigm, the statistical characteristics of the selected damage features can be used in such a way that allows for the decisions on the state of the structure to be made. In order for decision to be made about the state of the structure some form of machine learning has to be done in order to make an informed decision. There are two flavors of machine learning which are classified as supervised and unsupervised. In the case of supervised learning the algorithm used for the statistical calcification train on undamaged as well as damaged cases. The more damage classifications provided the more detailed the classification can be assuming there is a decent amount of separation in the damage feature distributions. The two most common forms of supervised learning are known as group classification and regression analysis. In the case of unsupervised learning only the undamaged state is known and in this case of machine learning it is much more difficult to perform further classification of damage other than damaged or undamaged. The methods most commonly used in unsupervised learning are known as outlier detection and novelty detection. Where the decision of damaged or undamaged is made based on the damage feature value exceeding some specified confidence interval determined from the normal operating conditions.

On the most basic level the model should be able to distinguish if there is damage present or not. If possible and the appropriate features were extracted, further classifications can be made to decide where and what type of damage is present. The next level of diagnostic information involves determining the extent of the damage. Lastly is providing a prognosis of the system which is the holy grail of structural health monitoring. Being able to provide a prognosis implies being able to provide a remaining useful life of a structure. With an accurate prognosis the parties responsible for operating and maintain a structure can make informed decision on when to perform maintenance plan on the replacement of a structure and establish the appropriate business model that will maximize the use of a structure and potentially save lives.

Of course none of this matters much if the machine learning and statistical models developed lead to poor decision being made. As such the level of classification is determined by the statistical performance characteristics of the damage features themselves. There are two types of poor decisions that can be made which are known as false positives and false negatives. For example in the case of SHM the null hypothesis is often damage is present, a false positive would be a damage feature values that indicates damage when there is none, where as a false negative would indicate no damage when there is damage present. Often is the case that the latter is the more costly decision from a Bayes risk point of view as the consequences for not detecting damage can lead to catastrophic failure or loss of life. On the other hand for false positive the risk involves losing operational time during maintenance and inspection which need not be performed in the first place. This knowledge reiterates the point that the best damage features are those that can distinguish damage and classify the extent of damage with the highest probability of detection and the least probability of false alarms.

1.3. Condition Based Monitoring of Rotating Machines

Condition based maintenance of rotating machinery is a successful and commonly-used subdivision of the SHM field. Its techniques have been used, many industries, ranging across manufacturing, automotive, aerospace, and energy sectors. It has been used to implement health monitoring systems which are useful for life safety in the case of monitoring drive trains of helicopters [4], [5], where a failure in flight could have catastrophic consequences, to being used on an online system connected to inventory networks where ordering parts has become an automated process [6]. By predicting when parts are going to fail, it is possible to pre-order only the needed parts and have them readily available for when maintenance is needed. It also has remote use applications such as monitoring the generators in a wind turbine farm [7]–[11]. In addition to the diverse applications, condition based monitoring has shown some of the best results in terms providing robust detection of damage.

1.3.1. Operational Evaluation

When considering the implementation of a condition based monitoring system the benefits that implementing the system will provide must outweigh the cost of implementation. There are a number of documents that show strong evidence that CBM implementation has a very good chance of saving the user money in term of reducing unwarranted maintenance, reducing downtime of operating machines, and increasing reliability in the system's ability to operate [12]–[16]. As such, the implementation of condition based monitoring for the most part is dependent upon the availability of the funding to implement it.

The damage to be detected, operational and environmental conditions, and data acquisition constraints are all going to be system dependent. Some of the more common

damage types to be identified are gear and bearing failures. A large body of literature exists which discuss the damage features with specific applications. Primarily CBM of rotating machines involves monitoring gears and bearings of machines.

1.3.2. Data Acquisition

The selection of the data acquisition is also going to be system-specific. There are a number of different sensing techniques that have been used in CBM in order to monitor rotating machines without interrupting its operations. Some of the most common techniques are vibration-based techniques, oil/oil debris optical (or similar) techniques, and infrared thermography [6].

Infrared thermography has been used to monitor slight changes of temperature to certain components of a machine. The idea behind it is that when bearings wear down there will be an increase of friction, which emits heat. As such an increase in heat may be an indication of damage. Some applications of this technique have been to monitor train bearings and braking systems [17].

Oil debris analysis is a technique that involves monitoring the oil that lubricates parts of the machine for any debris that may be present. Gears and bearings over time begin to spall and chip, leaving particles of debris in the oil that can be collected from a reservoir without having to interrupt the operation of the machine. Detection of metal particle in the oil would be a sign of damage in this case.

Vibration analysis of rotating machines is the most popular of the three methods discussed in this section due to its ability to localize damage within the machine based on known attributes associated with gear mesh frequencies and bearing frequencies. Vibration analysis also has the ability to provide real time data on the machines

condition at any given moment allowing for it to be implemented as an online monitoring system. It is this class of techniques that this thesis will consider.

1.3.3. Feature Selection

Feature selection for rotating machines can be difficult, as there is a lot of environmental and operational variability unique to each machine. Things that need to be considered include the operational speeds the loading and noise level of the environment. Depending on these variables different methods are available to refine and clean the data before extracting the desired damage feature. The majority of the CBM literature has focused on this step of the SHM paradigm.

Pre-processing the vibration signal before extracting a feature is a very common step. One of the reasons for this is that many times frequencies of the machine present in the vibration signal are phase locked to the shaft position and can be enhanced or separated using a method like angular resampling, time synchronous averaging, or discrete random separation. It is also possible to remove the phase locked frequencies using these same methods for detecting damage of components that are not phase locked such as bearing damage frequencies, which are reported to be quasi periodic due to slip in the bearing housing [17].

Some of the more traditional methods of pre-processing include filtering out various bandwidths of an angular resampled signal in order to enhance frequency content that is expected to change during certain damage types. At times it is desirable to filter out the gear meshing harmonics using band-pass filtering as is the case in the residual and difference signal. Other pre-processed signals filter out frequency content in bands between gear meshing harmonics such as the band-pass mesh signal [18]–[22].

Other methods involve decomposing the vibration signal into a 2D time-frequency domain; the continuous wavelet transform, short time Fourier transform, and Wigner-Ville distribution are some of the more common time frequency methods that have been used to study damage present in rotating machines [23]–[26]. Some methods presented in the literature for use in condensing the dimensionality of time-frequency decompositions involve taking the summation of the frequency components or computing the Holder exponent as a function of time [27]–[30].

Other methods have been presented that look at the kurtosis of the frequency domain or dissect it into different bandwidths and look for the maximum kurtosis in each bandwidth as a way of determining which frequency bands are responsive to damage [31]–[34]. For bandwidths of interest, demodulation and signal envelope analysis is often a common technique used to enhance the detection of bearing fault frequencies [35].

Though there are many techniques for extracting damage features that have been shown to work well in the literature, setting the parameters and establishing a damage feature that is intolerant to changes in environmental and operational conditions can still be an appreciable challenge at times.

1.3.4. Statistical Model Development

Statistical model development applied to rotating machines is the least mature section of the four steps in the SHM process; some of the work that is being done involves making prognosis of useful remaining life of machines [36]–[38]. There are essentially two types of modeling used which are physics based models and data driven models. In the physics based model, primarily work has been done in predicting crack

growth and spalling. In the case of data driven modeling, trending is predicted based on data taken in known conditions [17].

1.4. Scope of Thesis

The scope of this thesis is to study and report on the detection capabilities of the various commonly-used CBM damage feature extraction algorithms that have been described in the academic literature to date and characterize their detection perfection using experimental data for binary damage states using receiver operating characteristic curves. The literature to date has primarily involved an extensive pursuit of new techniques that are proved in theory or using models but lack real world application or statistically significant results. There have been some articles that have applied the algorithms to testbeds, but the method of testing usually only considers one test run, or a very few (due to cost) run-to-failure tests. By performing multiple test runs as is done in this thesis, it is possible to provide a better understanding of the variability of the damage features. Some papers have written about some of the uncertainty that exists in the extraction of the damage features from real world applications; for example, in one article, tests were performed on a helicopter gear box in flight and it was discovered that false alarms would occur during strenuous maneuvers [4]. Another article indicated that some of the damage features would increase then decrease as a certain level of wear proceeded on the gears and suggested that multiple features be used in order to classify damage [18]. Lastly, a considerable amount of work has been done on optimal sensor placement and multisensory data fusion in the scope of CBM [39], [40] but could benefit from a more informed decision based on known feature variability under changing environmental and operational conditions.

Due to the large variability in damage features under certain conditions and the lack of recommendations for DAQ specifications it was decided that an important contribution to the field would be to pursue a study on what damage features may have improved performance under specified conditions and why certain damage features may experience increased variability as known events occur, such as increased torsional load under a difficult flight maneuver or a belt drive loosening over time. This study will help develop a firm foundation and provide a better overview of which damage features might experience false alarms under some conditions but not in others. Features that are not affected by certain environmental conditions may make them better damage features than others under specified conditions. In general, this thesis is an attempt to lay out the ground work for future study in developing optimal detectors for classifying damage as well as providing a platform to continue off of by systematically exploring the damage features under controlled conditions.

In addition to the detailed comparative study of traditional damage features, a new damage feature was developed and labeled FMH. The FMH features uses the frequency spectrum of the Hölder Exponent as a measure of the periodicity of non-linearities associated with gear mesh harmonics. FMH was compared with traditional damage features under variable operational conditions and has shown superior performance compared to traditional damage features used in practice.

Chapter 2

Technical Background

2.1. Introduction

In Chapter 2 the technical background needed to understand the algorithms used in this study are presented and explained in greater detail than previously referred to in the previous chapter. Some examples are presented as well which will assist in demonstrating the use and limitations of all the various digital signal processing techniques that have been used in this study. Firstly, techniques in digital signal processing will be covered. These digital processing techniques provide the foundation for some of the more advanced techniques used in condition based monitoring. Then, more feature extraction techniques are presented which are more specific to CBM of rotating machinery. Lastly, a review of traditional damage features as well as the new damage feature will be introduced.

2.2. Digital Signal Processing Techniques

Various digital signal processing techniques are used in the feature extraction process for condition based monitoring, and to fully understand the reason behind how

the features are acquired and why they may experience reduced detection performance, it is of value to provide some basic understanding of some of the more important techniques used throughout this thesis as well provide some examples to verify that the application of the techniques work. This section is dedicated to reviewing relevant digital signal processing and related technical background used in vibration-based CBM applications.

2.2.1. Fourier Transform & Power Spectral Density

The Fourier transform is a central pillar of many digital signal processing applications. Its primary purpose is to transform a signal from the time domain to the frequency domain by decomposing it to its sinusoidal basis (phase and magnitude). The complex discrete Fourier Transform can be defined as:

$$X(k) = \frac{1}{N} \sum_{n=1}^N x(n) \exp(-j2\pi(k-1)\frac{(n-1)}{N}), \text{ for } 1 \leq k \leq N \quad (2.1)$$

where n is the sample number, N is the total number of samples, and k is the frequency bin. Using the magnitude of the complex Fourier transform it is possible to determine the power of a signal associated with a specified frequency. The advantages of the Fourier transform became even greater when the development of the Fast Fourier Transform. The Fast Fourier Transform (FFT) uses what are known as twiddle factors to reduce the number of operations by half if the sampling length is a factor of two which can have large computational cost savings for large signal lengths.

There are some tradeoffs to consider when using the Fourier transform in regards to time- frequency resolution. Longer signals provide better frequency resolution but poorer time resolution whereas short signals have better time resolution

and poorer frequency resolution. For example, say a one second signal is sampled at 10 kHz; this would provide a digital signal with 10,000 samples. Because the FFT frequency range spans a length of 10 kHz, a frequency resolution of 1 kHz can be achieved. To get better time resolution than 1 second, a shorter length signal must be used. A shorter length signal would have less samples but the FFT would span the same frequency range. This shorter signal would lead to poorer frequency resolution as there are now fewer samples for the same range of frequencies.

Noisy and non-stationary signals suffer from fluctuations of the frequency components which can cause smearing in the power spectrum and at times-frequency content within the FFT difficult to resolve. One way to deal with this is to use spectral averaging to estimate the power spectral density, one of the most common forms of spectral averaging is Welch's method [41]. The PSD using Welch's Method is defined as:

$$\hat{P}(f_n) = \frac{1}{K} \sum_{k=1}^K \frac{L}{U} |A_k(n)|^2, \text{ where } U = \frac{1}{L} \sum_{j=0}^{L-1} W^2(j), \text{ for } k = 1, 2, \dots, K \quad (2.2)$$

In Welch's method the power spectral density consists of first segmenting the signal into K number of L length segments with a specified number of overlapping samples; typically the number of overlapping samples is 50-75% of the segment length. The segments are then windowed to help prevent spectral leakage due to the discontinuities at the ends of the signal. The Hamming, Hanning and Kaiser windows are some of the more common window functions used in PSD computations. After windowing the segments in the time domain the FFT of all the segments are taken and their magnitudes averaged together. The PSD average then needs to be normalized by

L/U to compensate for loss of power due to the windowing. The overlapping also helps regain some of the lost power due to windowing.

2.2.2. Time-Frequency Analysis

The purpose of time-time frequency analysis is to decompose a signal into its frequency components as a function of time. There are many different time frequency decompositions, but this study focuses on three of some of the more popular methods. The three time-frequency decompositions to be discussed in this section are the Short Time Fourier Transform (STFT), Linear Predictive Coding (LPC) spectrogram, and the Continuous Wavelet Transform spectrogram. Each of the mentioned time-frequency analysis methods have their own different tradeoffs and some examples will be shown.

The STFT quite simply is the FFT of a moving window of a specified length that is shorter than the length of the signal. The shorter the window the better the localization of the frequency components are in time with the tradeoff that the shorter the window, the lower the frequency resolution that can be achieved. The STFT can be defined as:

$$S(f, \tau) = \int_{-\infty}^{\infty} x(t)w(t - \tau) \exp(-j2\pi ft) dt \quad (2.3)$$

where x is the signal, w is a windowing function, S is the STFT time-frequency decomposition of the signal x , f is the frequency, and τ is the time delay of the window function.

The LPC Spectrogram has been used for a long time in speech processing [42]. The advantage of the LPC spectrogram is that better spectral resolution can be achieved for short time windows giving it an advantage over the STFT. Like the STFT

it involves first sectioning the signal into a series of time-delayed windows.

Autoregressive coefficients are then computed which can be used to compute the spectrum of the window.

The Continuous Wavelet Transform (CWT) scalogram is also another alternative to STFT for use in time frequency analysis. The CWT scalogram is different from the STFT and LPC scalogram due to the fact that time-frequency resolution tradeoffs change throughout its domain. In the high frequency registers it has very poor resolution but good time resolution, whereas in the lower frequency range it has good frequency resolution but poor time resolution. The CWT scalogram can be defined as:

$$\Psi(\tau, s) = \frac{1}{\sqrt{|s|}} \int x(t) \psi^* \left(\frac{t-\tau}{s} \right) dt, \text{ where } \psi^*(t) = \frac{1}{(f_b^2 \pi)^{1/4}} e^{2\pi i f_c t} e^{\frac{-t^2}{2f_b^2}} \quad (2.4)$$

is the mother wavelet, s is the scale factor, and τ is the time lag. The CWT scalogram can be calculated digitally by developing a filter bank of mother wavelets with scales varying logarithmically and convolving a mirrored signal with each mother wavelet for each scale.

There are many mother wavelets, e.g., Morlet, Paul, Shannon, B-Spline and Daubechies among others. The choice of a mother wavelet dictates time resolution and frequency resolution in the scalogram. Paul wavelets tend to have good time resolution and poor frequency resolution whereas B-splines have good frequency resolution but poor time resolution [43]. Morlet wavelets were used in this paper as they have shown positive results in detecting transients in signals [28], [29], are easy to implement, and have a balanced tradeoff between time and frequency resolution.

The scale of the wavelet is dictated by the central frequency f_c and is varied on a log scale from a desired minimum frequency to a desired maximum frequency. By varying of the scales in such a manner the CWT scalogram has a dyadic sampling grid with increased time resolution at high frequencies and reduced time resolution at low frequencies.

2.2.3. Signal Envelope and the Hilbert Transform

The Hilbert transform is a way of transforming a signal from its real components to its analytical form. There are a number of ways to compute the Hilbert transform, but one of the more cost effective methods is to calculate the FFT of the signal, double its positive frequency components and remove its negative frequency components. After performing these steps, the inverse FFT of the modified spectrum will result in the analytic version of the original signal. The analytic signal can then be used to compute the enveloped signal by taking the magnitude of the analytic signal. The enveloped signal can be defined as:

$$E(t) = \sqrt{\text{Re}[A(t)]^2 + \text{Im}[A(t)]^2} \quad (2.5)$$

where $A(t)$ is the analytic signal.

2.3. Condition Based Monitoring Feature Extraction

Part of the feature extraction process involves manipulating the raw signal in a way that will later improve the detection of damage and in some cases improve classification of the damage as well. In Section 2.3 some of the more relevant

techniques to condition based monitoring of rotating machines are presented and their applications discussed.

2.3.1. Angular Resampling

Angular resampling is the process of resampling a vibration signal that was sampled in equal intervals in the time domain to a signal with equal angular interval relative to some shaft position in a rotating machine. The purpose of angular resampling is that often times rotating machines will operate with varying speeds, and during the feature extraction process it is desirable to track certain frequency components that can be associated with specific shaft, bearing, and gear frequencies. By using this method it allows for localization of damaged components at varying speeds. Furthermore, periodic frequency components at varying shaft speeds will tend to be smeared in the time domain but remain periodic in the angular domain.

Some systems have shaft encoders and are able to sample at equal angular shaft interval directly from the DAQ, but often times this is very costly [44]. A less expensive alternative uses a tachometer, which involves an optical sensor to detect the passing of a reflector on the shaft, which will generate a pulse for every full rotation of a machines shaft. Yet another method involves using the vibration signal itself if a known periodic component is present in the signal and can be correlated with the rotation of the shaft.

The procedure for angular resampling using a tachometer signal is summarized in the schematic shown in Figure 1. It involves using the tachometer signal to determine the period crossings of the shaft and using those to crossing to estimate the shaft position for the remaining samples using some sort of interpolation method. The original signal is then up sampled by a specified constant L and low passed filtered to remove any frequency content that may not have been present in the original signal. The

value of L is dependent on the desired samples per revolution and the minimum angular resolution that was present in the tachometer signal, which can be determined from the estimated angular intervals. After interpolating the time series signal to the angular domain, the final step is to down-sample the signal to the highest order of interest by first low pass filtering to prevent aliasing of higher frequency content, and then decimating by the desired value.

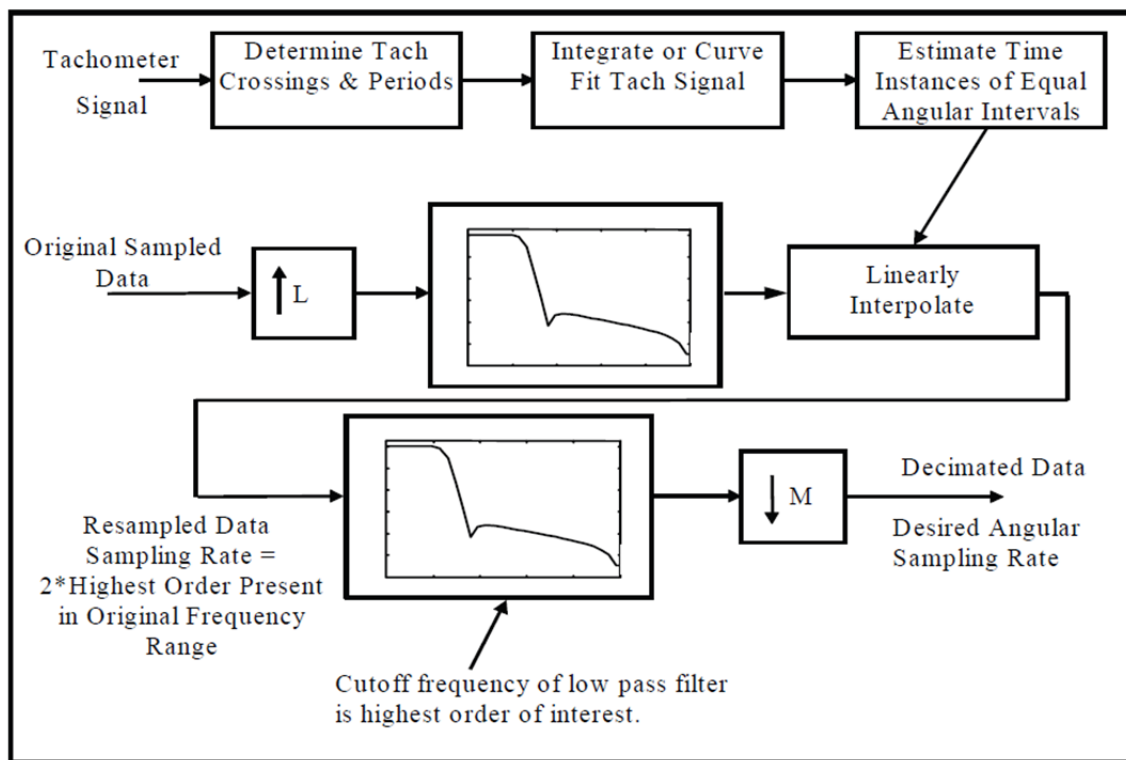


Figure 1: Angular Resampling Schematic [45].

If no tachometer signal is available it is possible to use a periodic gear mesh frequency component within the signal itself for angular resampling [44]. The process is similar to the tachometer process but instead of using a tachometer signal to estimate the shaft position corresponding to each sample of the time domain signal, the shaft

phase has to be estimated using prior knowledge of the system being monitored. If the general rotational frequency of the shaft, the number of teeth present on the gear and the harmonic order present in the vibration signal are known, that frequency can be band pass filtered out of the raw signal. Once this has been done, it is possible to compute its analytical form using a Hilbert transform. From the analytic signal, the phase can be determined and the shaft position estimated from the phase of a gear mesh harmonic. Using this estimate of the shaft position, the process is the same as was described for angular resampling using a tachometer signal.

2.3.2. Time Synchronous Averaging

The name time synchronous averaging (TSA) in context of CBM is a bit of a misnomer in that the method is not averaging the time domain at all. It is absolutely crucial to first resample to the angular domain, otherwise it will have little benefit. The purpose of the TSA technique is to further remove any non-periodic components from a signal. The TSA signal involves averaging each revolution of the resampled signal together. The TSA signal can be defined as:

$$x_{TSA}(t) = \frac{1}{N} \sum_{n=0}^{N-1} x(t + nT) \quad (2.6)$$

Here N is the number of revolutions present in the resampled signal, T is the number of samples per revolutions and t is representative of the angular position. By averaging the resampled signal revolutions together, the non-periodic components will phase cancel with each other, and only the periodic components are left. These periodic components can be said to be unique to gear specific damage whose teeth mesh frequencies are strongly correlated to the position of the shaft. The TSA signal can also

be used to remove periodic components from an angular resampled signal. This technique can be achieved by removing the TSA signal from each revolution in the angular resampled signal by subtraction. Though this method is simple and has been used and examined for many years in the CBM community [19], [46]–[49], it is also one of the most erroneous methods for separating discrete and random components from an angular resampled signal.

2.3.3. Discrete Random Separation

Discrete Random Separation (DRS) is an alternative to self-adaptive noise cancellation signal processing to filter out periodic components from a vibration signal [50], [51]. It can be used to separate or remove periodic components from a signal for feature extraction. The method of performing DRS involves computing the average cross-power spectrum of a signal by a delayed portion (Figure 2) of itself over the average auto-power spectrum of the delayed portion.

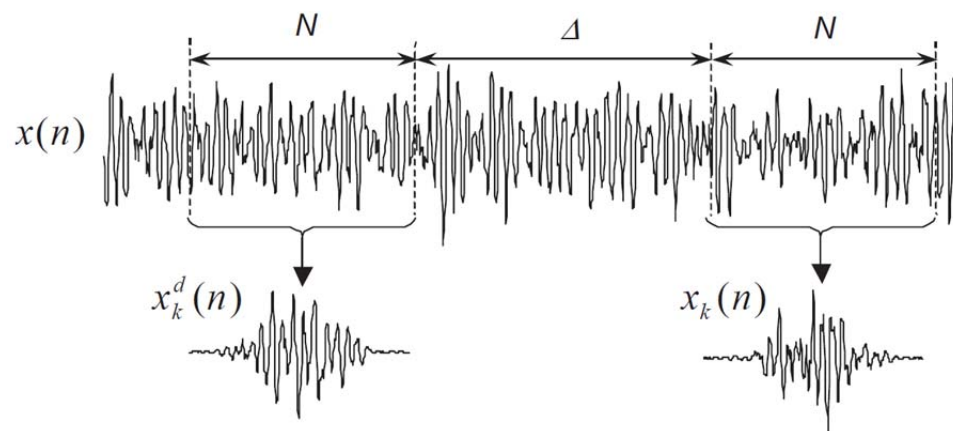


Figure 2: Example of Short Delayed Window Structure for use in determining the DRS filter transfer function [51].

This transfer function can be results in theory with values close to 1 at frequencies that are periodic in the signal and lesser values for non-periodic frequencies. The estimate of the optimal filter transfer function can be defined as:

$$\hat{H}(f) = \frac{\sum_{k=1}^K \tilde{X}_{k,M}^d(f) \tilde{X}_{k,M}^d(f)^*}{\sum_{k=1}^K \tilde{X}_{k,M}^d(f) \tilde{X}_{k,M}^d(f)^*} \quad (2.7)$$

Once the estimate of the optimal filter transfer function has been computed the filter's impulse response can be computed by taking the inverse FFT and convolved with the original signal in order to filter out the periodic components. To get the random component of the vibration signal, the periodic component may be removed by subtraction, but in order to do this it is important to note that the filter consists of a phase delay that must be compensated for before removing the periodic component.

2.3.4. The Difference, Residual and Band-pass Mesh Signal

The difference, residual, and band pass mesh signals are all vibration signals which have undergone some sort of filtering process and are traditionally used in extracting damage features for condition monitoring of rotating machines [4], [52]–[54]. Computing the residual signal involves filtering out the gear main shaft frequencies and the gear mesh frequencies but retaining any remaining side bands that may be present in the signal. For computing the difference signal, again it involves filtering out the main shaft and a gear mesh frequencies, but in addition to these, the first order side bands are also to be filtered out. Essentially the bandwidth of the band stop filter becomes wider to incorporate the first-order frequencies. In the case of processing the band pass mesh signal, is precisely to band-pass filter the gear mesh frequencies. An example of the

power spectral densities for the difference, residual and band-pass mesh signal is presented in Figure 3. For each plot the left and right halves are representative of a baseline and worn tooth system state.

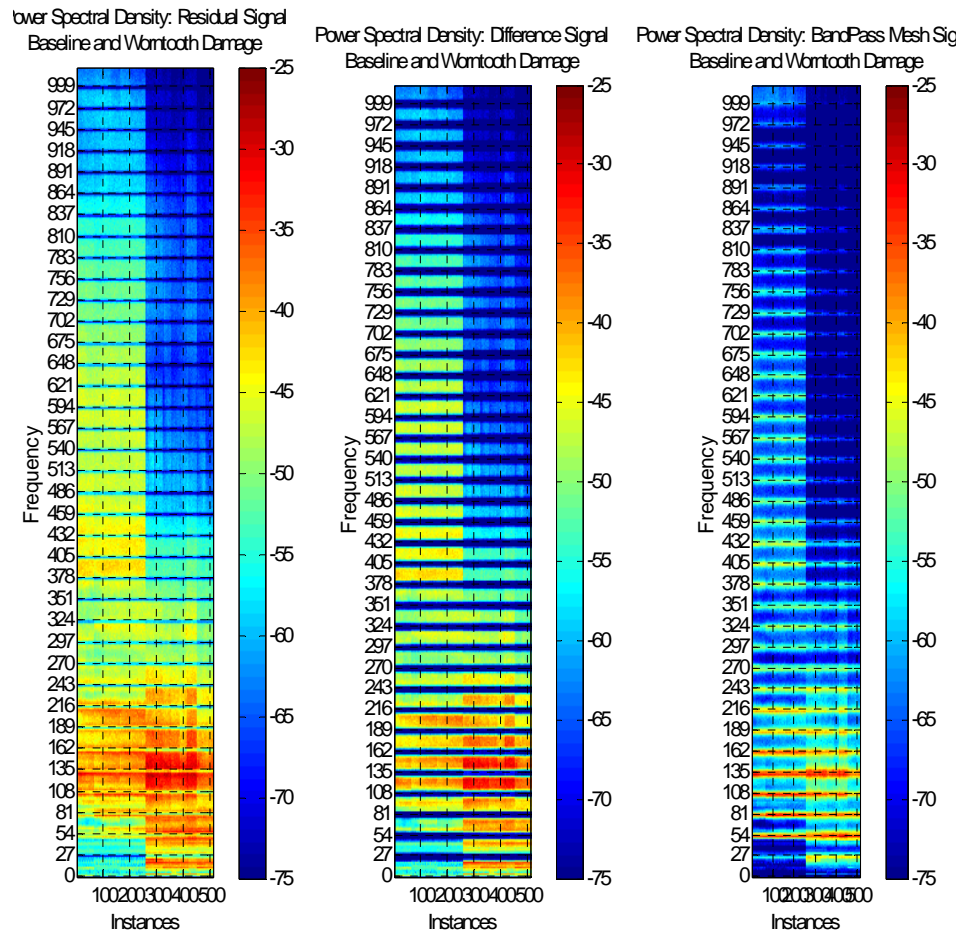


Figure 3: Residual Difference and Band Pass Mesh Power Spectral Densities for Baseline\Worn tooth Damage @ 1000 RPM Resampled to 2048 Samples per Revolution with 20 revolutions.

2.3.5. Traditional Damage Features

Three of the classical damage features operate on the conditioned raw signal. The RMS, is effective in tracking overall noise levels and damage, but is not very good in determining which component is failing. The crest factor is the ratio of the peak level

of the signal and the RMS. This feature is more sensitive to damage incurred in early stages of gear and bearing damage. The kurtosis is the fourth statistical moment and a measure of the peaked-ness of the raw conditioned signals distribution. It is used as an indicator of major peaks that may appear as damage occurs [54].

FM0 monitors the amplitude of the frequency bins that correspond to the gear mesh harmonics in the frequency domain of the TSA signal. The PPA is defined as the peak-to-peak amplitude of the TSA signal. The FM0 is not a good detector for minor tooth damage [54].

NA4* is an enhanced version of NA4 developed to detect progressive damage. It normalizes the 4th statistical moment of the residual signal by the variance of a baseline (healthy) residual signal variance [20], [54].

FM4, M6A, and M8A all operate on the difference signal. FM4 was developed to detect damage on a limited number of gear teeth. FM4 is 4th statistical moment of the difference signal normalized by its variance squared [54]. M6A and M8A were developed to detect surface damage on machinery components. M6A and M8A are expected to be more sensitive than FM4 [54].

NB4* is computed using the enveloped signal of the band-pass meshed signal. It is used to detect transients that differ from normal tooth load fluctuations that are detected by the enveloped signal. The enveloped signal (E) is determined by taking the magnitude of an analytic signal determined using a Hilbert transform [54] and is normalized by the variance of a baseline (healthy) enveloped signal.

Table 1: Traditional Damage Features [4], [52]–[54].

Damage Feature	Feature Equation	Signal Used	Filtering Operation
RMS	$\sqrt{\frac{1}{N} \sum_{i=1}^N [x_i]^2}$	Raw Conditioned Signal	--
Crest Factor	$\frac{PeakLevel}{RMS}$	Raw Conditioned Signal	--
Kurtosis	$\frac{\frac{1}{N} \sum_{i=1}^N [x_i - \mu_x]^4}{[\sigma_x^2]^2}$	Raw Conditioned Signal	--
FM0	$\frac{PPA}{\sum_{i=1}^N A(f_i)}$	Time Synchronous Averaged Signal	--
NA4*	$\frac{\frac{1}{N} \sum_{i=1}^N [r_i - \mu_r]^4}{(\tilde{M}_2)^2}$	Residual Signal	Band-Stop: Gear Mesh and Shaft Frequencies
FM4	$\frac{N \sum_{i=1}^N [d_i - \mu_d]^4}{\left\{ \sum_{i=1}^N [d_i - \mu_d]^2 \right\}^2}$	Difference Signal	Band-Stop: Gear Mesh +1 st Order Sideband and Shaft Frequencies
M6A	$\frac{N^2 \sum_{i=1}^N [d_i - \mu_d]^6}{\left\{ \sum_{i=1}^N [d_i - \mu_d]^2 \right\}^3}$	Difference Signal	Band-Stop: Gear Mesh +1 st Order Sideband and Shaft Frequencies
M8A	$\frac{N^3 \sum_{i=1}^N [d_i - \mu_d]^8}{\left\{ \sum_{i=1}^N [d_i - \mu_d]^2 \right\}^4}$	Difference Signal	Band-Stop: Gear Mesh +1 st Order Sideband and Shaft Frequencies
NB4*	$\frac{\frac{1}{N} \sum_{i=1}^N [E_i - \mu_E]^4}{(\tilde{M}_{2,E})^2}$	Enveloped Band-Passed Mesh Signal	Band-Pass: Gear Mesh Frequencies

2.3.6. Hölder Exponent and the FMH Feature

The Hölder exponent is computed by calculating the slope of the log-log analysis of the frequency vs. scale values of the CWT scalogram for each instance of time. The Hölder exponent as a function of time is defined as:

$$H(\tau) = \frac{(-m(\tau) - 1)}{2}, \text{ where } m(\tau) = \frac{\log|\Psi(\tau, s)|}{\log(s)} \quad (2.8)$$

Non-linearities caused by tooth impacts of gears generate high frequency energy in the system. Detecting this increase in high frequency energy can be utilized using the CWT scalogram and its Hölder exponent, which is known for its sensitivity to local (in time) non-linearities in dynamic response signals [4,6], making it an ideal candidate for health monitoring involving the presence or lack of non-linearities in rotating machines.

Healthy gear mesh signals, which consist of periodic tooth contact shocks dependent on shaft speed, create non-linearities picked up by the Hölder exponent. The result is a periodic signal associated with the meshing of the gear teeth. By monitoring the frequency bins of the Hölder exponent power spectral density associated with the gear mesh harmonics and its peak-to-peak amplitude, it is possible to achieve higher sensitivity than the traditional methods. The FMH is defined as:

$$FMH = \frac{PPA_{Holder}}{\sum_{i=1}^N A_{Holder}(f_i)} \quad (2.9)$$

An example of the new FMH damage feature for use in detecting worn tooth damage is provided below. The data were taken from a gearbox mounted sensor with

the gear box drive shaft speed operating at approximately 4.49 Hz and 27 teeth per gear. A single instance of a baseline and damaged CWT scalogram and their corresponding Hölder exponent series are shown below (Figure 4 and Figure 5).

When computing the CWT scalogram for the healthy gearbox, the gear mesh is clearly visible in the high frequency bins as can be seen in Figure 4. The corresponding Hölder exponent series appears to be periodic in nature and similar to an amplitude-modulated sinusoid with the frequency at the fundamental mesh frequency. For every tooth mesh impact there is a rise in the high frequency energy content due to the broadband response of the gear mesh impacts. The high frequency mesh-pattern shows an expected 27 impacts per full rotation, which agrees with the maximum number of 27 teeth in the drive shaft gear.

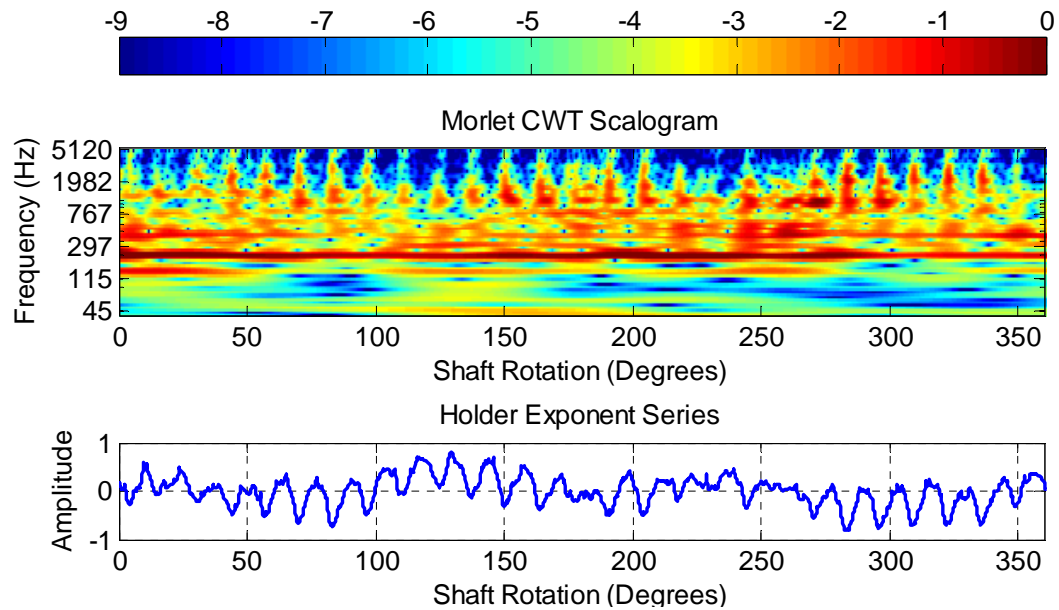


Figure 4: CWT scalogram and Hölder exponent series for a baseline condition gearbox signal.

In the case of the damaged gearbox, the pattern associated with the gear mesh has clearly decayed (Figure 5). There is now a smearing in the high frequency energy content instead of the clearly periodic pattern that was seen in Figure 4. When looking at the Hölder exponent series, the peaks have also been substantially reduced and no longer resemble the amplitude-modulated sinusoid that was seen in the case of the healthy gearbox; a decrease in the peak to peak amplitude is also observed.

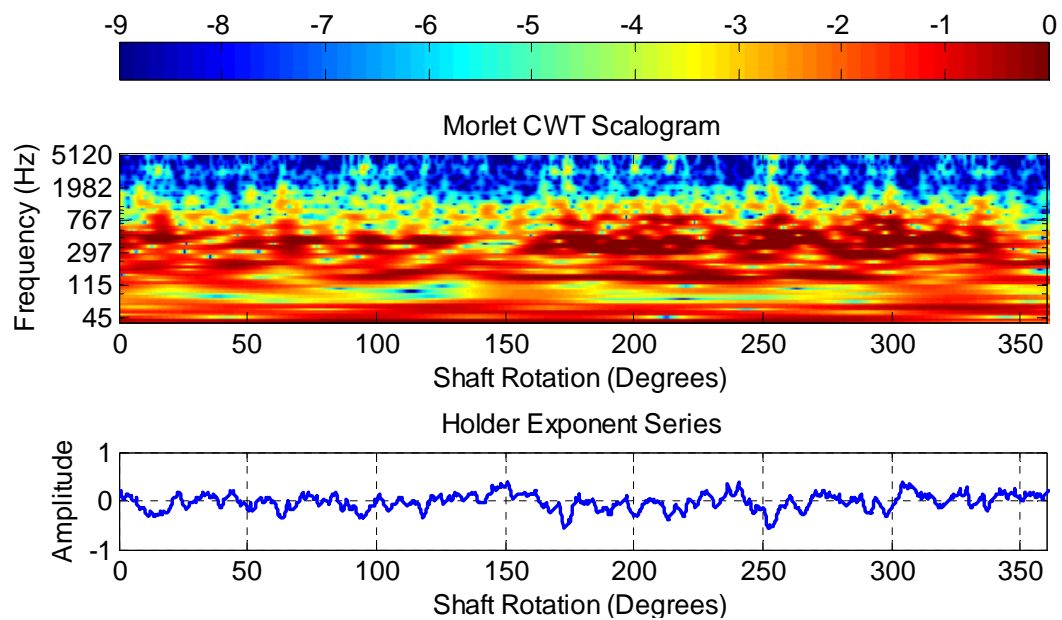


Figure 5: CWT scalogram and Hölder exponent series for a worn tooth condition gearbox signal.

The power spectral densities of the Hölder exponent series were taken using Welch's method. A comparison of the healthy Hölder exponent power spectral density for one instance of a healthy gearbox and a damaged gearbox can be seen below in Figure 6. In the case of the healthy gearbox, the first three harmonics can be clearly seen using a dB amplitude scale. In the case of the damaged gearbox, the amplitudes drop as the intensity of the gear mesh has reduced due to the tooth wear. The decrease

seen here in the amplitude of frequency bins associated with the gear mesh harmonics make them a good candidate for a damage detection feature of gearboxes.

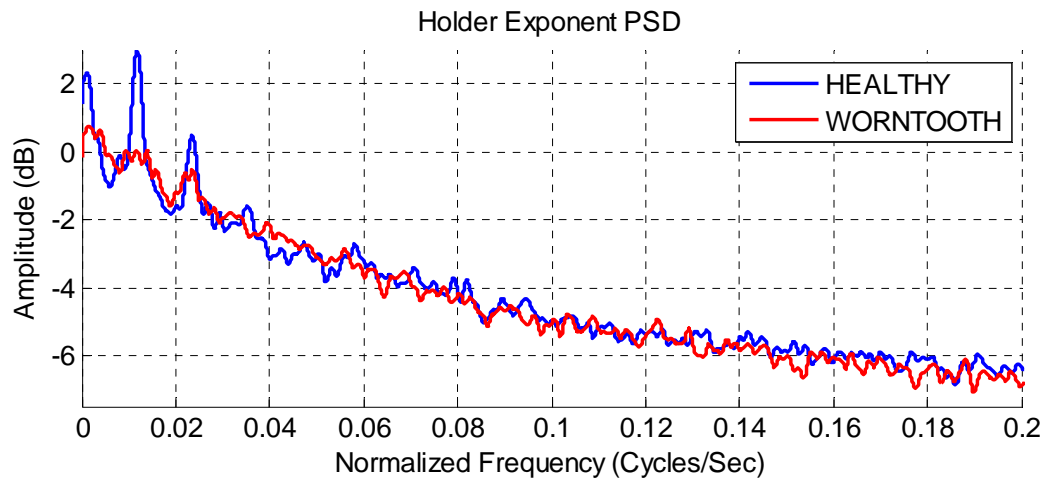


Figure 6: Power Spectral Densities of Hölder exponent series for undamaged and worn tooth damaged gearbox signals.

From the example it can clearly be seen that the FMH feature has potential to be a very effective damage detector for worn tooth damage. The performance of FMH damage feature is compared to traditional damage features in the results section of this thesis. Using a statistically significant comparison the FMH feature will be shown to have superior detection capabilities over traditional methods for early onset gear damage.

Chapter 3

Experimental Setup & Feature Extraction Results

3.1. Damage Types and Descriptions

In this study there were four types of damage that were rigorously compared using the damage features described in the previous chapter. The four types of rotating machinery damage examined were worn tooth gear box damage, ball fault bearing damage, outer race bearing damage, and inner race bearing damage. Varying operational loads such as the tension of the drive belt and torsional gear box load were also examined. These studies were performed to examine the robustness of the damage features but were not considered to be damage.

3.2. Experimental Setup

3.2.1. Testbed Description and Evaluation

The data in this study were acquired via the SpectraQuest Inc., Magnum Machinery Fault Simulator. The fault simulator simulates many faults but the damage

types of primary interest for this study were worn tooth (WT) damage on the gearbox and various bearing faults that were on the main shaft bearing, including ball bearing outer race faults (BBO), ball bearing inner race faults (BBI), and ball bearing ball faults (BBB). Some operational parameters that were varied over a number of different tests were the torsional load (TOR) on the gear box, main shaft speed in revolutions per minute (RPM), and belt tension (BT) of the belt connecting the gearbox drive shaft to the main drive shaft. Lastly two different main shaft bearings were used in this study. System states 1-4 involved using fluid film oil bearing and all other states involved using ball bearings to support the main shaft.

The testbed consisted of a main shaft driven by an electric motor (Figure 8), which had a single rotation tachometer signal that indicates the main shaft rotation in these experiments. The main shaft was set up to be supported by two fluid film oil bearings for states 1-4 but used ball bearings for the main shaft support for all other states. The main shaft was a 3/4 inch diameter steel shaft with a support length of 28.5 inches center to center between bearings. Two aluminum masses were supported on the main shaft, one 8.5 inches to the right from the motor side bearing and the other 6.5 inches from the belt drive side bearing. A belt drive (Figure 9) was used to drive a gearbox (specifications provided in Table 2) with a magnetic break which applied a torsional load (Figure 10). The belt drive consisted of two double groove belt sheaves with a sheave ratio of $\sim 1:3.71$ where the smaller sheave was attached to the main shaft and the larger sheave to the gearbox shaft.

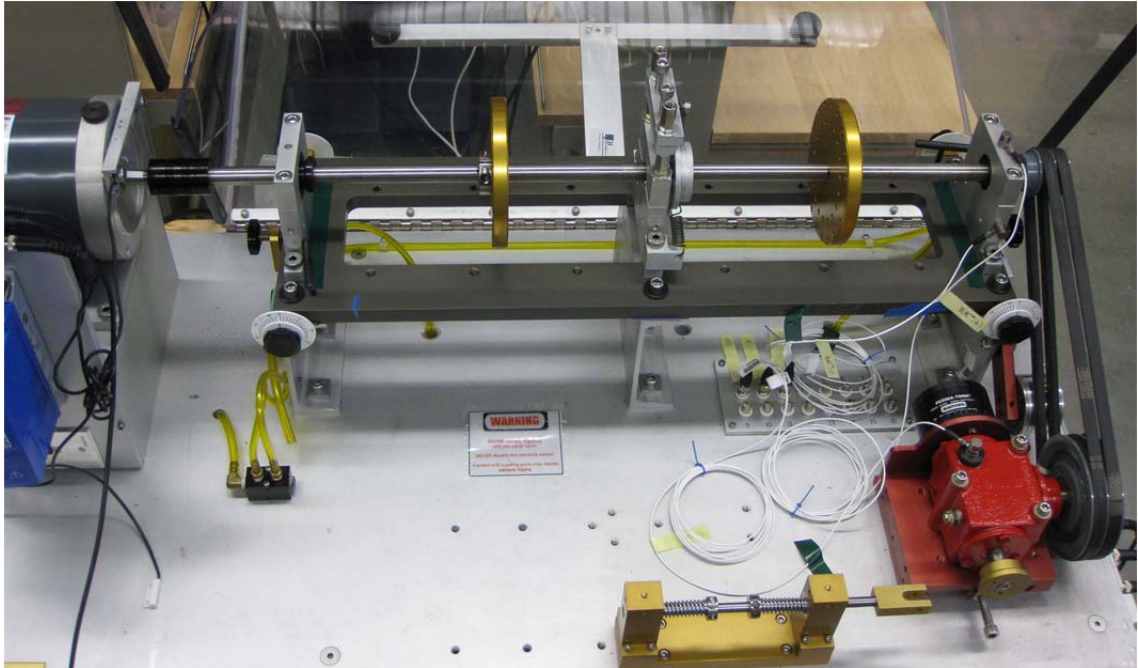


Figure 7: Machinery Fault Simulator (Top View)

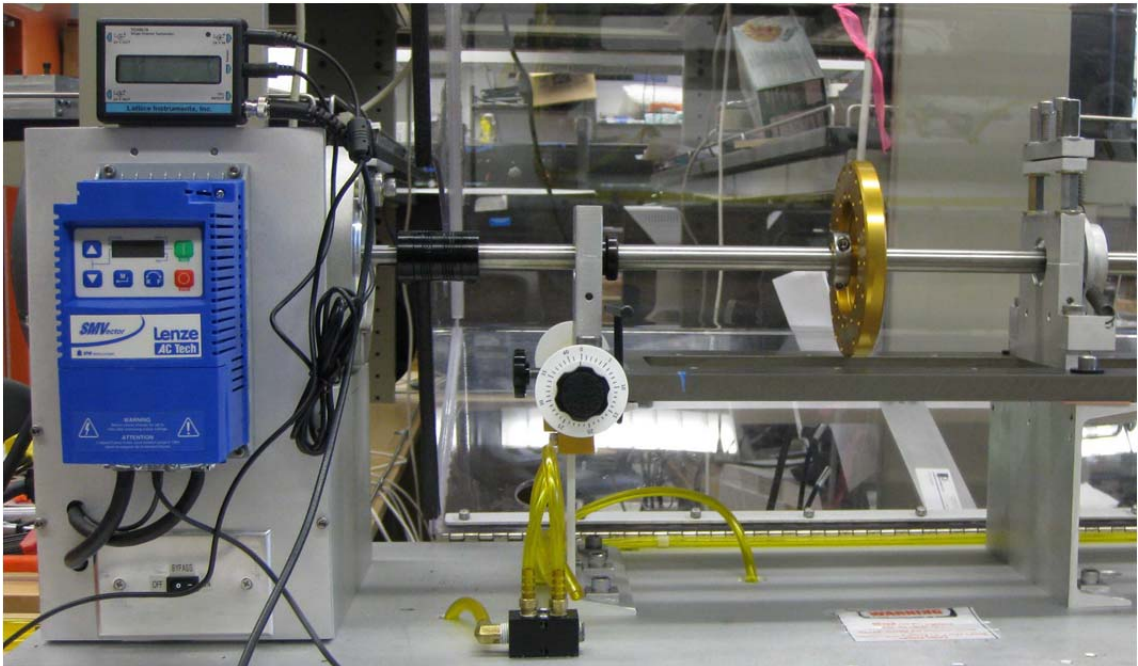


Figure 8: Machinery Fault Simulator Controller (Left Side)

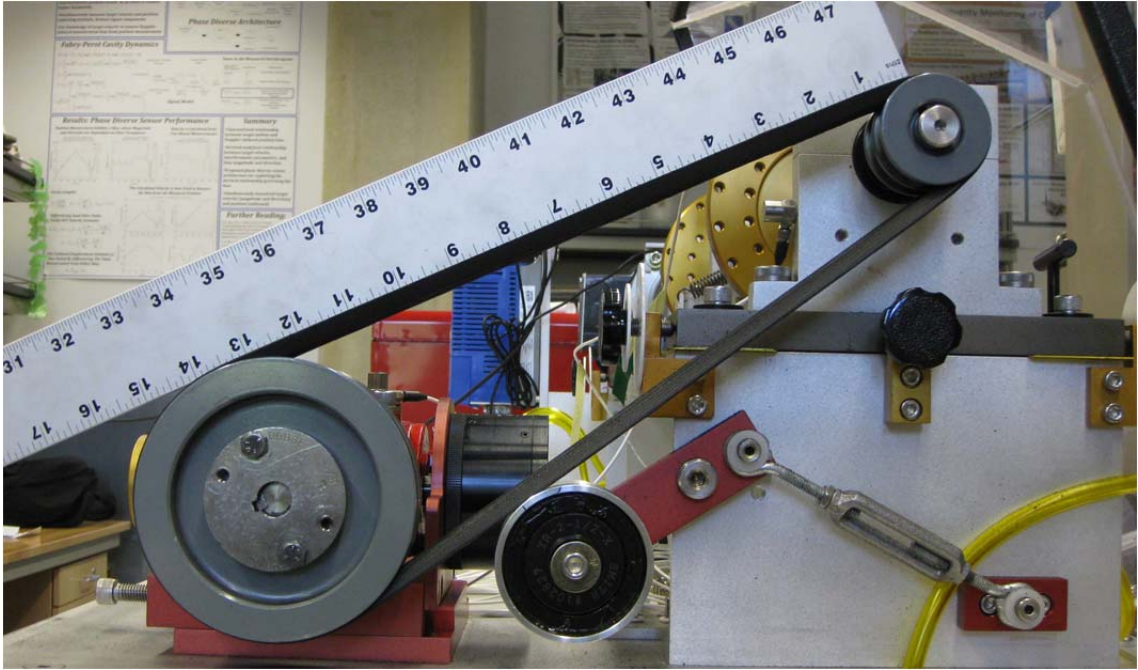


Figure 9: Gear Box Belt Drive (Side View)

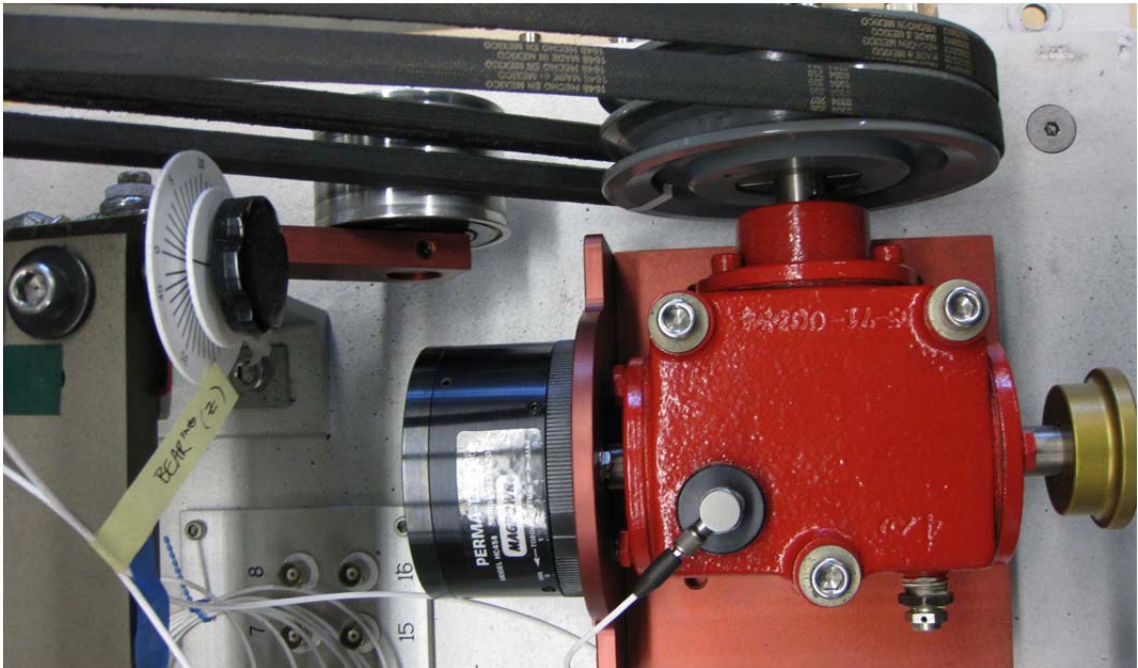


Figure 10: Machinery Fault Simulator Gear Box (Top View)

Table 2: Gear Box Specifications

Ratio:	1.5:1
Model:	Hub City M2
Pitch Angle Gear:	56 degrees 19 minutes
Pitch Angle Pinion:	33 degrees 41 minutes
Pressure Angle for Gear and Pinion:	20 degrees
Material:	Forged Steel
Backlash Tolerance:	0.001-0.005 inches
Pitch Diameter Pinion:	1.125 inches
Pitch Diameter Gear:	1.6875 inches
Number of teeth (Pinion):	18
Number of Teeth Gear:	27
Pinion Bearing:	NSK 6202 (1 Bearing)
Gear Bearing:	(2 Bearings)

3.2.2. Data Acquisition

The choice in sensors and data acquisition hardware was determined based on a couple of factors. The first factor was the limitations of the fault simulator. The literature that came with the hardware recommended that the fault simulator not be run at speed higher than 6000 RPM for periods longer than 30 seconds as well it was recommended not to run the near 20% of critical speeds for more than 20 seconds. As such it was decided so as not to damage any components uncontrollably and run only 1000 RPM and 2000 RPM tests. This limitation meant mesh frequencies and bearing fault frequencies would be relatively low compared to what the maximum sampling rates offered by the DAQ systems available in the lab. Lastly, to minimize data storage space and processing times, lower sampling rates were used.

The sensors chosen were PCB 352-C33 accelerometers, and the DAQ card was an NI 9234 DAQ Card (Figure 11). Sensor specifications are summarized below in Table 3 and DAQ card specifications summarized in Table 4. The maximum sampling

rate using internal timers for the NI 9234 was 51 kHz whereas the maximum frequency range was only 0.5-10 kHz for the sensor. Due to the limitations of the sensor all data were sampled at 10.2 kHz. BNC cables were used in connecting the sensors to the NI DAQ card, for all data in this study the tachometer (Figure 12) was connected to Channel 0, the sensor mounted to the gear box (Figure 13) was connected to Channel 1, the top mounted bearing sensor was connected to Channel 2 and the side mounted bearing sensor was connected to Channel 3 (Figure 14).

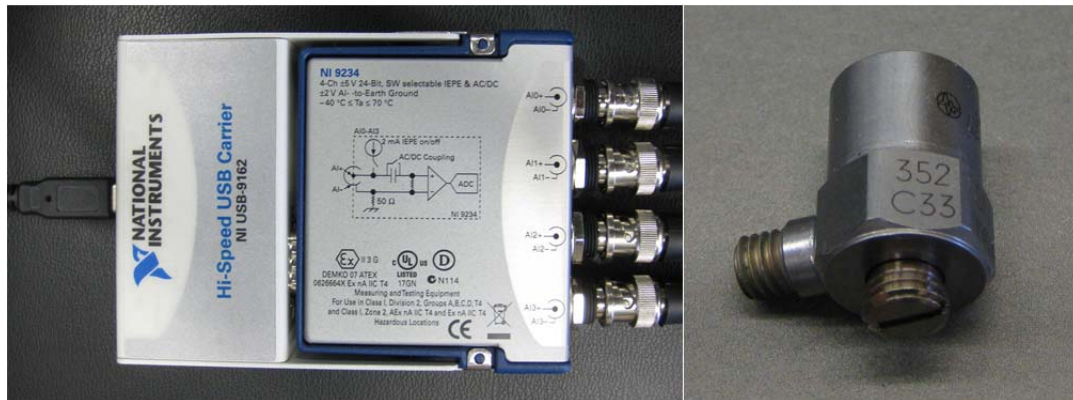


Figure 11: Data Acquisition Card and Sensor

Table 3: PCB 352-C33 Accelerometer Specifications

Sensitivity ($\pm 10\%$)	100 mV/g
Measurement Range	± 50 g pk
Frequency Range ($\pm 5\%$)	0.5 to 10000 Hz
Frequency Range ($\pm 10\%$)	0.3 to 15000 Hz
Resonant Frequency	≥ 50 kHz
Broadband Resolution (1)	0.00015 g rms
Non-Linearity	$\leq 1\%$
Transverse Sensitivity	$\leq 5\%$

Table 4: NI 9234 DAQ Card Specifications

Number of Channels	4
ADC Resolution	24 bit
Input Range	± 5 V
Sampling Mode	Simultaneous
Data Range Min (Internal Master Time Base)	1.652 kS/s
Data Range Max (Internal Master Time Base)	51.2 kS/s

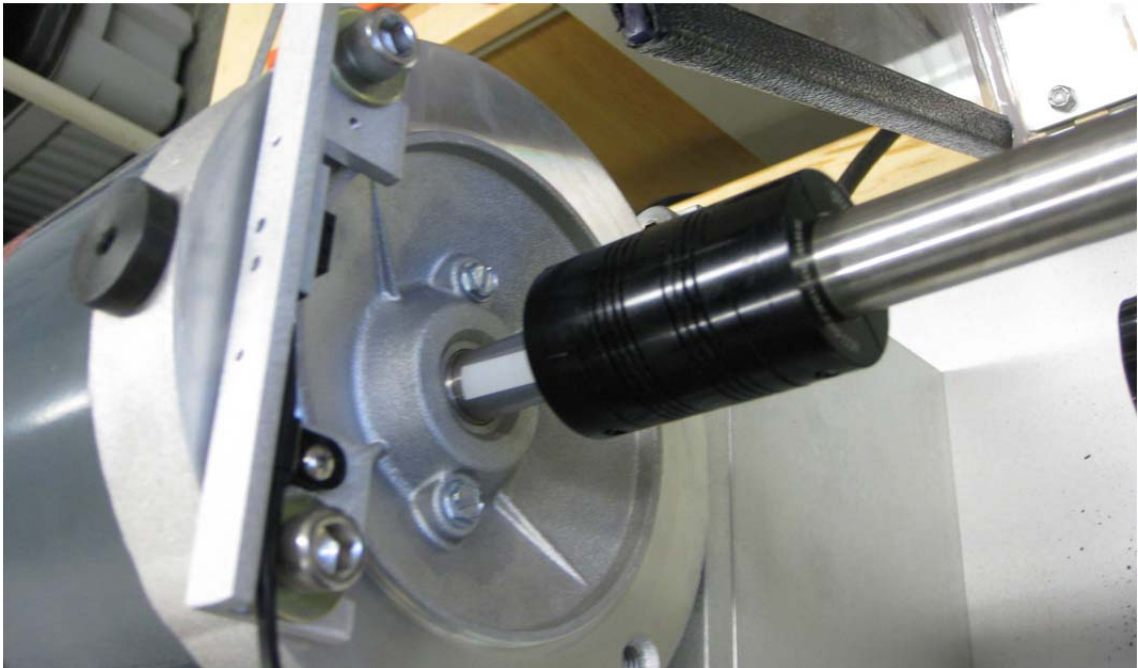


Figure 12: Tachometer Sensor Location (Channel 0)



Figure 13: Gear Box Sensor Location (Channel 1)

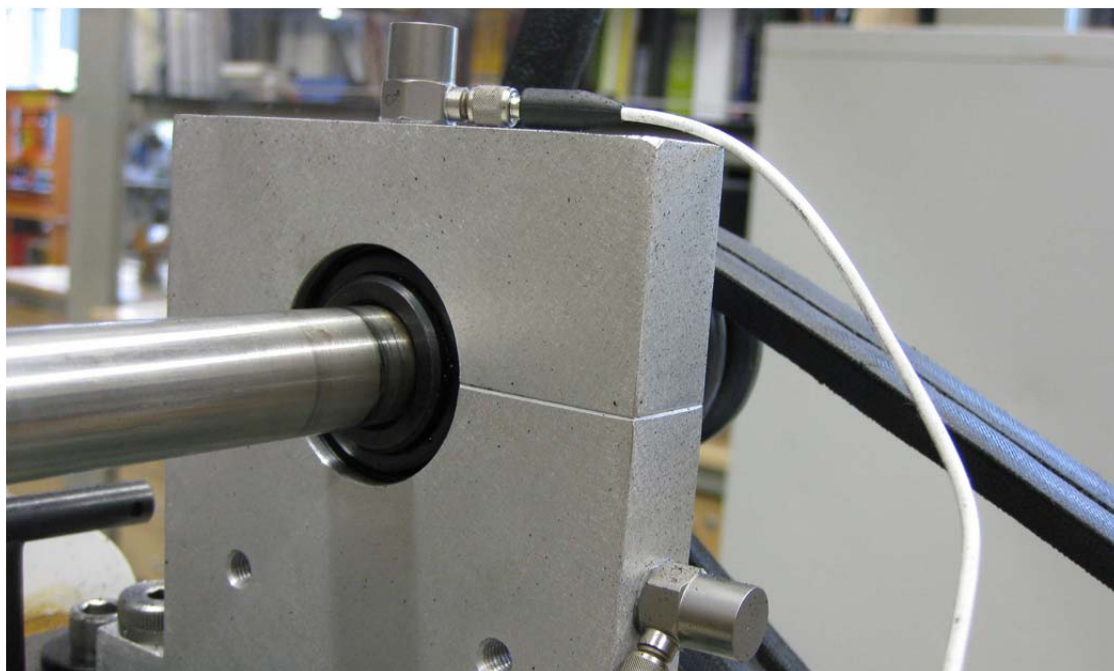


Figure 14: Bearing Sensor Location (Channels 2-3)

After connecting the sensors to the NI card, a USB cable was used to connect the NI card was connected computer. A MATLAB program developed by a colleague Dustin Harvey was used to collect data from the testbed during operation.

3.2.3. Description of System States

During the course of this study a number of data sets were collected over several days in some cases and others were taken in 1 hour sessions depending on what purpose each set served. Two procedures were used for the collection of data. The first procedure used for collecting the preliminary data sets (1-9) was not as formalized in an attempt to let environmental variability occur in the process and observe how that variability manifested itself in the data. The second procedure used was a more formalized procedure in an attempt to reduce environmental variability associated with assembly and breakdown. The various states collected for use in this study are summarized in Table 5.

Table 5: System States for Data Sets

State Number	Main Shaft Bearing	Damage Indicator	Damage Type	Main Shaft Speed (RPM)	Belt Tension (BT)	Break Torsion (TOR)	Number of Trials
1	Fluid	0	BASE	1	~MID	1	256
2	Fluid	1	WT	1	~MID	1	256
3	Fluid	0	BASE	2	~MID	1	256
4	Fluid	1	WT	2	~MID	1	256
5	Ball	0	BASE	1	~MID	1	256
6	Ball	1	BBB	1	~MID	1	256
7	Ball	1	BBB	1	~HIGH	1	192
8	Ball	1	BBO	1	~MID	1	256
9	Ball	1	BBOV	1	~MID	1	256
10	Ball	0	BASE	1	2	1	128
11	Ball	0	BASE	1	4	1	128
12	Ball	0	BASE	1	4	3	128
13	Ball	0	BASE	1	4	5	128
14	Ball	0	BASE	2	4	1	256
15	Ball	1	BBB	1	2	1	128
16	Ball	1	BBB	1	4	1	128
17	Ball	1	BBI	1	2	1	128
18	Ball	1	BBI	1	4	1	128
19	Ball	1	BBO	1	2	1	128
20	Ball	1	BBO	1	4	1	128
21	Ball	1	WT	1	4	1	128
22	Ball	1	WT	1	4	3	128
23	Ball	1	WT	1	4	5	128

State 1 consisted of 256 trials and was a baseline condition to be used for supervised learning. The main shaft was supported by fluid film bearings and its speed was monitored using a tachometer. The main shaft speed was approximately 1000 RPM or 16.7 Hz. The belt tension was set to an approximated medium tension level and the magnetic brake was set to apply 2lb-in of tension to the undamaged gear box pinion. Testing procedure 1 was used for the data collection.

State 2 consisted of 256 trials and was a damage gear box condition to be used for supervised learning. The main shaft was supported by fluid film bearings and its speed was monitored using a tachometer. The main shaft speed was approximately 1000 RPM or 16.7 Hz. The belt tension was set to an approximated medium tension level and the magnetic brake was set to apply 2lb-in of tension to a gear box pinion. The gear box here suffered from worn teeth. Testing procedure 1 was used for the data collection.

State 3 consisted of 256 trials and was a baseline condition to be used for supervised learning. The main shaft was supported by fluid film bearings and its speed was monitored using a tachometer. The main shaft speed was approximately 2000 RPM or 33.3 Hz. The belt tension was set to an approximated medium tension level and the magnetic brake was set to apply 2lb-in of tension to the undamaged gear box pinion. Testing procedure 1 was used for the data collection.

State 4 consisted of 256 trials and was a damage gear box condition to be used for supervised learning. The main shaft was supported by fluid film bearings and its speed was monitored using a tachometer. The main shaft speed was approximately 1000 RPM or 16.7 Hz. The belt tension was set to an approximated medium tension level and the magnetic brake was set to apply 2lb-in of tension to a gear box pinion. The gear box here suffered from worn teeth. Testing procedure 1 was used for the data collection.

State 5 consisted of 256 trials and was a baseline condition to be used for supervised learning. The main shaft was supported by ball bearings and its speed was monitored using a tachometer. The main shaft speed was approximately 1000 RPM or 16.7 Hz. The belt tension was set to an approximated medium tension level and the magnetic brake was set to apply 2lb-in of tension to an undamaged gear box pinion. Testing procedure 1 was used for the data collection.

State 6 consisted of 256 trials and was a damaged main shaft ball bearing condition to be used for supervised learning. The main shaft was supported by a damaged ball bearing with a ball fault and its speed was monitored using a tachometer. The main shaft speed was approximately 1000 RPM or 16.7 Hz. The belt tension was set to an approximated medium tension level and the magnetic brake was set to apply 2lb-in of tension to an undamaged gear box pinion. Testing procedure 1 was used for the data collection.

State 7 consisted of 192 trials and was a damaged main shaft ball bearing condition to be used to examine the effects of an overly tensioned belt drive. The main shaft was supported by a damaged ball bearing with a seeded ball fault and its speed was monitored using a tachometer. The main shaft speed was approximately 1000 RPM or 16.7 Hz. The belt tension was set to an approximated high tension level and the magnetic brake was set to apply 2lb-in of tension to an undamaged gear box pinion. Testing procedure 1 was used for the data collection.

State 8 consisted of 256 trials and was a damaged main shaft ball bearing condition to be used for supervised learning. The main shaft was supported by a damaged ball bearing with a seeded outer race fault and its speed was monitored using a tachometer. The outer race fault position in this case was constant and located closest to the Channel 3 bearing sensor. The main shaft speed was approximately 1000 RPM or 16.7 Hz. The belt tension was set to an approximated medium tension level and the magnetic brake was set to apply 2lb-in of tension to an undamaged gear box pinion. Testing procedure 1 was used for the data collection.

State 9 consisted of 256 trials and was a damaged main shaft ball bearing condition to be used to examine the effect of varying position of an outer race fault in

relation to the sensor and load. The main shaft was supported by a damaged ball bearing with a seeded outer race fault and its speed was monitored using a tachometer. After every 32 trials the bearing was disassembled and reassembled with not particular attention being made as to the position of the where the fault was located in relation to the sensors or the loading of the shaft. The main shaft speed was approximately 1000 RPM or 16.7 Hz. The belt tension was set to an approximated medium tension level and the magnetic brake was set to apply 2lb-in of tension to an undamaged gear box pinion. Testing procedure 1 was used for the data collection.

States 1-9 were collected using testing procedure 1 and after examination of the performance of the damage features, it was notices that there was a considerable amount of variability in the damage feature statistical distributions. As such a new testing procedure was developed to reduce variability that may be cause due to maintenance issues such as the dismantling of the various damaged components and reassembly as was done in the preliminary results. By reducing this variability it was hoped that the distributions of the damage features would become less spread out and the variability due to torsional load and belt tension could be singled out. States 10-24 used the second testing procedure described in 3.2.4 Testing Procedures.

State 10 consisted of 128 trials and was a baseline condition to be used for supervised learning of low tensioned belt drive. The main shaft was supported by ball bearings and its speed was monitored using a tachometer. The main shaft speed was approximately 1000 RPM or 16.7 Hz. The belt tension was set using a deflection force of 2 lbs. for 13/64" of an inch deflection and the magnetic brake was set to apply 2lb-in of tension to the undamaged gear box pinion. Testing procedure 2 was used for the data collection.

State 11 consisted of 128 trials and was a baseline condition to be used for supervised learning of low torsional load on the gear box. The main shaft was supported by ball bearings and its speed was monitored using a tachometer. The main shaft speed was approximately 1000 RPM or 16.7 Hz. The belt tension was set to the recommended value using a deflection force of 4 lbs. for 13/64" of an inch deflection and the magnetic brake was set to apply 2lb-in of tension to the undamaged gear box pinion. Testing procedure 2 was used for the data collection.

State 12 consisted of 128 trials and was a baseline condition to be used for supervised learning of medium torsional load on the gear box. The main shaft was supported by ball bearings and its speed was monitored using a tachometer. The main shaft speed was approximately 1000 RPM or 16.7 Hz. The belt tension was set to the recommended value using a deflection force of 4 lbs. for 13/64" of an inch deflection and the magnetic brake was set to apply 6lb-in of tension to the undamaged gear box pinion. Testing procedure 2 was used for the data collection.

State 13 consisted of 128 trials and was a baseline condition to be used for supervised learning of high torsional load on the gear box. The main shaft was supported by ball bearings and its speed was monitored using a tachometer. The main shaft speed was approximately 1000 RPM or 16.7 Hz. The belt tension was set to the recommended value using a deflection force of 4 lbs. for 13/64" of an inch deflection and the magnetic brake was set to apply 10lb-in of tension to the undamaged gear box pinion. Testing procedure 2 was used for the data collection.

State 14 consisted of 256 trials and was a baseline condition to be used for supervised learning of low torsional load on the gear box at higher speeds. The main shaft was supported by ball bearings and its speed was monitored using a tachometer.

The main shaft speed was approximately 2000 RPM or 33.3 Hz. The belt tension was set to the recommended value using a deflection force of 4 lbs. for 13/64" of an inch deflection and the magnetic brake was set to apply 2lb-in of tension to the undamaged gear box pinion. Testing procedure 2 was used for the data collection.

State 15 consisted of 128 trials and was a damaged condition to be used for supervised learning ball fault bearing failure at low belt tension. The main shaft was supported by ball bearings and its speed was monitored using a tachometer. The main shaft speed was approximately 1000 RPM or 16.7 Hz. The belt tension was set to the low setting value using a deflection force of 2 lbs. for 13/64" of an inch deflection and the magnetic brake was set to apply 2lb-in of tension to the undamaged gear box pinion. Testing procedure 2 was used for the data collection.

State 16 consisted of 128 trials and was a damaged condition to be used for supervised learning ball fault bearing failure at recommended belt tension. The main shaft was supported by ball bearings and its speed was monitored using a tachometer. The main shaft speed was approximately 1000 RPM or 16.7 Hz. The belt tension was set to the recommended setting value using a deflection force of 4 lbs. for 13/64" of an inch deflection and the magnetic brake was set to apply 2lb-in of tension to the undamaged gear box pinion. Testing procedure 2 was used for the data collection.

State 17 consisted of 128 trials and was a damaged condition to be used for supervised learning inner race ball bearing failure at low belt tension. The main shaft was supported by ball bearings and its speed was monitored using a tachometer. The main shaft speed was approximately 1000 RPM or 16.7 Hz. The belt tension was set to the low setting value using a deflection force of 2 lbs. for 13/64" of an inch deflection

and the magnetic brake was set to apply 2lb-in of tension to the undamaged gear box pinion. Testing procedure 2 was used for the data collection.

State 18 consisted of 128 trials and was a damaged condition to be used for supervised learning inner race ball bearing failure at recommended belt tension. The main shaft was supported by ball bearings and its speed was monitored using a tachometer. The main shaft speed was approximately 1000 RPM or 16.7 Hz. The belt tension was set to the recommended setting value using a deflection force of 4 lbs. for 13/64" of an inch deflection and the magnetic brake was set to apply 2lb-in of tension to the undamaged gear box pinion. Testing procedure 2 was used for the data collection.

State 19 consisted of 128 trials and was a damaged condition to be used for supervised learning outer race ball bearing failure at low belt tension. The main shaft was supported by ball bearings and its speed was monitored using a tachometer. The main shaft speed was approximately 1000 RPM or 16.7 Hz. The belt tension was set to the low setting value using a deflection force of 2 lbs. for 13/64" of an inch deflection and the magnetic brake was set to apply 2lb-in of tension to the undamaged gear box pinion. Testing procedure 2 was used for the data collection.

State 20 consisted of 128 trials and was a damaged condition to be used for supervised learning outer race ball bearing failure at recommended belt tension. The main shaft was supported by ball bearings and its speed was monitored using a tachometer. The main shaft speed was approximately 1000 RPM or 16.7 Hz. The belt tension was set to the recommended setting value using a deflection force of 4 lbs. for 13/64" of an inch deflection and the magnetic brake was set to apply 2lb-in of tension to the undamaged gear box pinion. Testing procedure 2 was used for the data collection.

State 21 consisted of 128 trials and was a baseline condition to be used for supervised learning of low torsional load on a damaged gear box. The main shaft was supported by ball bearings and its speed was monitored using a tachometer. The main shaft speed was approximately 1000 RPM or 16.7 Hz. The belt tension was set to the recommended value using a deflection force of 4 lbs. for 13/64" of an inch deflection and the magnetic brake was set to apply 2lb-in of tension to the damaged gear box pinion with worn gears. Testing procedure 2 was used for the data collection.

State 22 consisted of 128 trials and was a baseline condition to be used for supervised learning of medium torsional load on a damaged gear box. The main shaft was supported by ball bearings and its speed was monitored using a tachometer. The main shaft speed was approximately 1000 RPM or 16.7 Hz. The belt tension was set to the recommended value using a deflection force of 4 lbs. for 13/64" of an inch deflection and the magnetic brake was set to apply 6lb-in of tension to the damaged gear box pinion with worn gears. Testing procedure 2 was used for the data collection.

State 23 consisted of 128 trials and was a damaged condition to be used for supervised learning of high torsional load on the damaged gear box. The main shaft was supported by ball bearings and its speed was monitored using a tachometer. The main shaft speed was approximately 1000 RPM or 16.7 Hz. The belt tension was set to the recommended value using a deflection force of 4 lbs. for 13/64" of an inch deflection and the magnetic brake was set to apply 10lb-in of tension to the undamaged gear box pinion. Testing procedure 2 was used for the data collection.

3.2.4. Testing Procedures

The two testing procedures used in the collection of data for this study are discussed in further detail here. In system states 1-9 the testing procedure used was

designed to be informal and allow environmental variability into the data. The second testing procedure was designed to reduce random environmental variability by not swapping components between tests and quantifying belt tension and torsional load.

Though designed to be informal, basic guidelines were established for the first procedure. Several parameters were always kept constant during the preliminary data collection for states 1-9. The first parameter kept constant was the location of the sensors. The tachometer was always positioned directly above the main shaft and monitored the main shaft rotational speed. The accelerometers monitoring the vibration signals were always mounted at the same locations and in the same way. Channel 1 was always mounted on top of the gear box, Channel 2 was always mounted on the top of the second main bearing housing closest to the gear box and belt drive, and Channel 3 was always positioned to the side of the main shaft bearing housing closest to the gear box and belt drive. The accelerometers were always mounted in the same fashion, using stud mounting with a wax film to provide good contact between the bottom of the accelerometer and the surface of the testbed, then hand tightened.

During the course of a trial set using testing procedure 1, the machine fault simulator was allowed to warm up at the desired speed for the experiment for a period of ten minutes before any data were collected. Data were collected using the seDAQ program a single set at a time by hand and the time interval between each instance varied. The sets were always collected in groups of 32 instances and total time of collection could range anywhere from 30-45 minutes. The trial sets of 32 instances later were concatenated to produce a larger state set.

In between trial sets there involved a large amount of modification to the fault simulator. In the case of gear box fault sets, the worn tooth and baseline gear boxes

were two separate gearboxes, between each set the belt drive had to be loosened and belts removed. Then the gearbox was unfastened and removed, there was only one large sheave so that too had to be removed and swapped to the new gear box for the next set. When replacing the gear box the belt drive had to be tensioned with an approximated level of tension using a ruler and estimated feel of the force being applied.

In the case of bearing damage trial sets, the belt drive again had to be loosened and removed, the bearing housing was dismantled, and bearings removed to be swapped with a new bearing. Once the new bearing was replaced, the belts were put back in place and re-tensioned using the same approximated method as was done for gear box trial sets.

For States 10-24 the amount of variability due to dismantling and moving around components was undesirable due to the fact that the purpose of the experiments was to study the effect of varying mechanical states such as torsional load and belt tension, not variability due to maintenance and repairs. As such the procedure was changed from testing procedure 1. The program seDAQ was modified to change the way each instance of the state was collected. Each instance was no longer collected at varying time intervals but instead was collected at specified times controlled by the computer's internal clock.

Between each state set the system was allowed first to run for ten minutes before the first trial set of 32 instances were collected. Trial set were spaced at 10 minutes apart and each instance of a trial set was spaced at 5 seconds apart. State sets were collected in groups of 4 trial sets and during this time the machine never stopped and no components were altered by swapping parts, changing the torsional load or belt tension.

The method for determining belt tension was also changed to reduce any variability associated with the approximated method using feel and a ruler. Here in procedure 2 a belt tension tester was used which measured the force applied to the belt for a given deflection. The manufacturer of the belts provided recommended deflection to force ratios for specified belts and span lengths to achieve recommended belt tensions. In the case of low belt tension system states the force was reduced by half for the same deflection. To change the torsional loads two screws on the magnetic break needed to be loosened, the break was rotated to a clearly marked setting and the screws were retightened.

3.2.5. Sources of Variability

There were a number of sources of variability in the system. One major contributing factor of variability was the substitution of damaged and undamaged components between the collections of data sets. The substitution of these components effected belt tension and caused it to change on a case by case basis. Changing the gearbox and the sheaves also led to slight changes in the way that the belts were lined up. Procedures were used to insure the belt drive was orientated in the correct manner, but slight changes from its previous position was unavoidable and suspected to be a contributing factor to variability in the statistical distributions of the damage features.

Variability due to operational conditions was also observed. The belt tension tended to loosen during operation as the belt heated up during longer runtimes. The force applied for a deflection of 13/64 inches was typically a pound less than it was at the start of a trial for the longer runs. The speed of the main shaft also varied over the course of a data collection session. Though the motor controller was set to a constant power level, the RPM of the main shaft fluctuated by roughly 1-2 RPM.

3.3. Statistical Modeling and Detection Performance

To better understand the results section a brief overview of how the damage features performance was compared is explained here. The damage features were computed using some of the recommended techniques in the literature, but their values would vary for every measurement of the signal as the environment changed. The purpose of the various states that were explained earlier was to see how the different states affected the statistics of the damage features. A good damage feature is one that detects a specific condition of the system and whose value does not change excessively under potential changes in the environment except for changes that indicate the damage it was designed to detect (“statistical specificity”). In order to quantify the ability to detect this damage receiver operating characteristics (ROC) curves were used.

3.3.1. Hypothesis Testing & Receiver Operating Characteristic Curves

In order to generate an ROC curve first a null hypothesis needs to be made. For the results presented the hypotheses answered the question of is there damage present. Two hypotheses were possible as the data were trained on a binary case where a baseline state was always compared with a known damage states under different environmental conditions. The hypotheses were determined by an automated algorithm where the means of the statistics for the baseline data set and the damaged data set. Then using this knowledge a hypothesis could be made.

When the mean of the damage feature was larger than the mean of the baseline feature, the hypothesis leading to the best probability of detection was that damage was present if the feature value was larger than a specified threshold (Figure 15). When the mean of the baseline damage features was greater than the mean of the damage features, the hypothesis was made that damage was present if the feature values were less than

some specified threshold (Figure 16). Two visualizations of the different hypothesis are presented in the figures below where the green is representative of a baseline damage features distribution and the red a damaged features distribution.

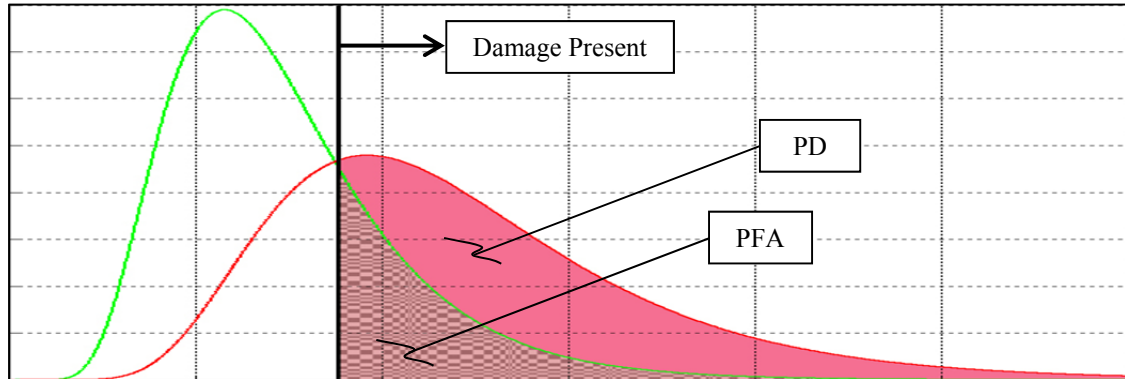


Figure 15: Example of hypothesis for damage feature mean greater than baseline feature mean.

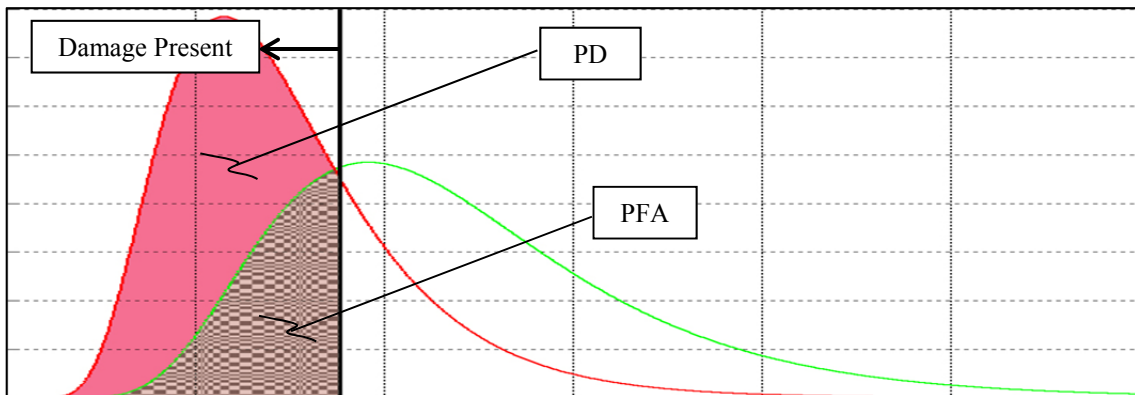


Figure 16: Example of hypothesis for damage feature mean less than baseline feature mean.

With a known hypothesis and known distributions for the damage features it is possible to generate an ROC curve. ROC curves provide information on the probability of false alarm (PFA) verse the probability of detection (PD) for varying thresholds. The PFA can be defined as the probability that an undamaged system may generate feature

values that would indicate damage, or that a damaged system may generate values that would not indicate damage for a given hypothesis.

In the case of the experiments, the analytical distributions were unknown; as such no analytical ROC curves could be generated. In order to generate the ROC curves, an empirical method was used. As mentioned earlier the hypotheses were made based on the mean values of known damaged and undamaged states under the same environmental conditions. After a hypothesis was established a threshold was moved along the range of features values and the number of feature values that generated false alarms were counted and plotted against the number of feature values which indicated damage by satisfying the hypothesis made. In this way the performance of the damage features could be quantified and compared to each other.

When reading an ROC curve plot the best performing damage feature is the one with the greatest PD to PFA. Features with distributions that have less variance and greater separation in their means give the best performance. The ROC curves of the better performing damage features will tend to shift to the upper right corner of the plots which is representative of higher PD to PFA ratios. When the features tend to be poor performers due to little distinction in the statistics of the distributions the performance will be close to a straight line that runs from one corner of the plot to the other. This line is the 50/50 line whose performance is no better than a coin toss. In Figure 17 ROC plots were generated for 5 hypothetical features. The features were of Gaussian distribution for both damaged and undamaged states. The separation in the means between the damaged and undamaged conditions for the five features was increased by a factor of 1 for every feature starting at 0. From the ROC curve it can clearly be seen that features with large separation in statistics between the damaged and undamaged

condition move to the upper right of the ROC plot as was the case with Feature 5. For Feature 1, the distributions were exactly the same and little information is available to distinguish the system as being damaged or undamaged.

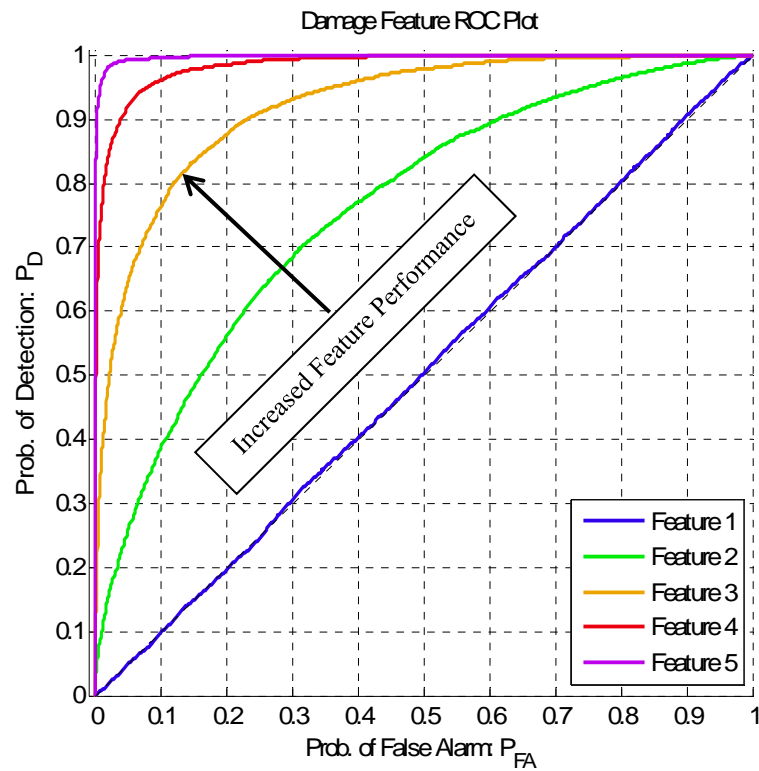


Figure 17: Example ROC curves for Gaussian Distributions with increasing separation of means.

For certain distributions types, the ROC curves generated from using a single moving threshold may generate abnormal ROC curves. Such distributions include bi-modal distributions or distributions with the same mean and different variances (Figure 18). In the case of the bi-modal damage state distribution compared to the single mode distribution, the ROC curve begins to develop an S shape curve. This same ROC curve shape can be seen in the case of two distributions with the same mean but differing variances (Figure 19). When establishing hypotheses from these distribution types a

multi threshold approach should be used in the hypothesis test. One approach would be to hypothesize that damage is present given the feature value is not within a certain range between two thresholds. This range can then be increased to provide a ROC curve for that feature.

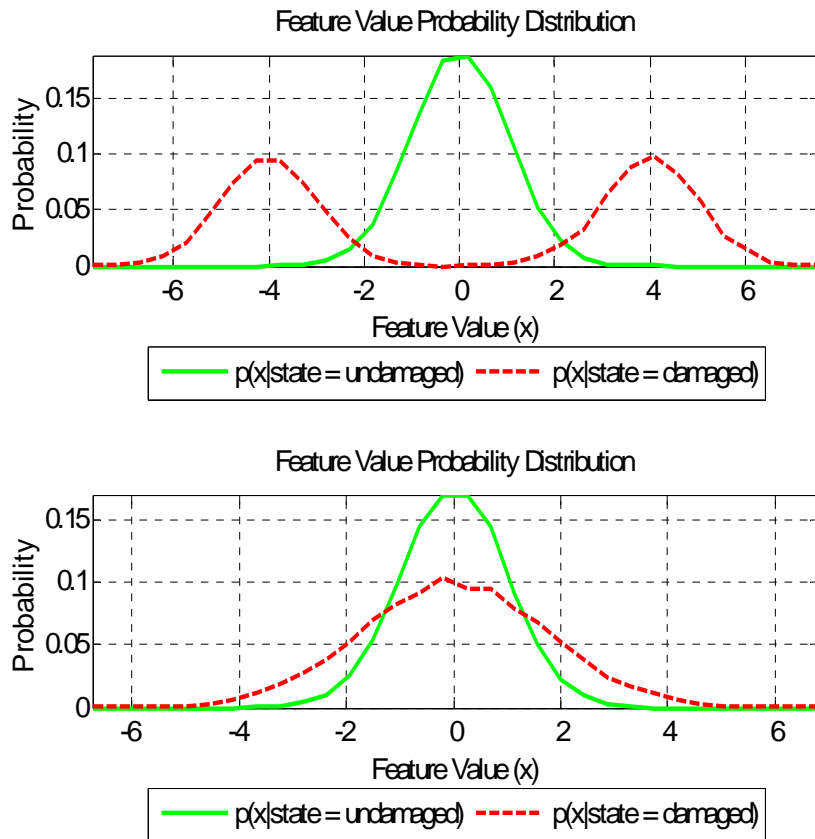


Figure 18: Hypothetical bi-modal (top) and changing variance (bottom) damage distributions.

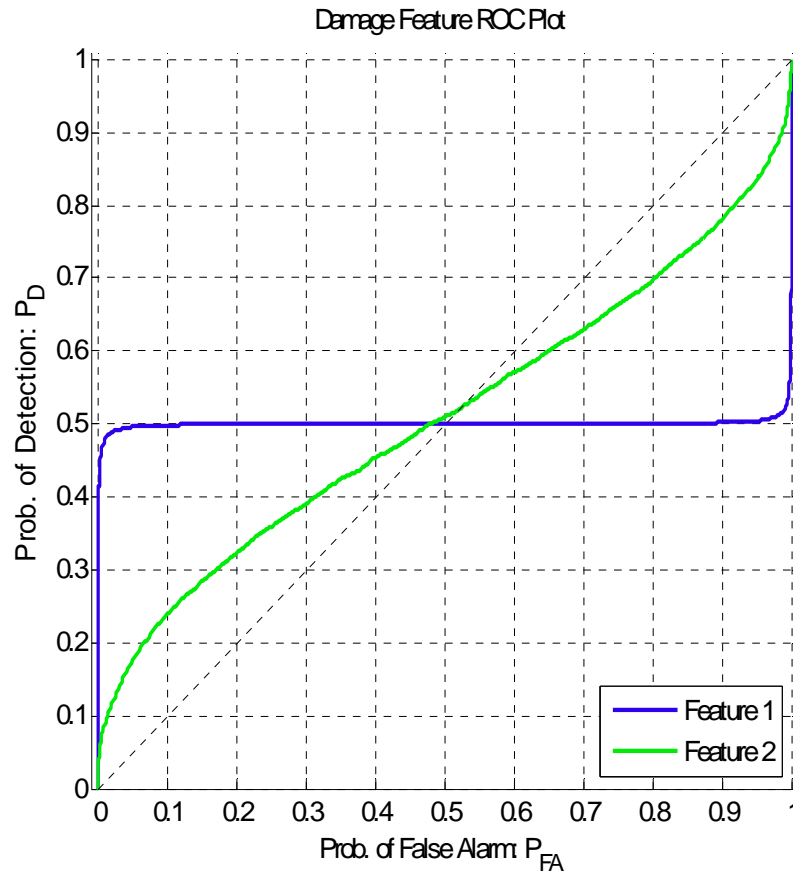


Figure 19: ROC curves of bi-modal damaged distribution (Feature 1) and changing variance damaged distributions (Feature 2).

Depending on the cost of a false alarm vs. the cost of detection, thresholds can be determined and implemented in a CBM system. In the absence of any cost functions for a particular application, the area under the curve (AUC) of an ROC curve is often used as a means of evaluating machine learning algorithms using a scalar metric [55]. The AUC is computed by integrating the ROC curve over the total PFA range. Damage features with better statistical performance will have AUC values closer to 1 whereas poor performing damage features will have a value closer to 0.5. Damage features with an AUC value less than 0.5 indicate a poor choice in hypothesis. In the case that the

AUC is less than 0.5 swapping the hypothesis would regain any statistical advantage in the damage features ability to detect damage. The calculation of the AUC for empirical data can be performed by two methods. One method involves fitting a polynomial to the ROC data and integrating along the polynomial. A more direct method involves using trapezoidal integration. In the case of this study the trapezoidal method was used for computing the AUC of all ROC curves.

3.4. Testing Results

A number of tests were performed to determine the effects that varying system states had on damage feature detection performance. Testing procedures and system states were mentioned in previous sections and the results of traditional damage features will be discussed further in this section. Preliminary results are provided which compared damage feature detection performance under a number of different damage classes as well as how different system parameter affected their performance. Two types of damage were examined and included worn tooth damage in the gearbox, ball fault damage in the main shaft bearing and outer race fault in the main shaft. DAQ limitation will dictate signal parameters like sampling frequency and signal length. The performance of worn tooth damage features were examined under varying signal parameters that consisted of sampling frequency and number of revolutions present in the angular resampled signal. Operational parameters also had an effect on damage detection performance for worn tooth damage. The effect to damage detection performance caused by increased shaft speed for worn tooth damage detection is also examined. The performance of bearing damage detection was examined for ball fault bearing damage and outer race bearing damage. Ball fault bearing damage was

examined under medium belt tension and high belt tension. Outer race bearing fault damage detection was examined when the fault location was randomized and unknown as well as having a constant position relative to the tension load of the belt.

Because the preliminary results showed there was a lot of variability in the power spectra from trial to trial. Subsequent test were performed that minimized the variability associated with substituting parts with different damage classifications and taking data in short sessions on multiple days in an attempt to identify the extent of variability caused by specified operational states. The effect of belt tension on bearing damage detection was examined further for three ball bearing faults: Inner Race, Outer race and Ball Fault. The affect torsional load had on detecting worn tooth damage and which damage features detection performance at alternate sensor locations on the structure was examined as well.

For all the results shown below the only parameters changed in the computation of damage features were the samples per revolution used in the angular resampling algorithm, the number of revolutions kept in the signal, the channel the data were collected from, and the data sets used in the computations; these are all labeled in the figure titles for clarity.

To compute the damage features the data were loaded and the mean values of the signals were removed giving them a zero DC value at zero frequency. The signals were then angular resampled at varying rates to see how the sampling rate would affect the results of the damage detectability. The following examples were not time synchronous averaged, as it was observed that this had a reduction of performance for the damage features in earlier experiments. For the power spectrum plots the power spectrums were computed for all the samples and the average power spectrum is

displayed for both the baseline conditions and damaged conditions. Once all features had been computed their distributions were plotted using box plots as the actual statistical distribution was unknown. Damaged classes were plotted in red and undamaged classes were plotted in green. ROC curves were plotted for each damage feature using empirical results and the area under the curve was calculated to provide a measure of total probability of detection. The values of the area under the curve are presented as green and red arrows to provide some knowledge of what hypotheses were used for the computation of the ROC curves. The determination of the null hypotheses used was an automated process determined by the mean of the damaged and undamaged features in relation to each other. Red arrows pointing down represented hypotheses of the structure was damaged given the feature value was lower than the specified threshold, whereas green arrows represented hypotheses of the structure was damaged given the feature value was greater than the threshold.

3.4.1. Worn Tooth Gearbox Damage Preliminary Results

In this section preliminary gear box system states are compared for a baseline and worn tooth damage cases to see how the power spectrums are affected by worn tooth gears during operation. It was desirable to see the performance of the damage features at varying signal lengths and sampling rates. Damage feature comparisons are also made at different operating speeds.

The frequency ranges of all power spectrum plots are marked by gear mesh harmonics. A value of one represents the fundamental meshing frequency which is 27 cycles per rotation of the gear shaft as the gear had 27 teeth. The fundamental meshing frequency is rarely present in all the experiments taken at 1000 RPM but does become more apparent at speeds of 2000 RPM. From looking at the PSD's of the damage cases

it is clear that the wearing of the gear teeth caused the frequency content to smear into other frequency bins and the peaks associated with the gear meshing begin to decay. There is more high frequency content in the undamaged case due to the contact shocks of the gear teeth meshing together, whereas in the case of the worn teeth more slipping occurs and there is less force per contact (Figure 20).

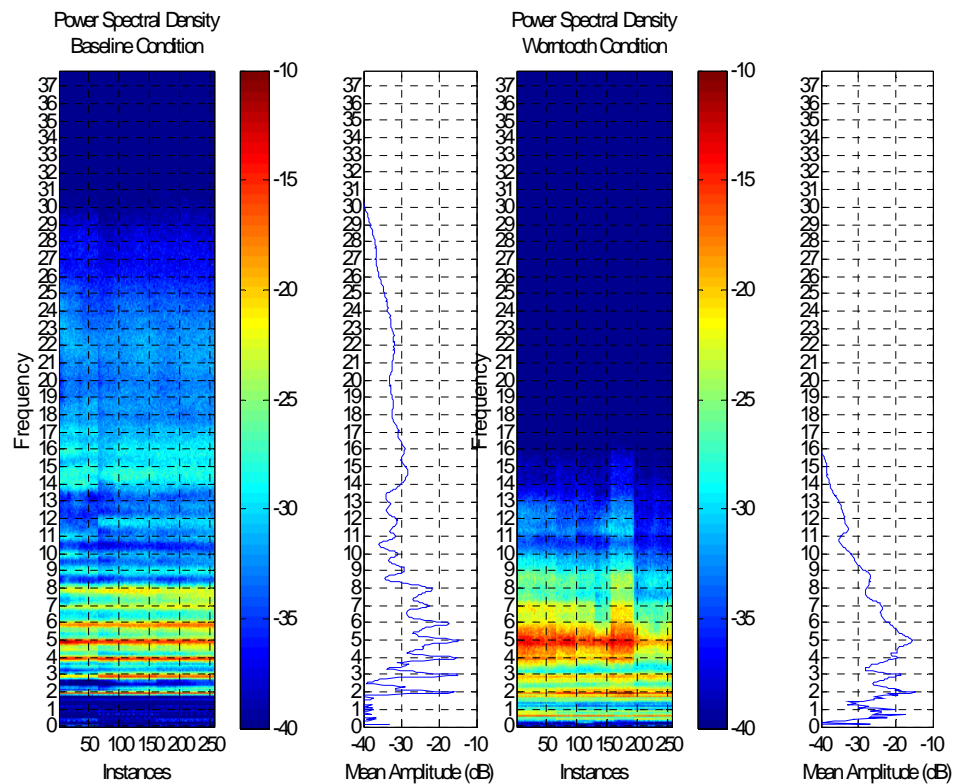


Figure 20: Trial Power Spectrums for Worn Tooth Damage @ 1000RPM, 2048 Samples per Revolution, Channel 1

The ROC curves for the damage features at a sampling rate of 2048 samples per revolution (Figure 22) showed that the dominant performing damage feature was FMH, followed by FM4 and M6A. These damage features had good separation of the damaged and undamaged distributions (Figure 21) giving them better detectability. The

number of revolutions used in the calculations of the damage features was reduced to only 4 revolutions. The damage feature distributions showed an increase in variance of the damaged and undamaged feature values when 4 revolutions were used (Figure 23). This increased variance caused a decrease in detection performance for damage features FM4, M6A and M8A observed from their ROC curves (Figure 24). The FMH damage feature continued to have good detection performance despite the reduction in signal length.

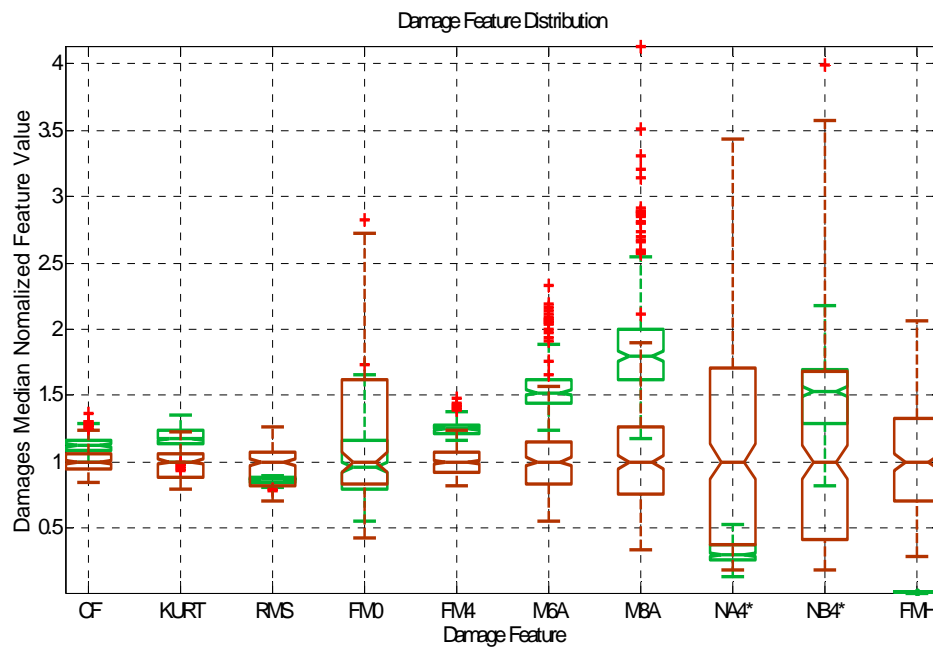


Figure 21: Damage Feature Distributions for Worn Tooth Damage @ 1000RPM, 2048 Samples per Revolution, 20 Revolutions, Channel 1

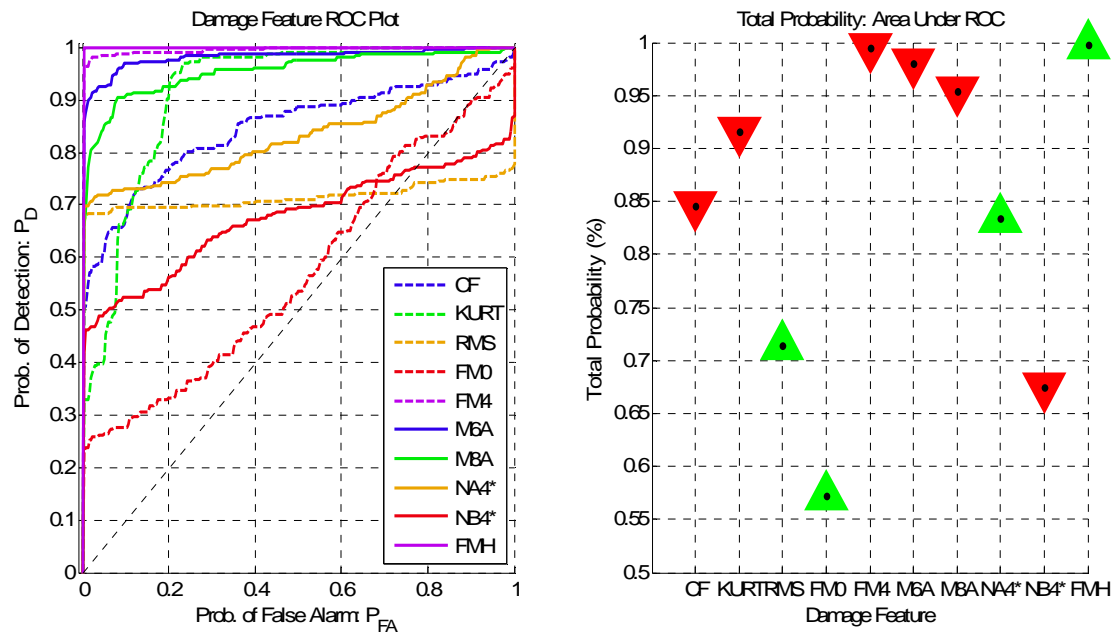


Figure 22: Damage Feature Statistical Performance for Worn Tooth Damage Detection @ 1000 RPM, 2048 Samples per Revolution, 20 Revolutions, Channel 1

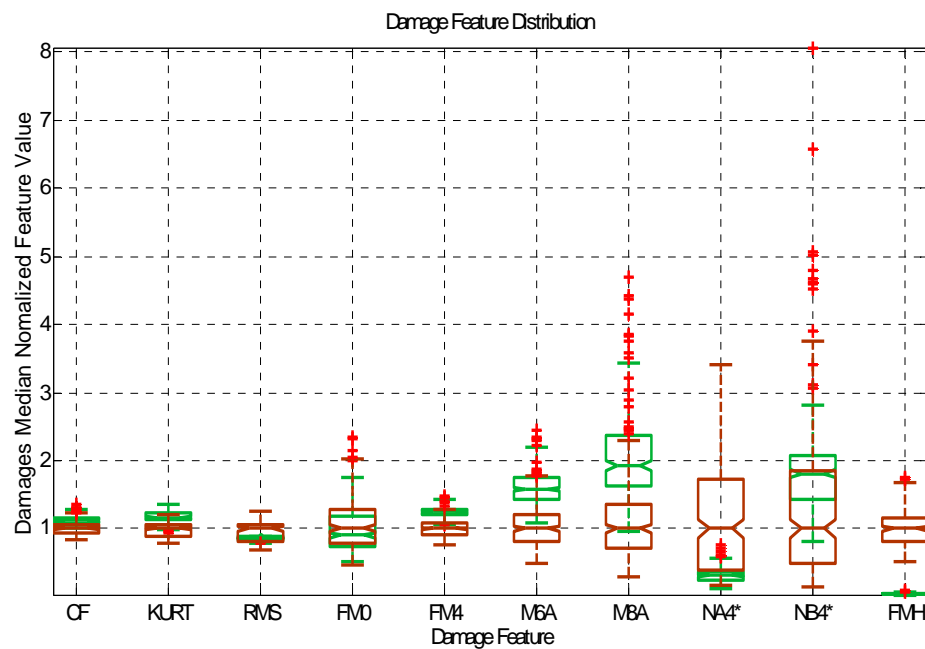


Figure 23: Damage Feature Distributions for Worn Tooth Damage @ 1000RPM, 2048 Samples per Revolution, 4 Revolutions, Channel 1

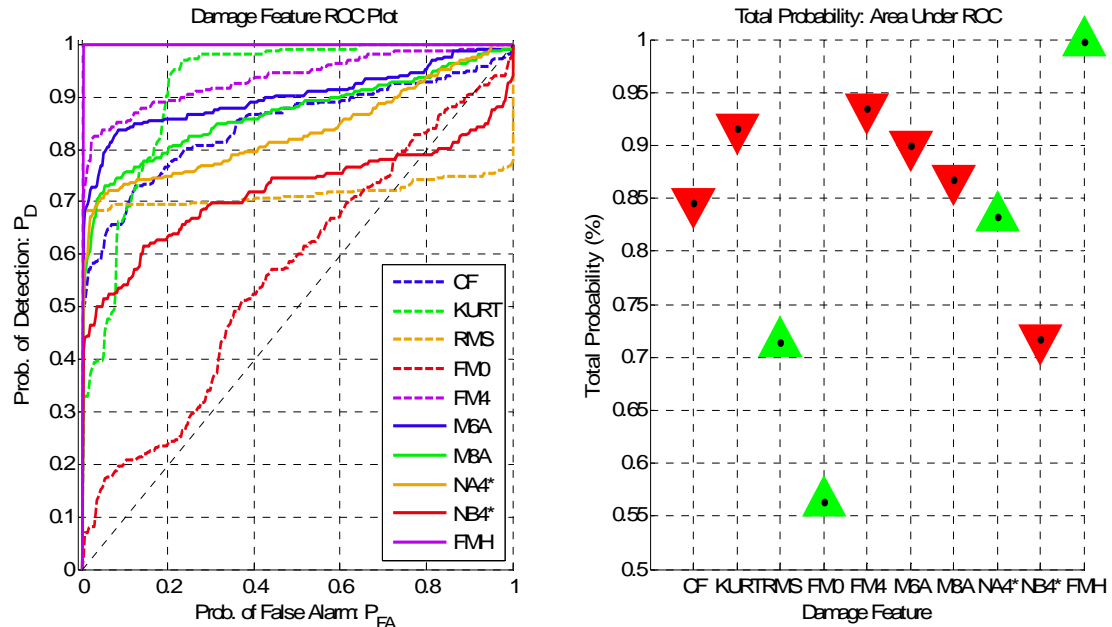


Figure 24: Damage Feature Statistical Performance for Worn Tooth Damage Detection @ 1000 RPM, 2048 Samples per Revolution, 4 Revolutions, Channel 1

The effect of reduced sampling rate on worn tooth damage detection performance was examined by first reducing the sampling rate to 512 samples per revolution. The PSD's of the trials (Figure 25) now only consisted up to 9 gear meshing orders but nothing appeared to change otherwise. The distributions of the damage features (Figure 26) showed overlap between most of the damaged and undamaged states. The ROC curves (Figure 27) showed that for a signal length of 20 revolutions sampled at 512 samples per revolution, most of the damage features suffered a reduction in performance compared to the features extracted from signals sampled at 2048 samples per revolution. The two damage features that did not suffer a performance loss were NA4* and FMH. When reducing the sampling frequency, NA4* had a large increase in performance and the FMH damage feature continued to perform well.

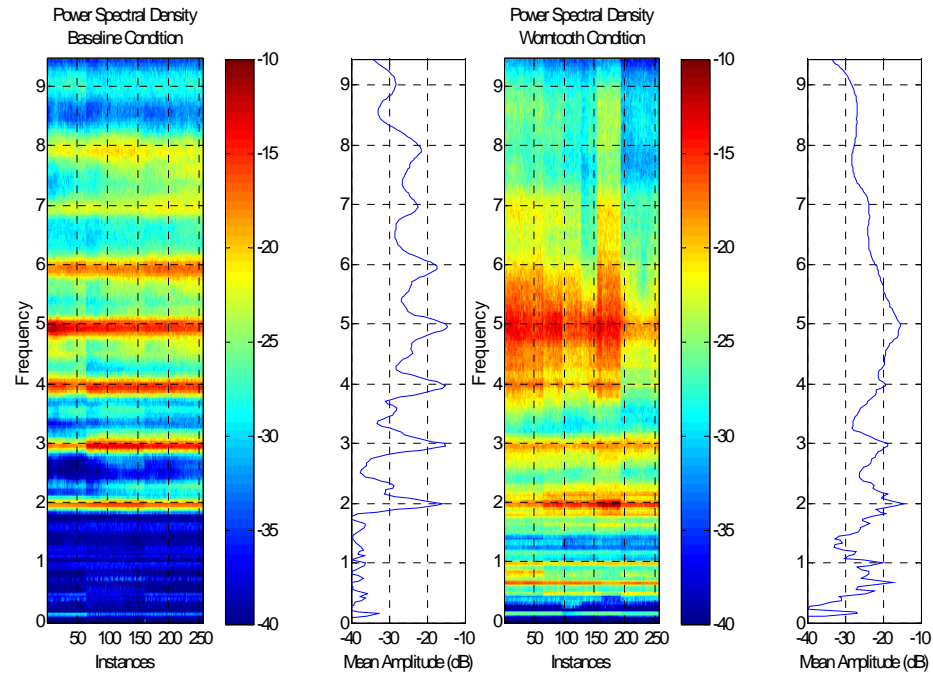


Figure 25: Worn Tooth Damage Power Spectrum @ 1000RPM, 512 Samples per Revolution, Channel 1

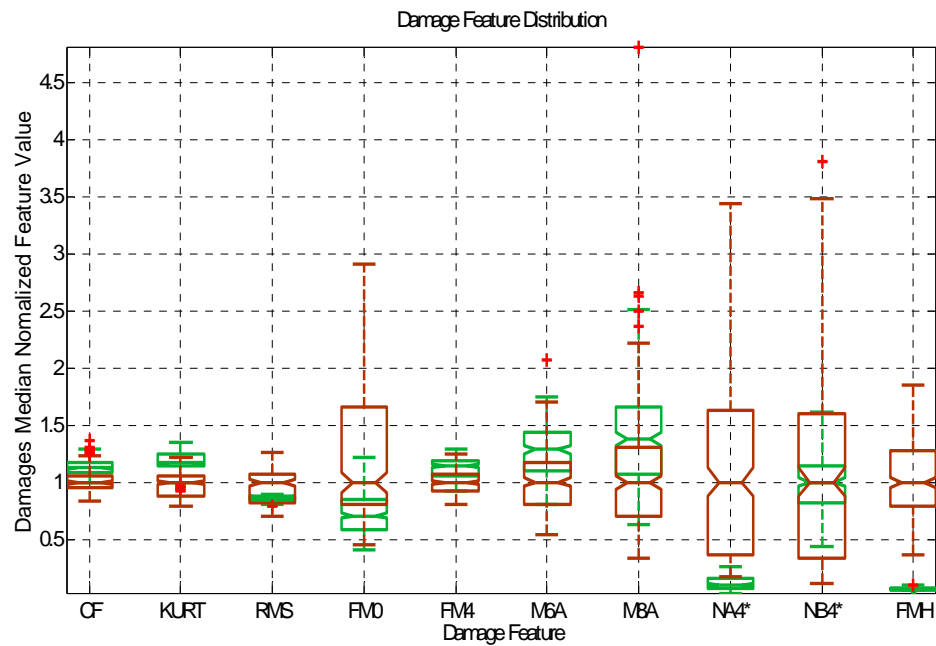


Figure 26: Damage Feature Distributions for Worn Tooth Damage @ 1000RPM, 512 Samples per Revolution, 20 Revolutions, Channel 1

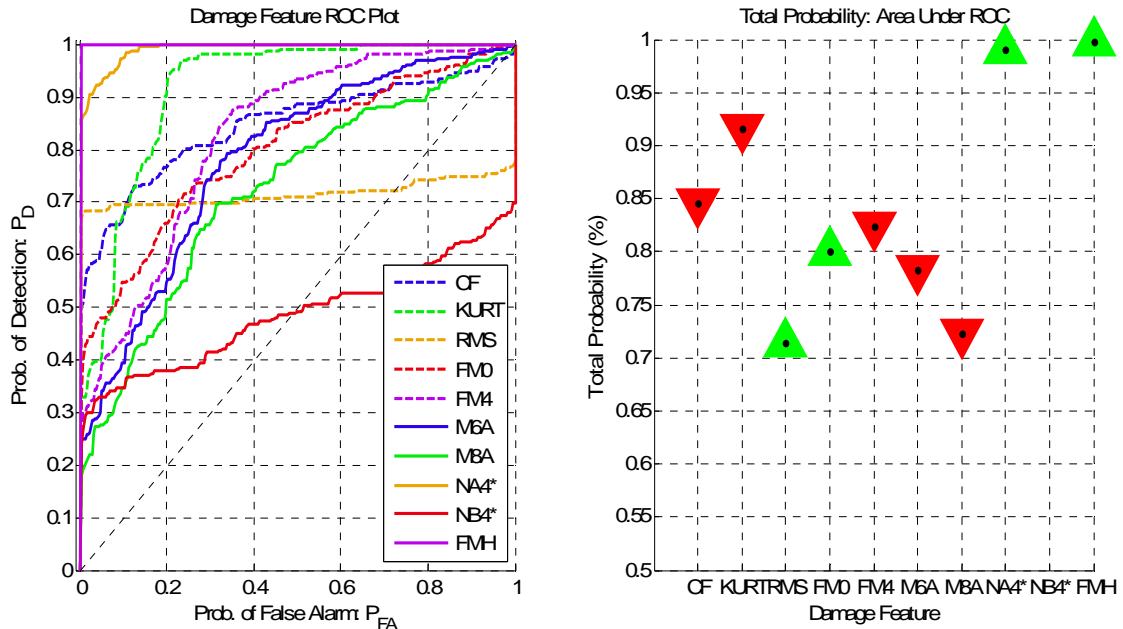


Figure 27: Damage Feature Statistical Performance for Worn tooth Damage Detection @ 1000 RPM, 512 Samples per Revolution, 20 Revolutions, Channel 1

Signals sampled at 512 samples per revolution were cropped to 4 revolutions to see which feature would perform well under short lengths as well as a reduced sampling frequency. The damage feature distributions (Figure 28) showed an increase in outliers and an increase in variance for damage features FM4 M6A and M8A. The ROC curves (Figure 29) showed that FM4, M6A and M8A had a reduction in performance. The NA4* and FMH feature remained the better performing damage features when compared to longer signal lengths at the same sampling frequency.

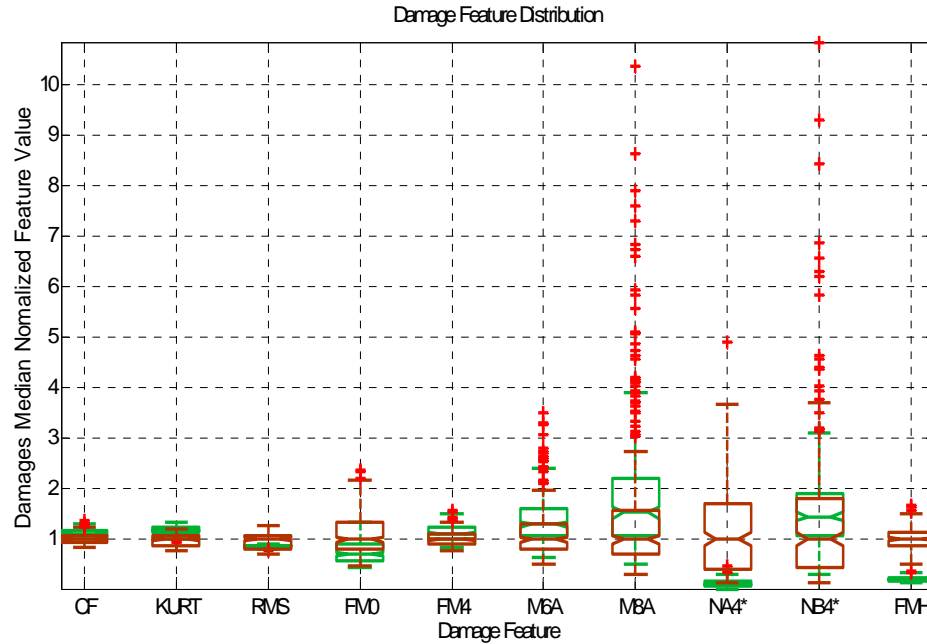


Figure 28: Damage Feature Distributions for Worn Tooth Damage @ 1000RPM, 512 Samples per Revolution, 4 Revolutions, Channel 1

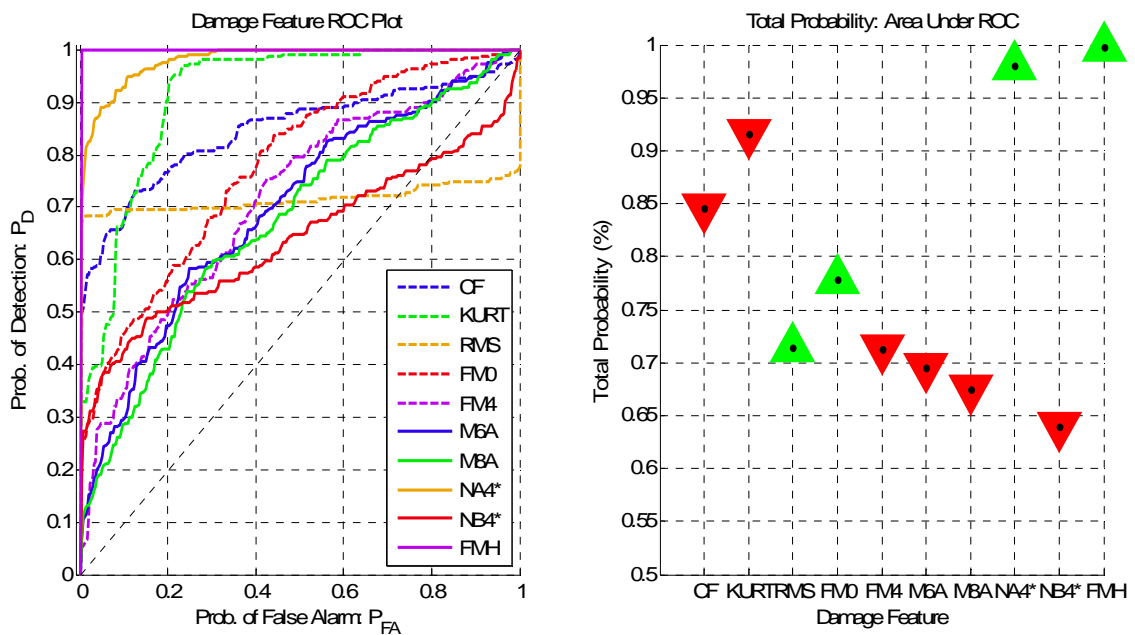


Figure 29: Damage Feature Statistical Performance for Worn Tooth Damage Detection @ 1000 RPM, 512 Samples per Revolution, 4 Revolutions, Channel 1

Out of all the damage features the top performing feature for detecting worn tooth damage at a main shaft speed of 1000 RPM was the FMH damage feature as it demonstrated good detection for both long and short signal lengths as well as multiple sampling frequencies. This feature property is beneficial because fewer false alarms will occur and the dependability of the damage feature is increased. The increased dependability for multiple sampling rates and signal lengths greatly reduces limitations that may arrive when determining which hardware to acquire or sensors to choose.

Data were taken at shaft speeds of 2000 RPM to observe how the damage features would perform at increased rotational speeds. The raw vibration signals were resampled to 2048 samples per revolution which required up sampling the original frequency content by an approximate factor of 2. The signal length in these trials consisted of 40 revolutions as a result of the increased shaft speed. The PSD's of signals taken at 2000 RPM (Figure 30) showed an increase in power throughout the entire spectrum compared to data taken at 1000 RPM. The PSD's also showed that the fundamental mesh frequency, previously not apparent at 1000 RPM, became more obvious in the PSD's at 2000 RPM. All other peaks associated with higher order gear meshing frequencies were not as apparent as they had been at slower shaft speeds.

The distributions of the damage feature taken at 2000 RPM for worn tooth damage (Figure 31) showed increased variability and outliers but also an increased separation in the means of the damaged and undamaged states. Most of the damage features had improved performance compared to features taken at 1000 RPM. The ROC curves (Figure 32) showed that the top three performers were the crest factor, FM0 and FMH. It was observed that the damage features that were extracted from the difference

signal all had swapped hypothesis from when they were extracted at the slower shaft speed.

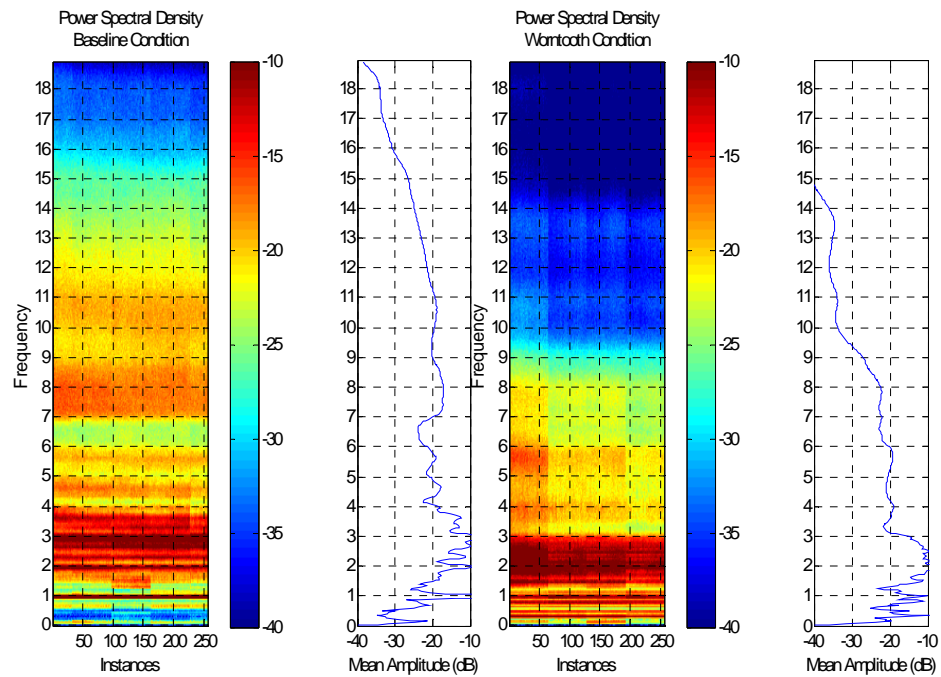


Figure 30: Trial Power Spectrums for Worn Tooth Damage @ 2000RPM, 2048 Samples per Revolution, Channel 1

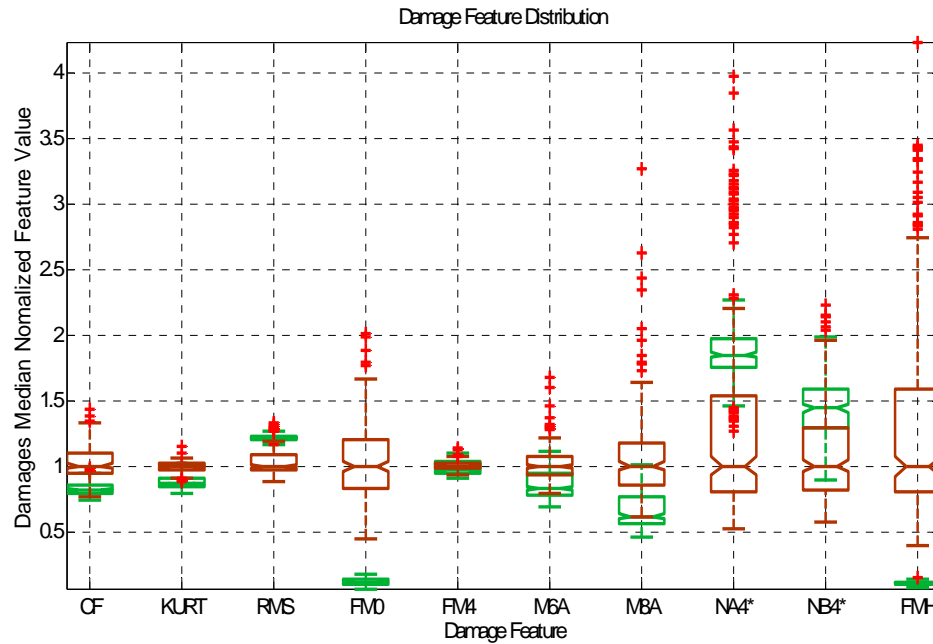


Figure 31: Damage Feature Distributions for Worn Tooth Gearbox Damage @ 2000RPM, 2048 Samples per Revolution, 40 Revolutions, Channel 1

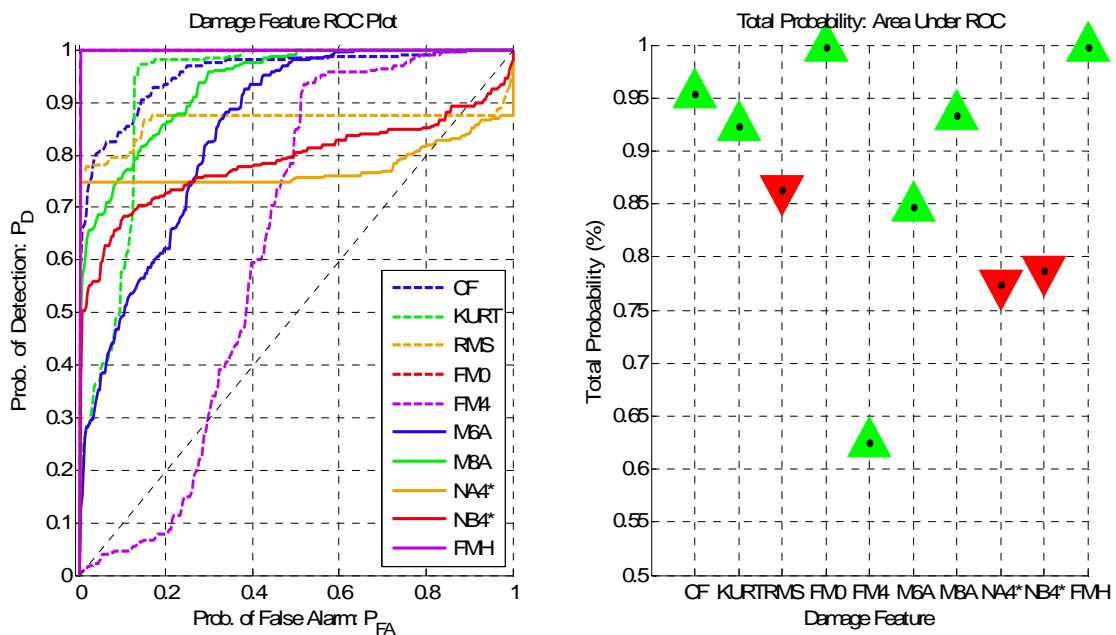


Figure 32: Damage Feature Statistical Performance for Worn Tooth Gear Box Damage Detection @ 2000 RPM, 2048 Samples per Revolution, 40 Revolutions, Channel 1

3.4.2. Main Shaft Ball Bearing Damage Preliminary Results

The next damage case to be examined was that of bearing damage. In the preliminary bearing damage examination two types of damage were examined under two different conditions. Damage features for ball fault damage were first examined under normal operating conditions then the belt drive tension was increase slightly to see how this would affect the detection performance of the damage features. After that a damage case of outer race bearing damage was explored as well as the effect of the position of the fault relative to the loading of the belt drive. For the extraction of the damage features, the angular resampling rate was always kept constant at 2048 samples per second and a total of 20 revolutions used. From experience it was determined that channel three was the best channel for detecting bearing damage using the damage features. Channel 3 was the side mounted bearing, which was in the path of the load vector from the belt drive.

When first looking at the power spectral densities of the various ball fault damage trials (Figure 33), groups of sporadic vertical lines spanning the entire range of frequencies can clearly be seen. These were representative of long periods of ball fault excitation that occurred within an instance of data collection. During machine operation while the ball fault bearing was in place, periods of low fault excitation would occur where the ball fault would not be active. The cause of these periods of low damage excitation was believed to be that the fault had slipped to the side and was not in the path of any loading. The damage excitation was observed to be somewhat of a random event and not always included in the acquired signal. The use of a longer signal sampling length was more advantageous for use in damage detection of ball fault damage in order to record periods of excitation. This property of ball fault damage

dictated the use of the maximum signal length taken which consisted of 20 shaft revolutions or roughly 5 seconds of data.

When looking at the damage features performance, all pick up on this damage very well. The three worst performers were FMH, NB4* and the root mean square. The null hypothesis for all the damage features all indicate that damage is present when the damage features showed an increase from their baseline values (Figure 35). Looking back at the worn tooth gearbox damage case some of the null hypotheses for the damage features indicated a reduction in value from their baseline means. When looking at the variances in the damage feature values (Figure 34), the range between the 25 and 75th percentile values has shown a large increase compared to variance in feature values for worn tooth damage.

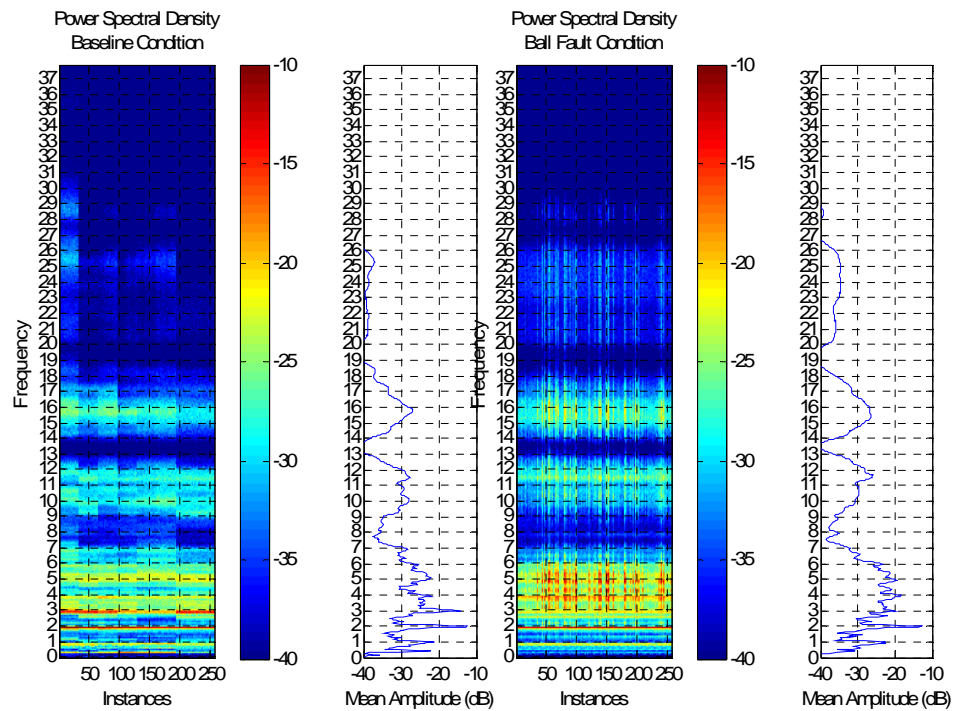


Figure 33: Trial Power Spectra for Main Shaft Bearing Ball Fault Damage @ 1000RPM, 2048 Samples per Revolution, Channel 3

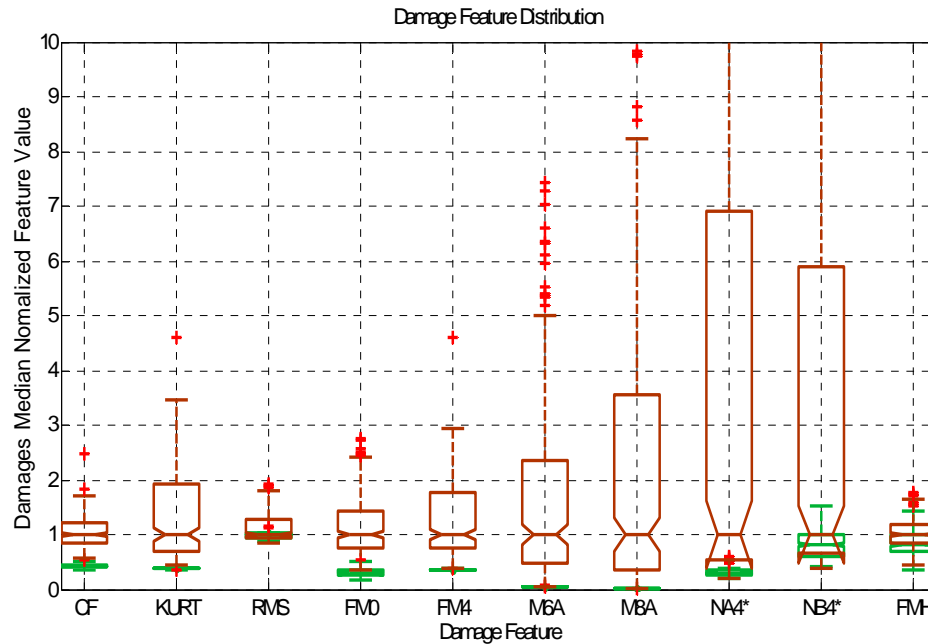


Figure 34: Damage Feature Distributions for Main Shaft Bearing Ball Fault Damage @ 1000RPM, 2048 Samples per Revolution, 20 Revolutions, Channel 3

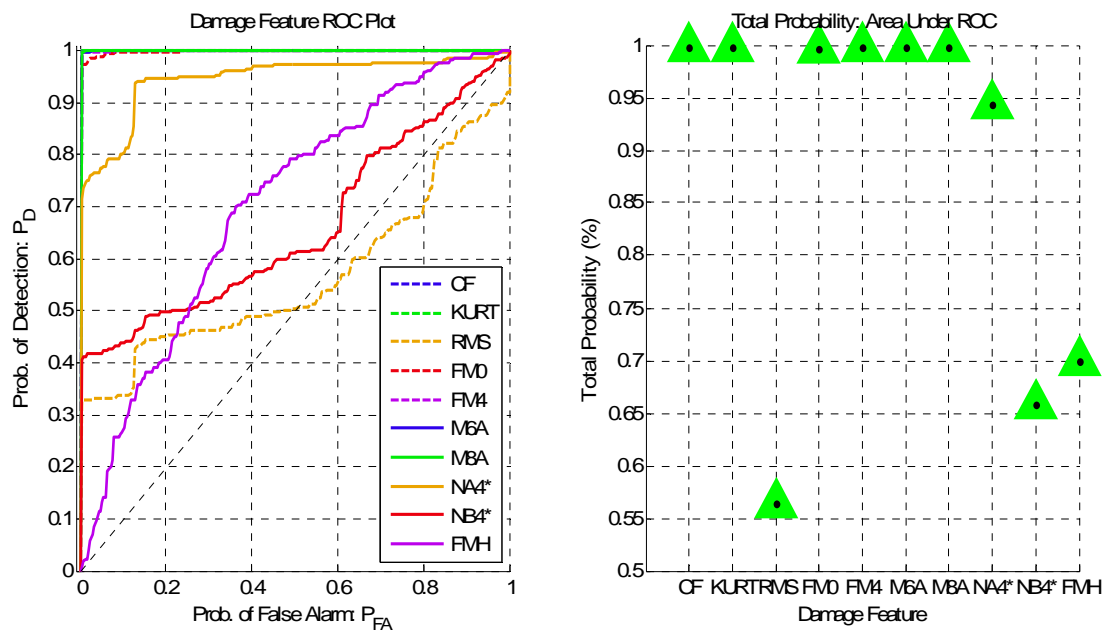


Figure 35: Damage Feature Statistical Performance for Main Shaft Bearing Ball Fault Damage Detection @ 1000 RPM, 2048 Samples per Revolution, 20 Revolutions, Channel 3

The high belt tension tests produced a noticeable increase in the spectral power from the majority of the frequency domain (Figure 36). There was limited overlap in the feature distributions (Figure 37) which resulted in increased detection performance had for all detection features (Figure 38) except for the FMH which was the lowest performing damage feature. FMH's poor performance occurs because it is tuned to detect impacts at the meshing frequencies of orders 1-3, it was the least likely to detect this class of damage, whereas the FM0 feature, also tuned to specific frequency orders associated with gear mesh signals is only monitoring for changes in a certain frequency bin. If impacts due to bearing faults are causing wide band frequency response then it will still register this increase in energy as damage. Though this isn't an issue for detecting damage, it does mean that its value as a good classifying statistic is limited, as it can't distinguish bearing damage from gear damage.

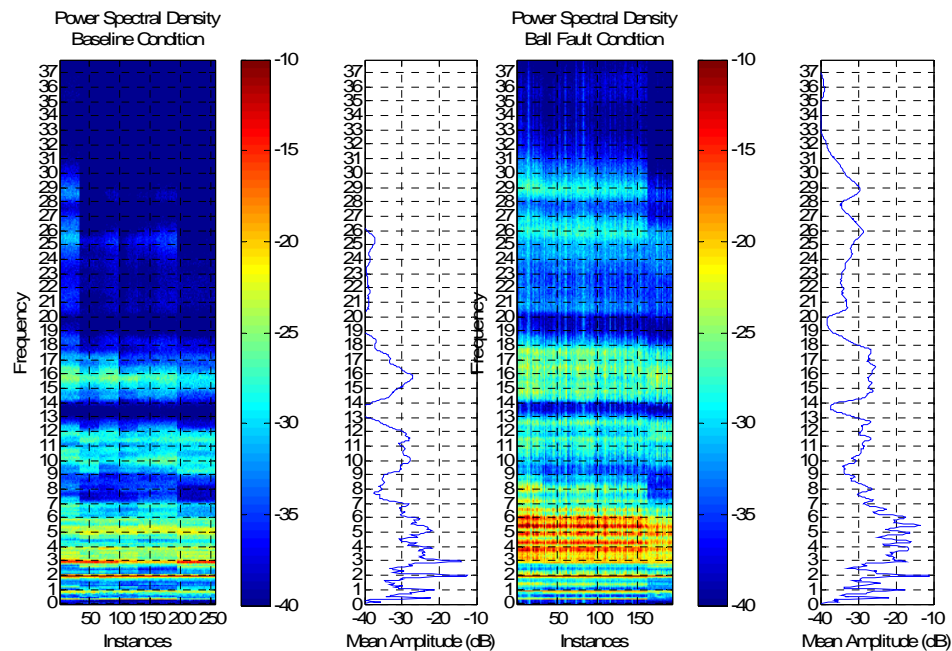


Figure 36: Trial Power Spectrums for Main Shaft Bearing Ball Fault Damage under High Belt Tension @ 1000RPM, 2048 Samples per Revolution, Channel 3

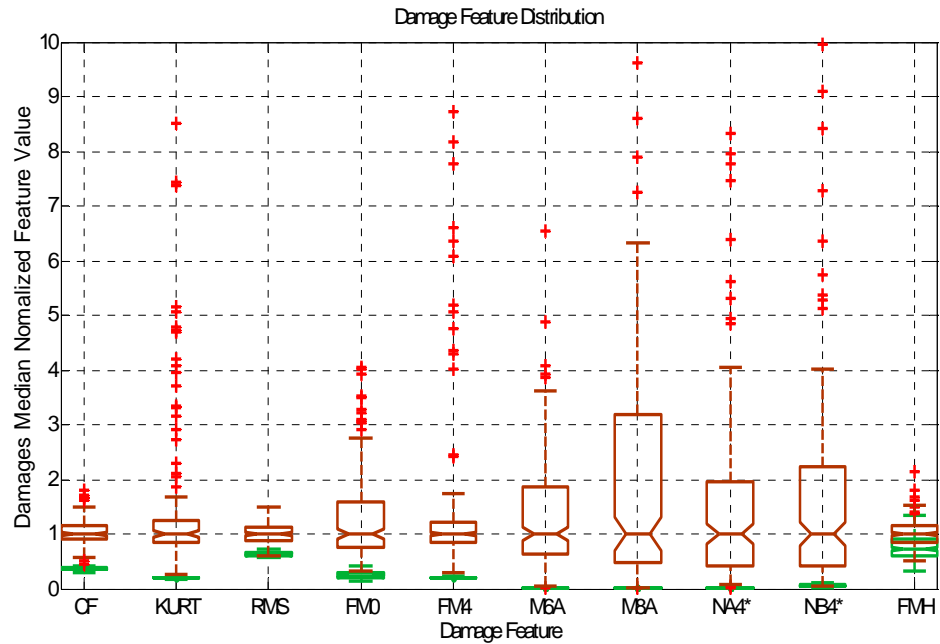


Figure 37: Damage Feature Distributions for Main Shaft Bearing Ball Fault Damage Under High Belt Tension @ 1000RPM, 2048 Samples per Revolution, 20 Revolutions, Channel 3

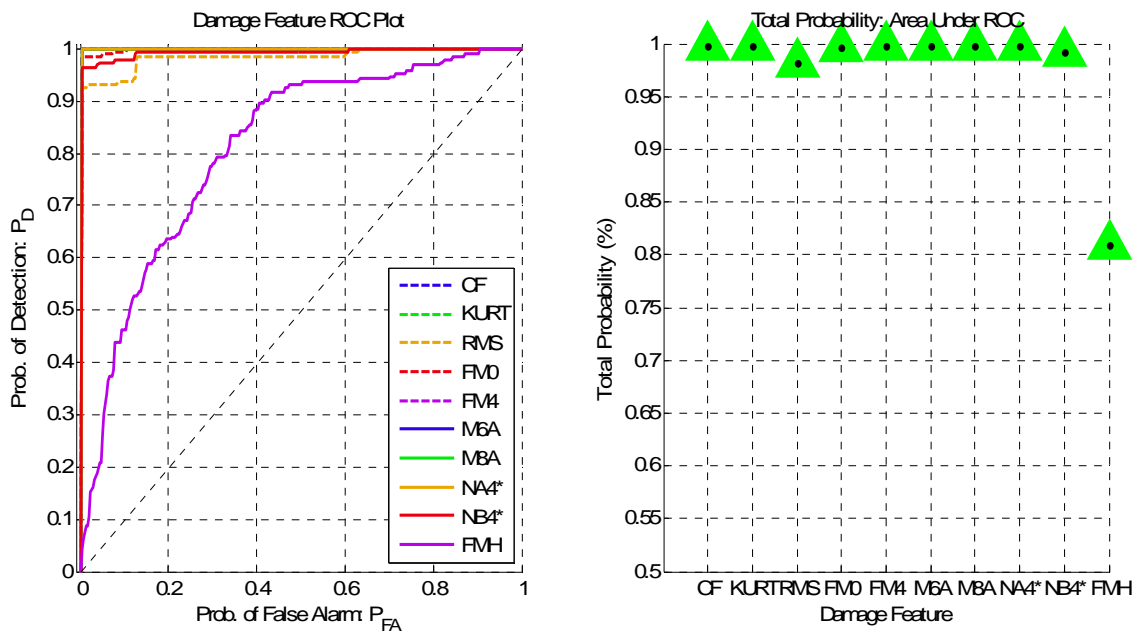


Figure 38: Damage Feature Statistical Performance for Main Shaft Bearing Ball Fault Under High Belt Tension Damage Detection @ 1000 RPM, 2048 Samples per Revolution, 20 Revolutions, Channel 3

In the case of outer race fault bearing damage the location of the bearing fault was marked on the side of the bearing casing with a little mark and the word outer was engraved on the outside of the bearing to clearly distinguish it from the other bearings. For the first test of outer race bearing damage the location of the bearing damage was located in the same position every time. This position was closet to channel 2 and also would have the highest normal force applied to it as it was in line with the force vector associated with the belt tension.

When examining the power spectral densities of the outer race bearing damage (Figure 39), it is difficult to tell if there is any damage present at all. There was less environmental variability from changing the machine components around than there was in the case of the baseline condition. The damage feature distributions (Figure 40) show a great deal less variance than the ball fault bearing damage feature distributions. These results appear to indicate that there is less damage in the damaged data than the undamaged data. When looking at the hypotheses (Figure 41), all but one damage feature hypotheses indicate that damage is being present when the value of the damage feature is less than the threshold. The best performers here were NA4*, RMS, and FMH.

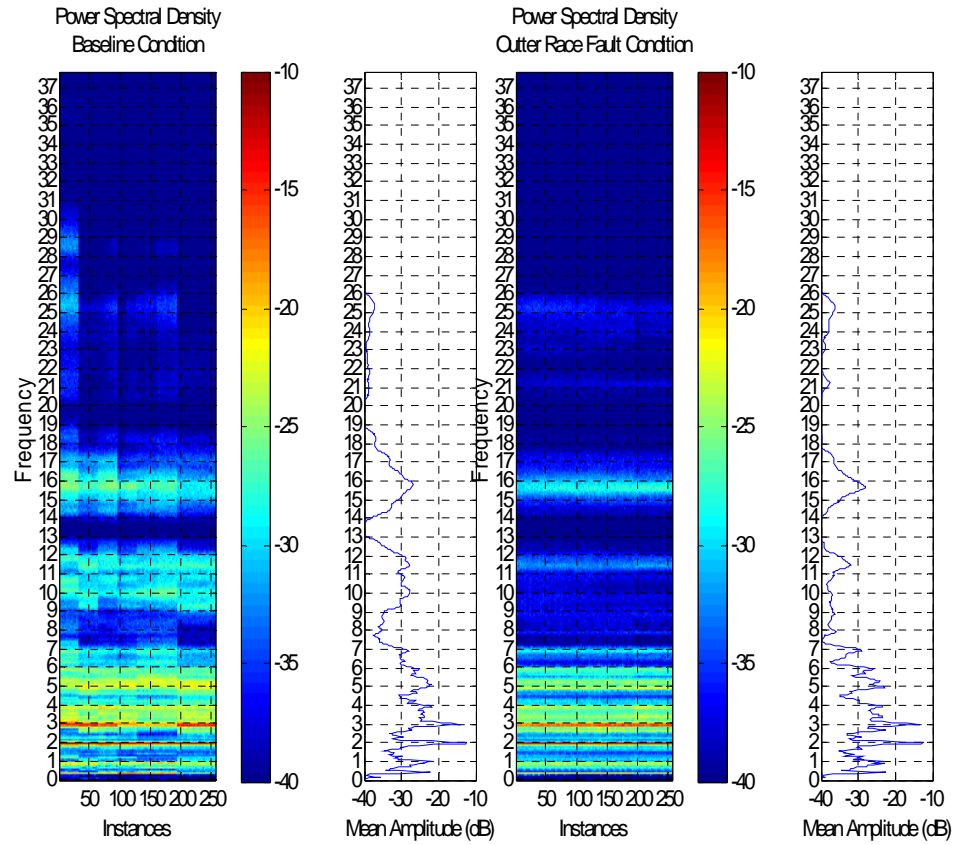


Figure 39: Trial Power Spectrums for Main Shaft Bearing Outer Race Fault Damage @ 1000RPM, 2048 Samples per Revolution, Channel 3

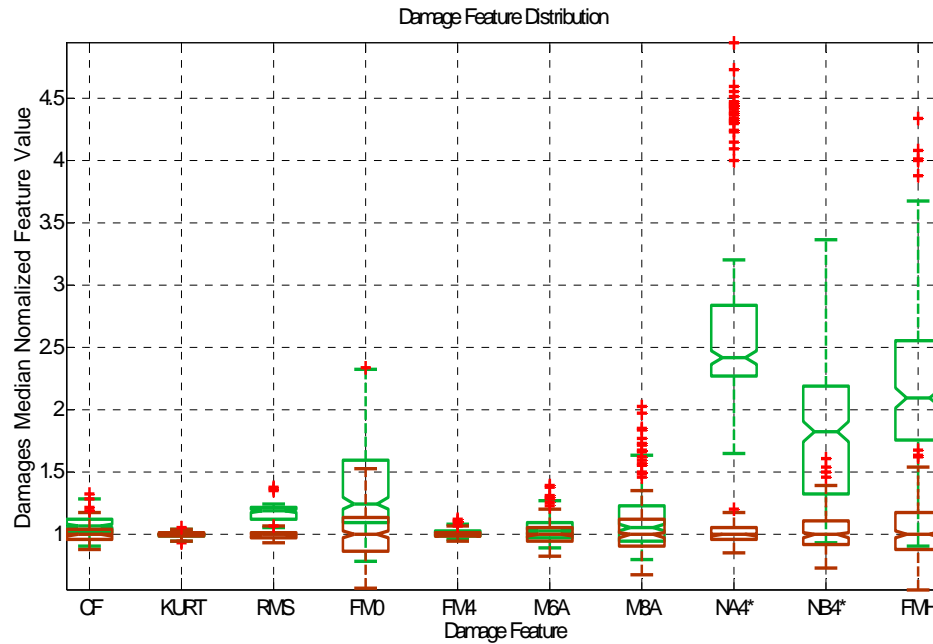


Figure 40: Damage Feature Distributions for Main Shaft Bearing Outer Race Fault Damage @ 1000RPM, 2048 Samples per Revolution, 20 Revolutions, Channel 3

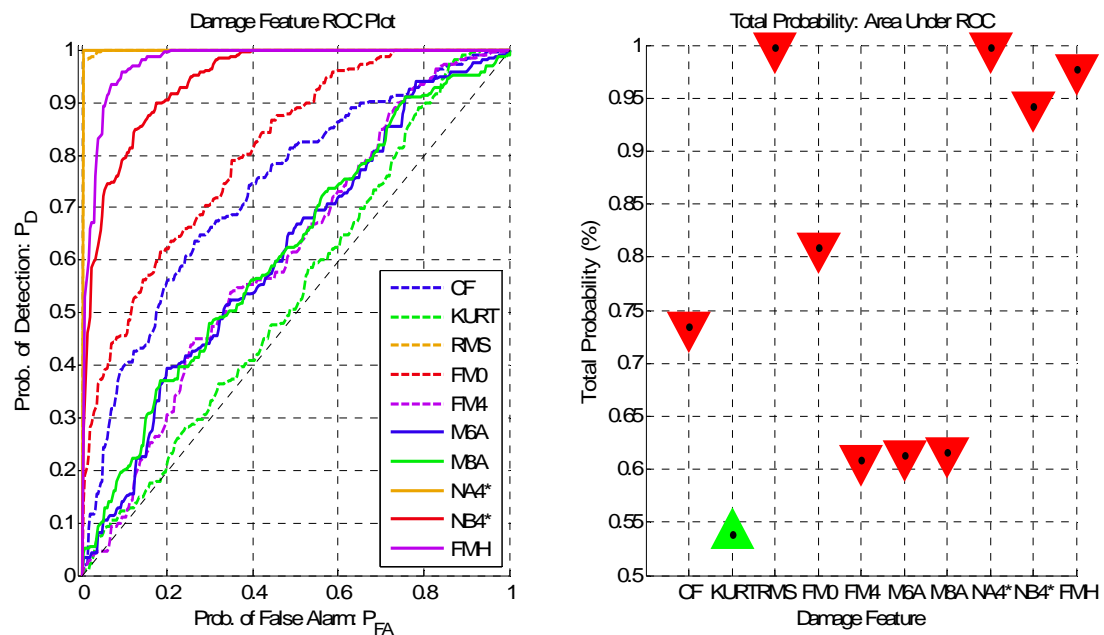


Figure 41: Damage Feature Statistical Performance for Main Shaft Bearing Outer Race Fault Damage Detection @ 1000 RPM, 2048 Samples per Revolution, 20 Revolutions, Channel 3

Data were taken for outer race fault bearing damage where the outer race fault was placed at random positions with no particular order. This random positioning of the outer race fault showed and increased variability in the PSD's (Figure 42) when compared to the previous outer race fault data with constant fault position. The variance in the damage features remained small (Figure 43) compared to the ball bearing fault damage feature values. This observed feature variance was consistent to the previous outer race fault damage feature distributions. Hypotheses made for optimal damage detection (Figure 44) indicated damage as being present when the value of the damage feature is less than the threshold for all but one damage feature. The best performing damage features were NA4*, RMS, and FMH. The FMH damage feature detected damage in the outer race fault even though it was designed for worn tooth damage detection. This result was unexpected because FMH is a measure of the periodicity of impacts associated with the gear mesh harmonics and is unknown why FMH is a top performer for this class of damage.

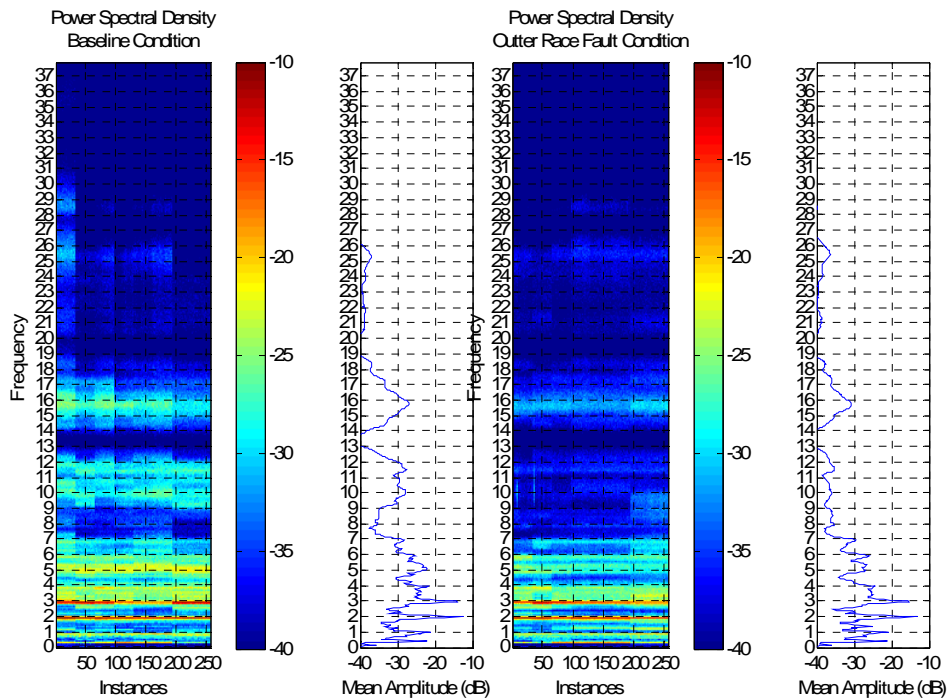


Figure 42: Trial Power Spectrums for Main Shaft Bearing Outer Race Fault Damage w/ Varying Fault Position @ 1000RPM, 2048 Samples per Revolution, Channel 3

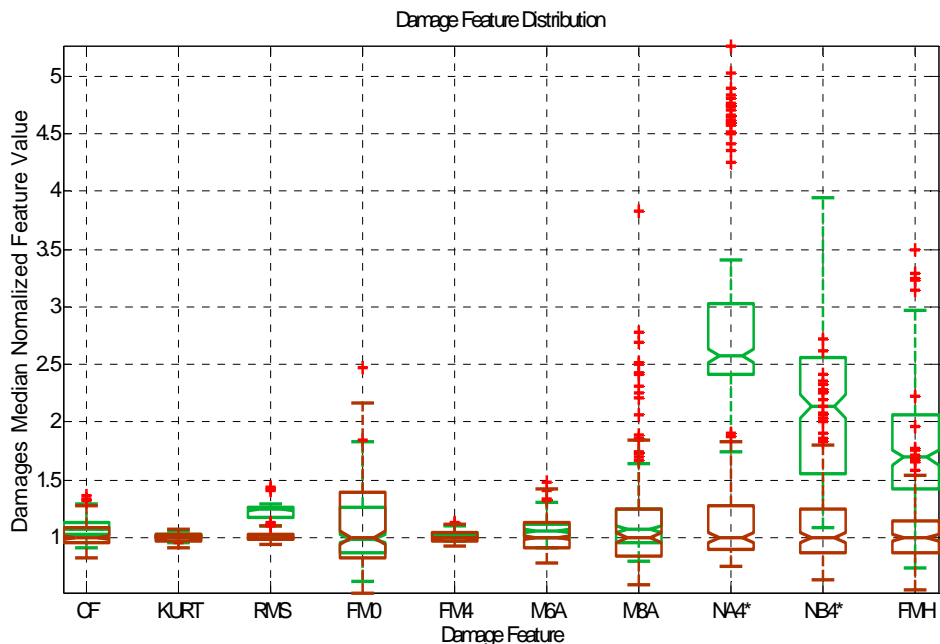


Figure 43: Damage Feature Distributions for Main Shaft Bearing Outer Race Fault Damage w/ Varying Fault Position @ 1000RPM, 2048 Samples per Revolution, 20 Revolutions, Channel 3

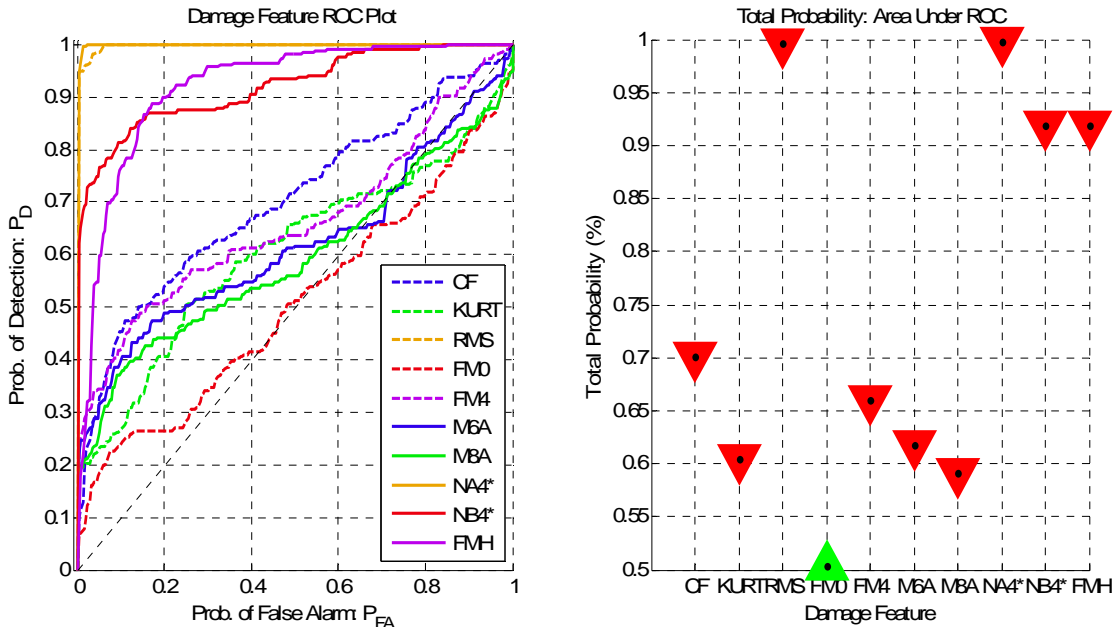


Figure 44: Damage Feature Statistical Performance for Main Shaft Bearing Outer Race Fault Damage Detection w/ Varying Fault Position @ 1000 RPM, 2048 Samples per Revolution, 20 Revolutions, Channel 3

3.4.3. Bearing Damage Detection and Varying Belt Tension

For the following results, it was desirable to try and reducing some of the variability associated with time and manipulation of the testbed caused by replacing parts. The effect of belt tension on bearing damage detection was to be examined in this section and testing procedure two was used where features were taken over a single long run with automated data collection. The results showed that the detection performance was greatly increased for many bearing damage types even though the belt tension was lowered by half that of the optimal belt tension for half the trials. For all the cases presented in this section, low level and high level belt tension are represented on the left and right half of the PSD's respectively.

For the ball fault damage case, by looking at the PSD of the baseline condition and the damaged condition (Figure 45), it is possible to see that there is an increase in

power to frequency components that were present in the low belt tension case. The ball fault bearing damage still exhibits the random events of increased broadband frequency energy that was present in the earlier case but the increase of belt tension seems to only increase the power of these events.

When looking at the distributions for the damage features (Figure 46), it can be seen that the performance is exceedingly well for all the damage features. The mean of all the damage features increased for the ball fault damage case as well the base line case had very little variability in the features when compared to the damage case. Because the features were extracted from data sets where there was less manipulation to the system as previous data sets, this is believed to be the reason for the drastic increase in performance of all damage features when compared to the previous results. The ROC curves (Figure 47) showed near perfect detection for all damage features.

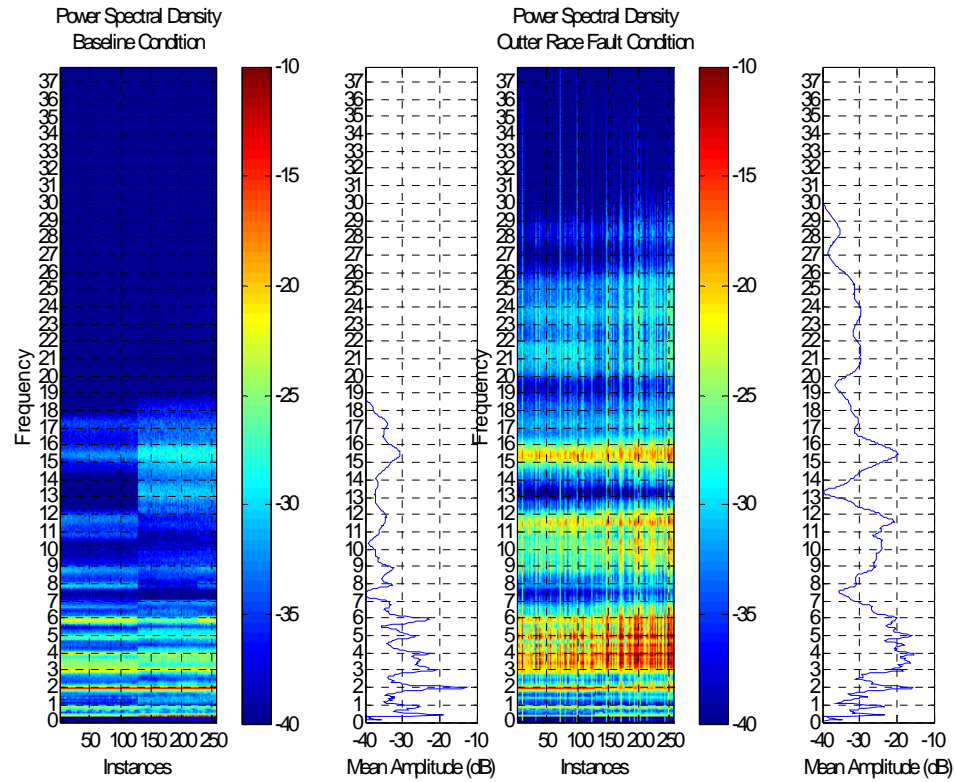


Figure 45: Trial Power Spectrums for Main Shaft Bearing Ball Fault Damage w/ Varying Belt Tension @ 1000RPM, 2048 Samples per Revolution, Channel 3

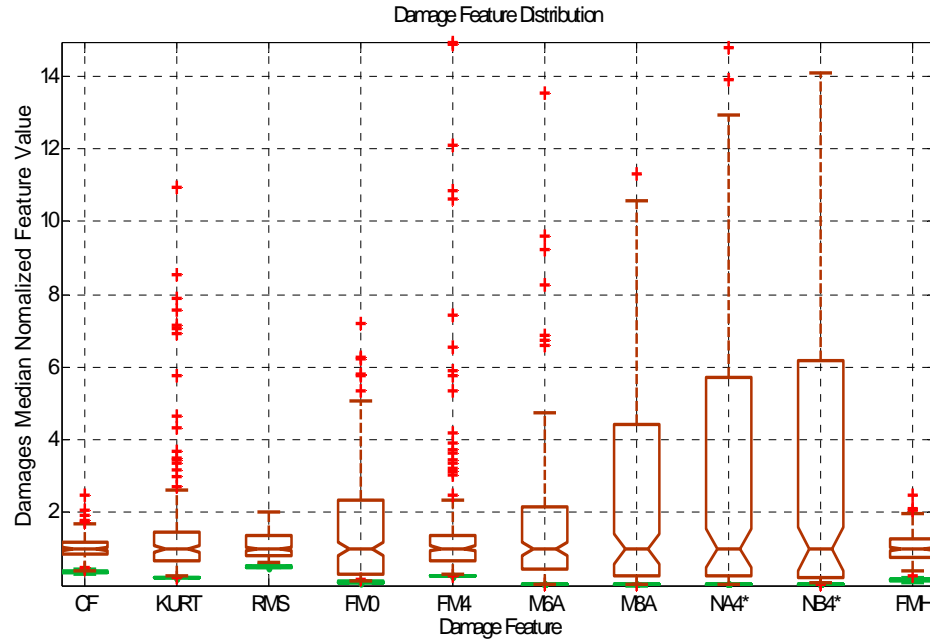


Figure 46: Damage Feature Distributions for Main Shaft Bearing Ball Fault Damage w/ Varying Belt Tension @ 1000RPM, 2048 Samples per Revolution, 20 Revolutions, Channel 3

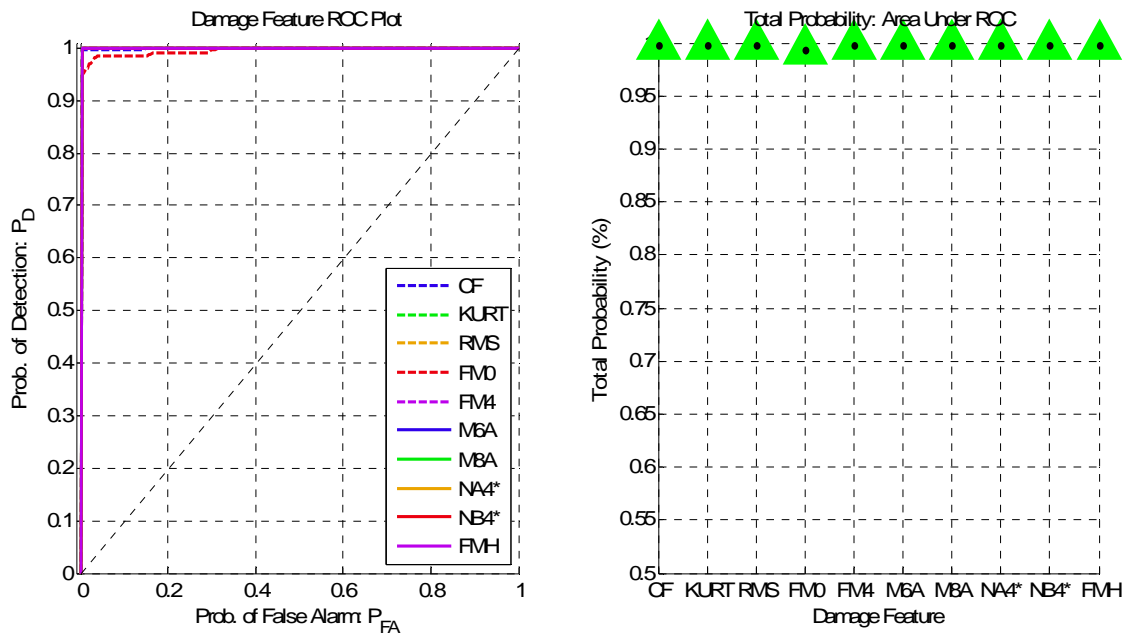


Figure 47: Damage Feature Statistical Performance for Main Shaft Bearing Ball Fault Damage Detection w/ Varying Belt Tension @ 1000 RPM, 2048 Samples per Revolution, 20 Revolutions, Channel 3

In the inner race fault bearing damage case the PSD of the trials (Figure 48) again show that increasing the belt tension amplified the frequency content that was originally present in low tension case. For the inner race fault, by comparing the PSD's of the trial it can be seen that there is a large increase in power in the band width of 3-7 orders of the gear mesh fundamental frequency. This increase in power dominates the gear mesh frequencies in that region, which were clearly present in the undamaged case. Because the damage on the inner race is static and cannot move around, the random events of broad band energy spikes for the ball bearing damage are no longer present. Instead it can be seen that there is a uniform increase in broad band power due to the inner race faults.

The distributions of feature values for the inner race fault (Figure 49) continually showed an increase for the damaged case for all feature values. The damage feature variances were again much larger than those for the baseline condition. The performance of the damage features (Figure 50) was essentially the same as it was for the ball fault damage. All features yielded superior detection capabilities for the inner race ball fault damage under varying belt tension. This increase in performance is most likely due to the reduced environmental variability that was attained by using testing procedure 2.

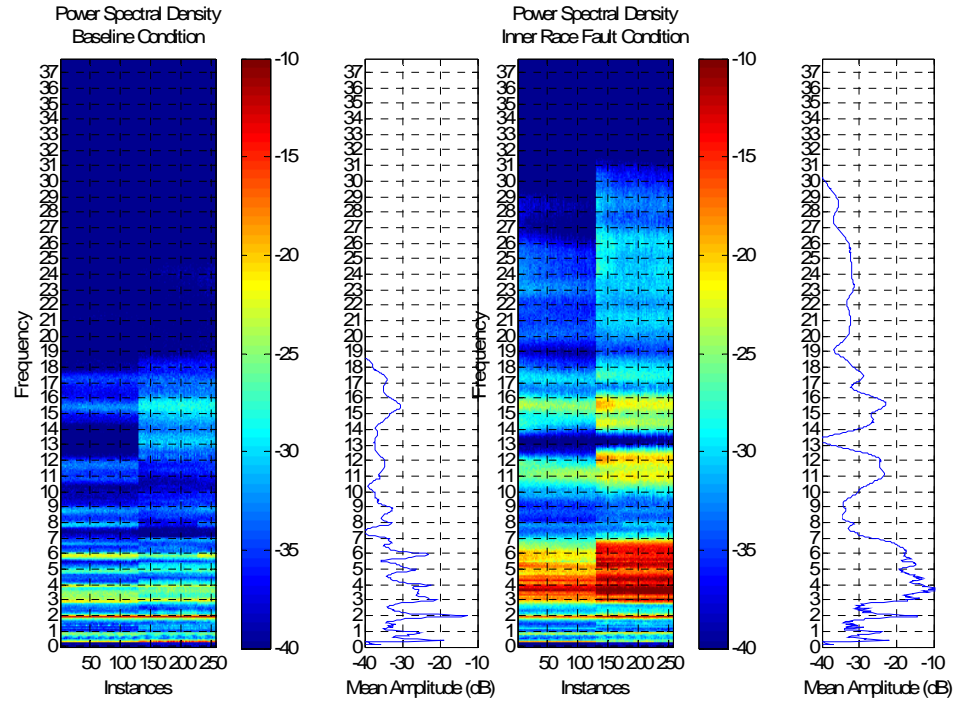


Figure 48: Trial Power Spectrums for Main Shaft Bearing Inner Race Fault Damage w/ Varying Belt Tension @ 1000RPM, 2048 Samples per Revolution, Channel 3

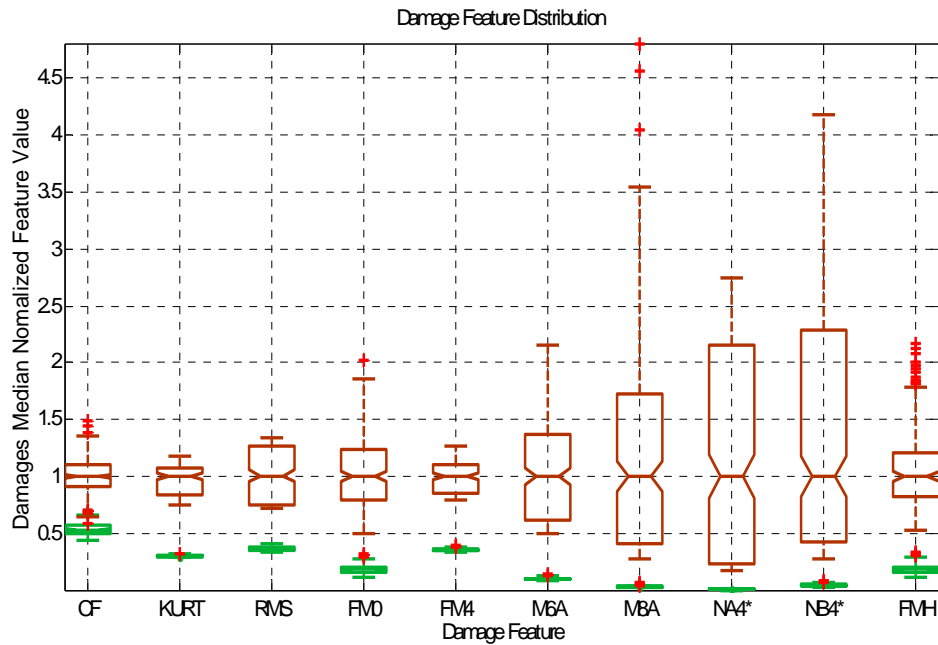


Figure 49: Damage Feature Distributions for Main Shaft Bearing Inner Race Fault Damage w/ Varying Belt Tension @ 1000RPM, 2048 Samples per Revolution, 40 Revolutions, Channel 3

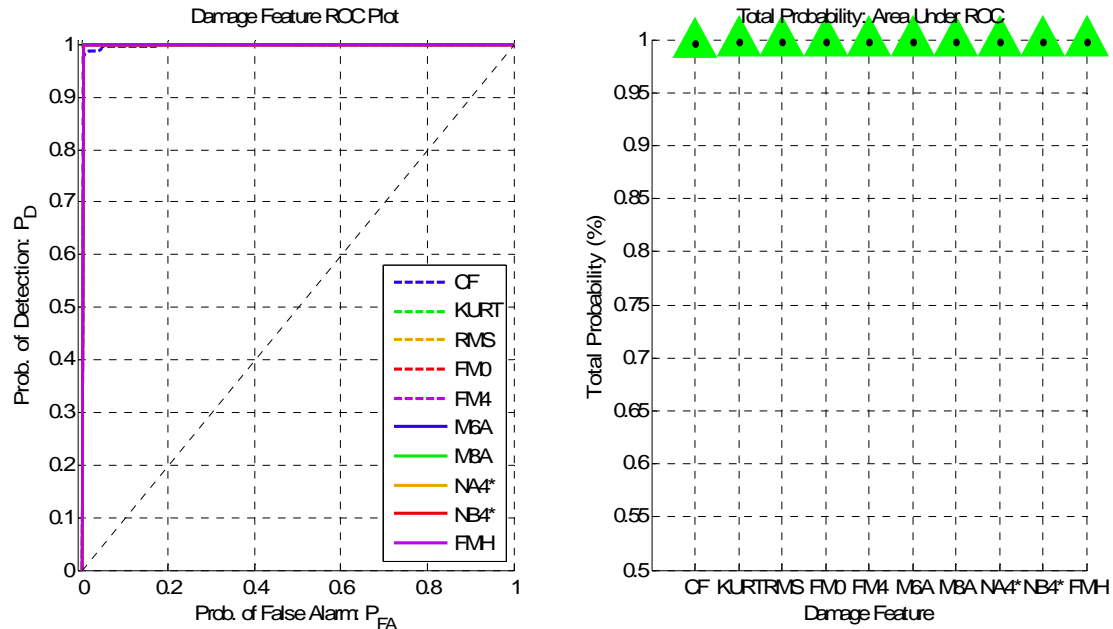


Figure 50: Damage Feature Statistical Performance for Main Shaft Bearing Inner Race Fault Damage Detection w/ Varying Belt Tension @ 1000 RPM, 2048 Samples per Revolution, 40 Revolutions, Channel 3

Lastly, the outer race bearing fault was examined using testing procedure 2 for varying belt tensions. The variability in the PSD's (Figure 51) for this comparison showed very little difference between the damaged and undamaged states. In the damage case there is a slight increase in high frequency power in the bandwidth of 20-25 orders of the gear mesh fundamental frequency. Though in the baseline condition there is a slight increase of power in the bandwidth of 19-12 orders of the fundamental gear mesh frequency for the results taken with the manufacturers recommended belt tension. These results strongly suggest that the damage seeded in the outer race fault was very small when compared to the ball fault and inner race fault damage cases. An inquiry was made to SpectraQuest about the procedures used in seeding damage for the different bearing faults but there has been no response as of this time.

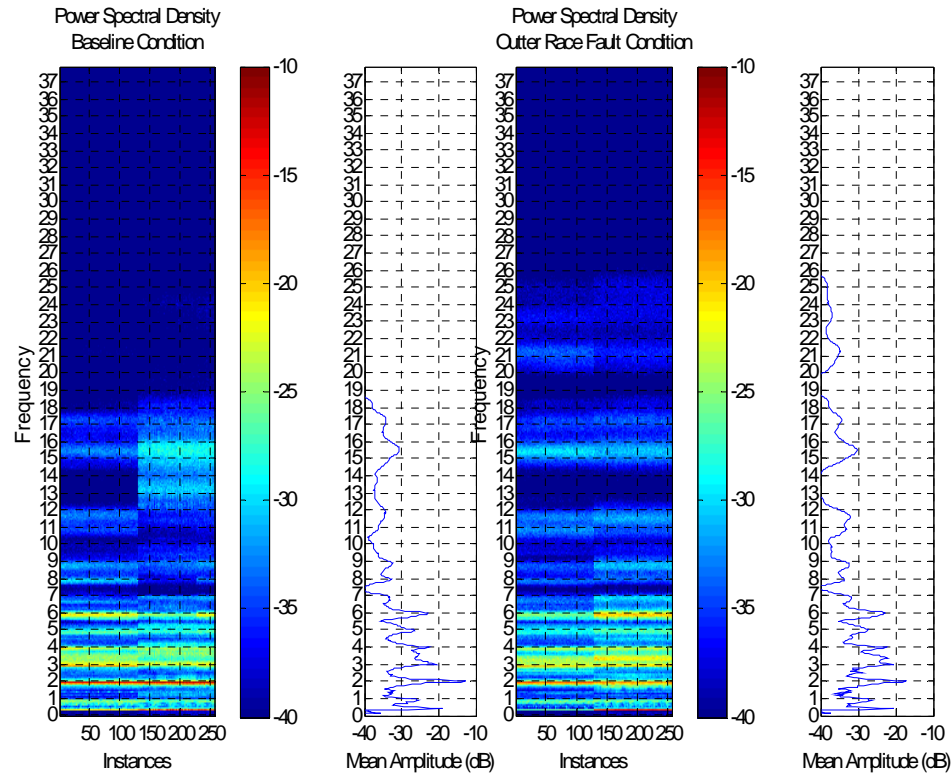


Figure 51: Trial Power Spectrums for Main Shaft Bearing Outer Race Fault Damage w/ Varying Belt Tension @ 1000RPM, 2048 Samples per Revolution, Channel 3

When examining the performance of the damage features for the outer race fault under varying belt tension (Figure 52), the large increase in performance that was seen in the previous two bearing damage cases is not observed. This observed result is most likely due to the small size of the outer race fault. The ROC plots (Figure 53) showed that the top three performers were FM0, NB4* and FMH. FM0 and FMH were tuned to track frequency content for the first three harmonic orders. It is uncertain why they would be the top performers for a bearing damage case taken from a sensor that positioned on the bearing housing. Clearly the bearing fault causes a change in frequency content that is primarily associated with the gear mesh harmonics.

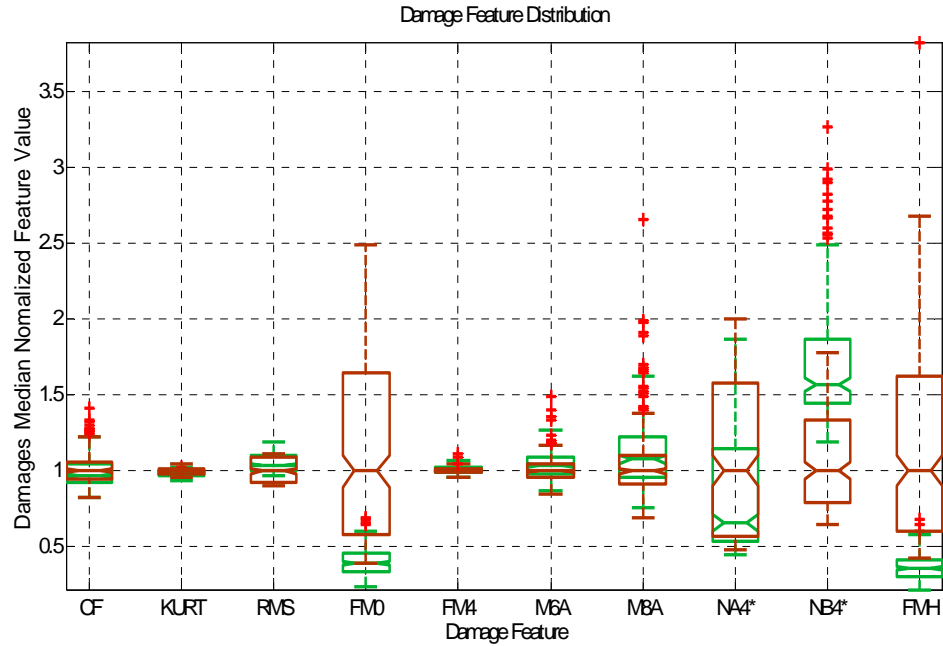


Figure 52: Damage Feature Distributions for Main Shaft Bearing Outer Race Fault Damage w/ Varying Belt Tension @ 1000RPM, 2048 Samples per Revolution, 40 Revolutions, Channel 3

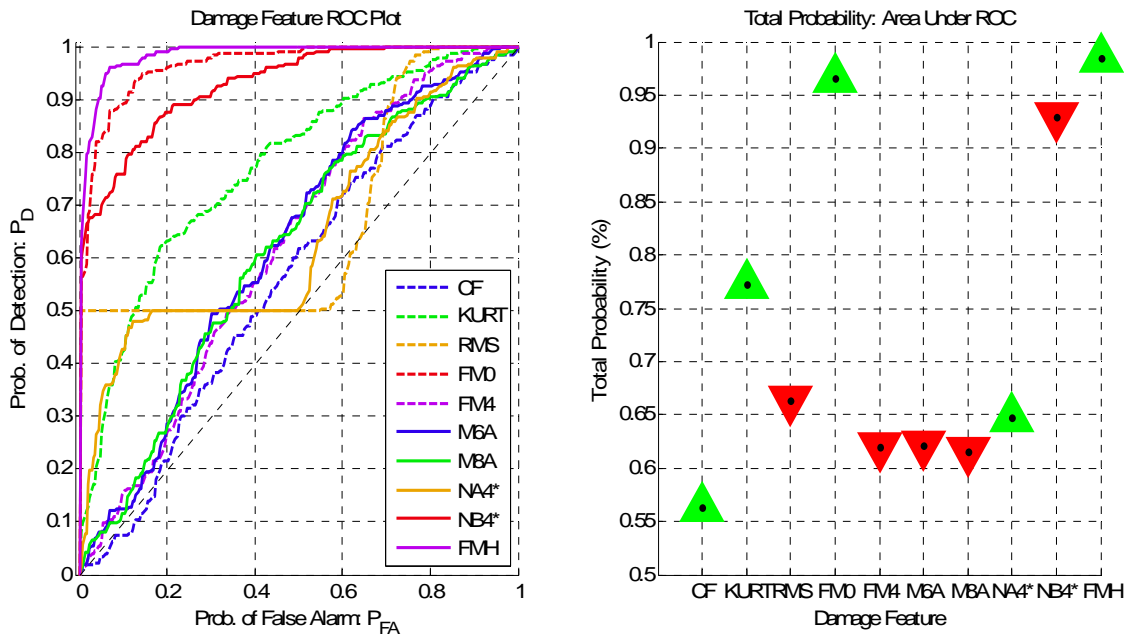


Figure 53: Damage Feature Statistical Performance for Main Shaft Bearing Outer Race Fault Damage w/ Varying Belt Tension @ 1000 RPM, 2048 Samples per Revolution, 40 Revolutions, Channel 3

Lastly, one other interesting observation made here is that the ROC plots for the root mean square and NA4* show a distinct step pattern. This result is due to a bimodal distribution in the damage features and indicates that the root mean square of the system and the NA4* damage features have a clear correlation with the belt tension.

Over all reducing the environmental variability showed a large increase in performance for all damage features in the case of the ball fault and inner race bearing damage conditions. This result of increased detection performance was not observed for the outer race bearing damage condition. The belt tension and normal force clearly has an effect on the power of the frequency content but not enough to affect the performance of the damage features in most cases, the exception being the RMS and NA4* damage features for outer race fault condition which is believed to be minimal in size compared the ball fault and inner race faults.

3.4.4. Worn tooth Damage and Varying Torsional Load

In this section testing procedure 2 was used to reduce environmental variability and isolate variability caused by varying torsional load applied to the gear box. The data sets used were ordered in increasing torsional load and can be view from left to right in the PSD plots below. 128 trials were taken at three levels of torsional load. To determine the effect that sensor placement has on worn tooth damage detection a comparison was made between Channel 1 and Channel 3 data. Channel 1 data were taken for a sensor directly mounted on the gear box while Channel 3 data were taken from a sensor mounted to the bearing housing.

The PSD's for Channel 1 data (Figure 54) showed similar results from the preliminary worn tooth damage case. The undamaged case showed more power in the high frequency range caused by the impacting of healthy gear teeth and reduced high

frequency content due to the slipping of worn teeth for the damaged case. When comparing the low and high torsional loads, the power spectrums show that there is a definite increase in power for frequencies associated with gear mesh harmonics under higher torsional loads.

The distributions of feature values using Channel 1 data for undamaged and damaged states (Figure 55) showed an increase in separation and reduced variance compared to the worn tooth damage feature distributions in the preliminary results. The ROC curves of the damage features (Figure 56) performance showed an overall increase compared to the preliminary results. This observed increase in performance is attributed to the reduced environmental variability achieved by using testing procedure 2. The variability of the torsional load did not reduce the performance of the various damage features.

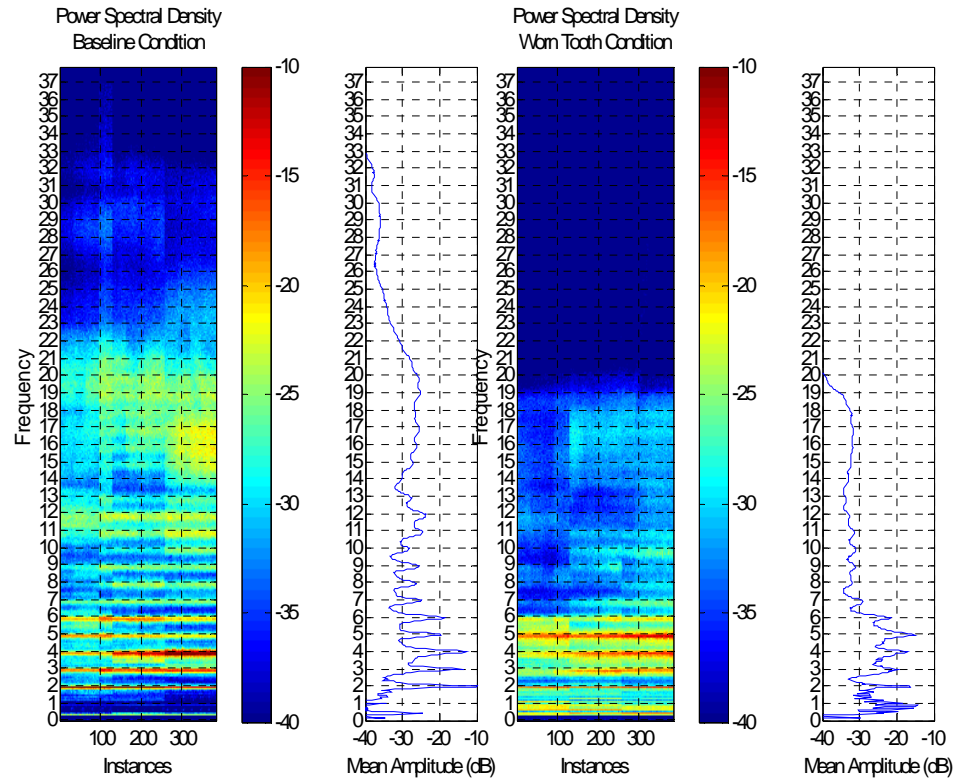


Figure 54: Trial Power Spectrums for Worn Tooth Damage w/ Varying Torsional Load @ 1000RPM, 2048 Samples per Revolution, Channel 1

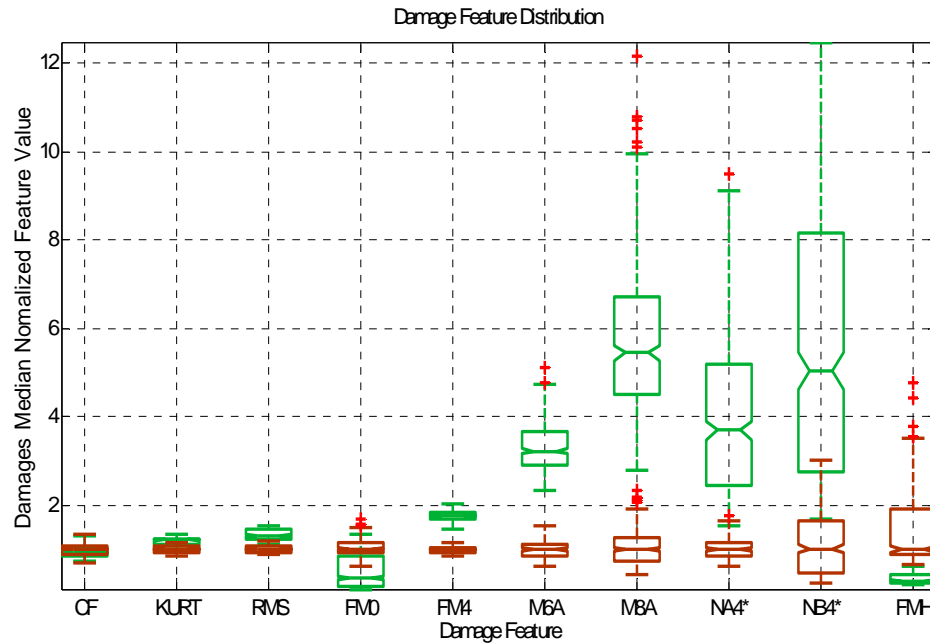


Figure 55: Damage Feature Distributions for Worn Tooth Damage w/ Varying Torsional Load @ 1000RPM, 2048 Samples per Revolution, 40 Revolutions, Channel 1

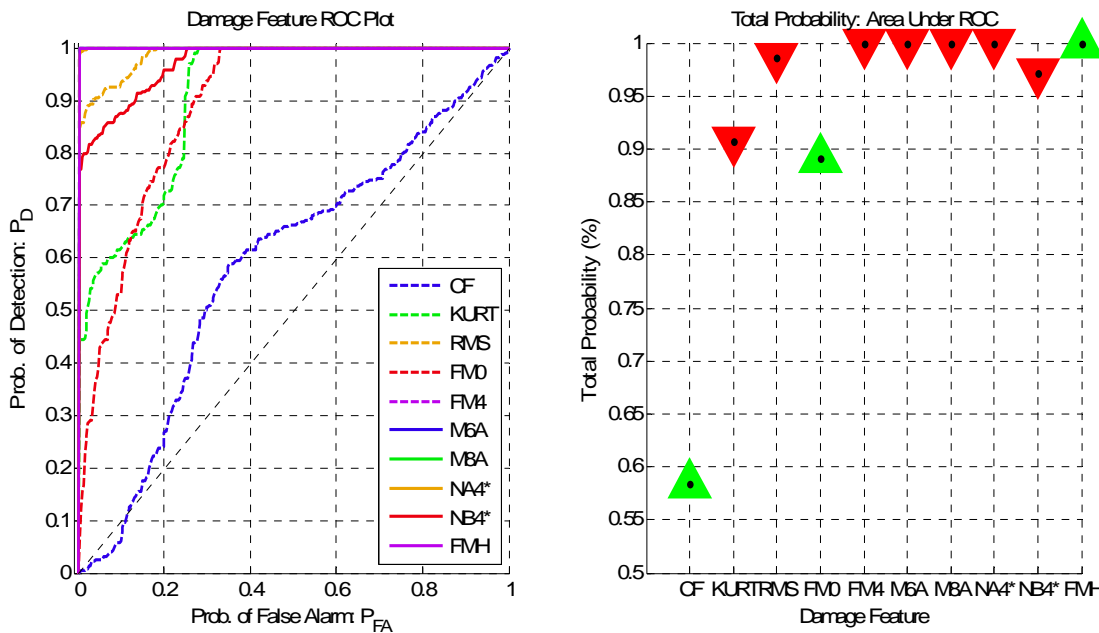


Figure 56: Damage Feature Statistical Performance for Worn Tooth Damage w/ Varying Torsional Load @ 1000 RPM, 2048 Samples per Revolution, 40 Revolutions, Channel 1

Data from Channel 3 showed presence of the gear mesh harmonics in their PSD's (Figure 57) though not as defined as the data taken from the sensor directly mounted to the gearbox. The reduction of power to higher ordered frequency content due to worn tooth slippage is present in the Channel 3 data again. The effect of the increase in torsional load on PSD's using Channel 3 data had the same result as the gear box mounted sensor data. This observed result was that the frequency power associated with the gear mesh harmonics is increased as the torsional load increases.

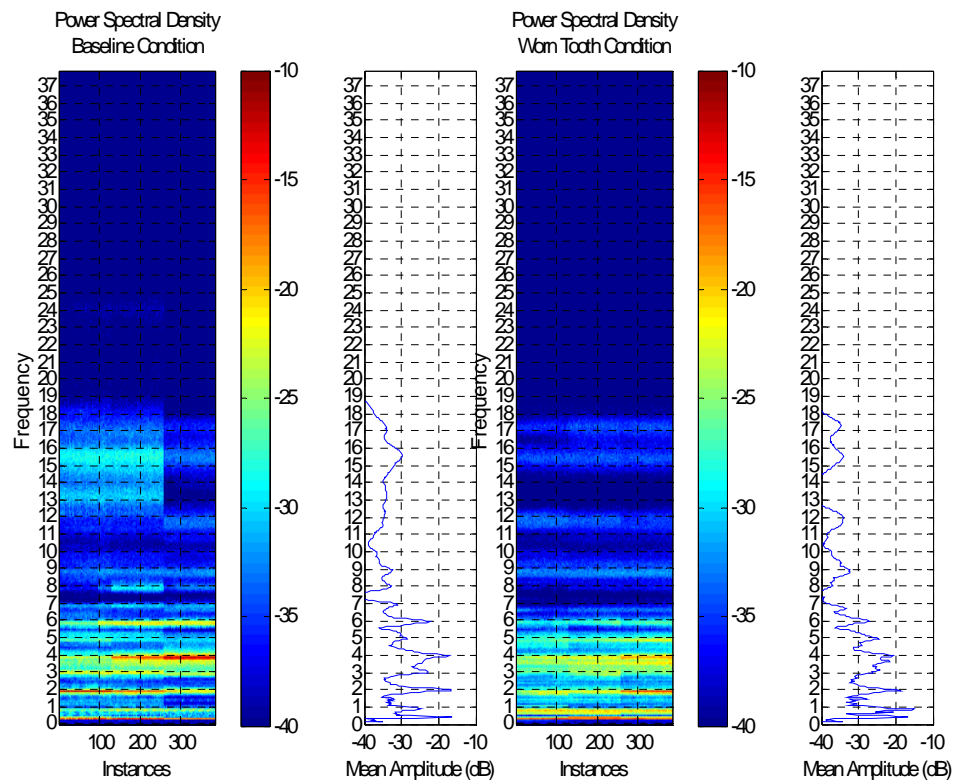


Figure 57: Trial Power Spectrums for Worn Tooth Damage w/ Varying Torsional Load @ 1000RPM, 2048 Samples per Revolution, Channel 3

The distributions of the damage feature values (Figure 58) showed more overlap between damaged and undamaged feature distribution than was observed for feature

values using data from Channel 1. The detection performance of the damage features using the Channel 3 data (Figure 59) showed the top two performing damage features were NB4* and FMH. The remaining damage features suffered a reduced ability to detect the worn tooth damage caused by their proximity to the damage. NB4* and FMH showed the most potential for monitoring worn tooth damage at greater distances from the source.

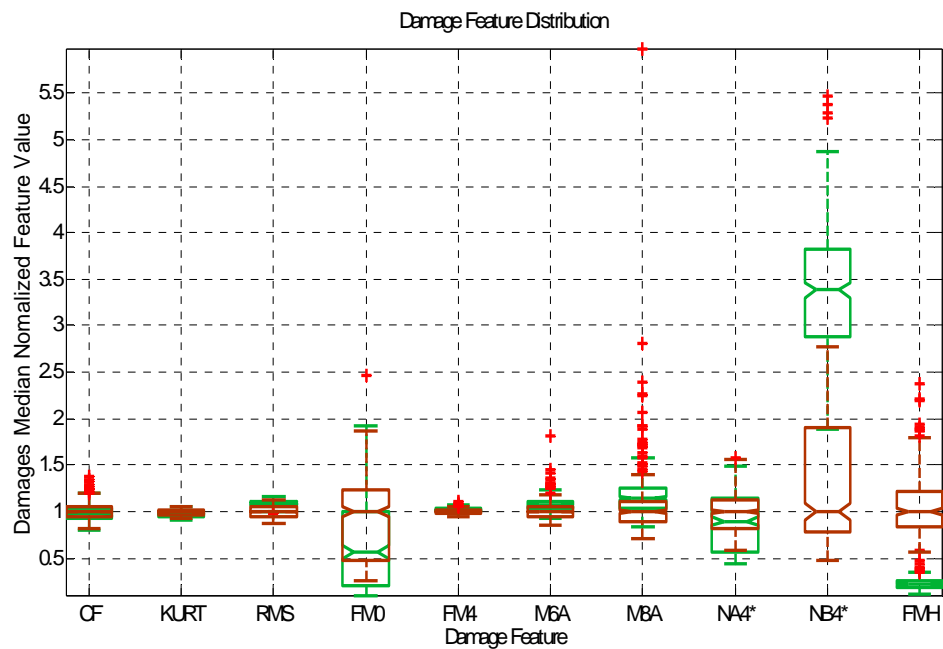


Figure 58: Damage Feature Distributions for Worn Tooth Damage w/ Varying Torsional Load @ 1000RPM, 2048 Samples per Revolution, 40 Revolutions, Channel 3

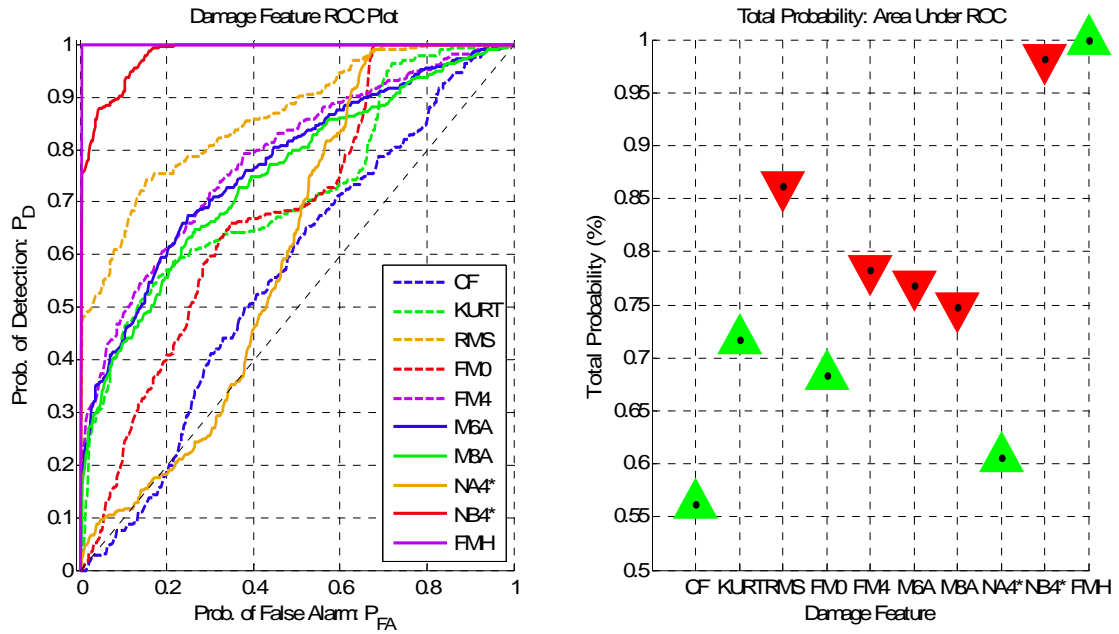


Figure 59: Damage Feature Statistical Performance for Worn Tooth Damage w/ Varying Torsional Load @ 1000 RPM, 2048 Samples per Revolution, 40 Revolutions, Channel 3

Chapter 4

Conclusion & Future Work

4.1. Conclusion

From the results of this study it was shown that the relation of the performance of various damage features to environmental variability and operational conditions is complex. Many of the damage features indicated good performance for the different damage types under different condition but suffered from hypothesis swapping, where for one system state, damage caused an increase in the mean of the feature value, but in others the damage caused a decrease. The change in damage feature distributions makes it hard to establish specified thresholds to detect if damage is present. Classification of damage types become increasingly also become difficult.

Out of the damage features covered, the newly proposed FMH feature continuously showed superior performance in detecting worn tooth damage compared to traditional gearbox damage features. This superior performance occurred for a number of different signal lengths, sampling frequencies and sensor locations. In addition to its superior performance in worn tooth damage detection, the FMH feature also was less sensitive to bearing damage than the traditional damage features. Lastly,

because damage nearly always produced an increase in the feature value of the FMH damage feature the hypotheses made for optimal detection was rarely swapped unlike the traditional damage features.

Two main contributions have been made in this thesis. The first contribution was providing a better understanding of traditional damage features performance under varying environmental and operational conditions. The survey of the damage detection performance for various damage states can be extrapolated for use in industry. The knowledge of which features perform better for certain classes of damage and don't suffer from swapping hypotheses can be used for more informed damage classification of damage types. This will allow CBM system to achieve better reliability and performance. The second and most fruitful contribution was the introduction of the FMH damage feature for use in detecting worn tooth damage. The results in this thesis showed the FMH damage to be an excellent candidate for detecting early stages of gear damage. With earlier detection of gear wear, better planning of maintenance and ordering of replacement parts can be achieved. This results in a reduction of cost and increase in potential safety.

4.2. Recommendations for Future Work

This study has provided valuable information on the effect of varying environmental and operational parameters of various damage features under a number of damage conditions that occur in rotating machines. The majority of the damage features performed well under certain conditions while others did not. As such they can be used for group classification of various damage types as well as location in multidimensional data driven analysis.

The next step after the work presented in this study would be for the damage features to be compared in a statistically significant way by using groups of features instead of a single one then compared against which type of damage was present. The multi-dimensional statistics of a group of features for each damage type can be learned and then machine damage can be classified using the Mahalanobis distance of the damage feature from the trained statistics in an attempt to be able to classify the type of damage present.

References

- [1] C. R. Farrar and K. Worden, "An introduction to structural health monitoring," *Phil. Trans. R. Soc. A*, vol. 365, no. 1851, pp. 303–315, Feb. 2007.
- [2] C. R. Farrar and T. A. Duffey, "VIBRATION-BASED DAMAGE DETECTION IN ROTATING MACHINERY," in *The International Conference on Damage Assessment of Structures (DAMAS 99)*, Dublin, Ireland, 1999.
- [3] C. R. Farrar, S. W. Doebling, and D. A. Nix, "Vibration-based structural damage identification," *Phil. Trans. R. Soc. Lond. A*, vol. 359, no. 1778, pp. 131–149, Jan. 2001.
- [4] M. Mosher, A. H. Pryor, and E. M. Huff, "Evaluation of Standard Gear Metrics in Helicopter Flight Operation," presented at 56th Meeting of the Society for Machinery Failure Prevention Technology."
- [5] R. B. Randall, "Detection and diagnosis of incipient bearing failure in helicopter gearboxes," *Engineering Failure Analysis*, vol. 11, no. 2, pp. 177–190, Apr. 2004.
- [6] P. A. Higgs, R. Parkin, M. Jackson, A. Al-Habaibeh, F. Zorriassatine, and J. Coy, "A survey on condition monitoring systems in industry," in *The 7th Biennial ASME Conference Engineering Systems Design and Analysis*, 2004, pp. 19–22.
- [7] F. P. García Márquez, A. M. Tobias, J. M. Pinar Pérez, and M. Papaelias, "Condition monitoring of wind turbines: Techniques and methods," *Renewable Energy*, vol. 46, pp. 169–178, Oct. 2012.
- [8] Z. Hameed, Y. S. Hong, Y. M. Cho, S. H. Ahn, and C. K. Song, "Condition monitoring and fault detection of wind turbines and related algorithms: A review," *Renewable and Sustainable Energy Reviews*, vol. 13, no. 1, pp. 1–39, Jan. 2009.
- [9] W. Lu and F. Chu, "Condition monitoring and fault diagnostics of wind turbines," in *Prognostics and Health Management Conference, 2010. PHM '10.*, 2010, pp. 1–11.
- [10] R. F. Orsagh, H. Lee, M. Watson, C. Byington, and J. Powers, "Advanced Vibration Monitoring for Wind Turbine Health Management."

- [11] L. F. Villa, A. Reñones, J. R. Perán, and L. J. de Miguel, "Angular resampling for vibration analysis in wind turbines under non-linear speed fluctuation," *Mechanical Systems and Signal Processing*, vol. 25, no. 6, pp. 2157–2168, Aug. 2011.
- [12] B. Al-Najjar and I. Alsyouf, "Enhancing a company's profitability and competitiveness using integrated vibration-based maintenance: A case study," *European Journal of Operational Research*, vol. 157, no. 3, pp. 643–657, Sep. 2004.
- [13] B. Al-Najjar, "The lack of maintenance and not maintenance which costs: A model to describe and quantify the impact of vibration-based maintenance on company's business," *International Journal of Production Economics*, vol. 107, no. 1, pp. 260–273, May 2007.
- [14] F. Barbera, H. Schneider, and P. Kelle, "A Condition Based Maintenance Model with Exponential Failures and Fixed Inspection Intervals," *The Journal of the Operational Research Society*, vol. 47, no. 8, pp. 1037–1045, Aug. 1996.
- [15] T. Biagetti and E. Sciubba, "A First Step Towards Unmanned Intelligent Process Management: A Procedure for the Diagnostics and Prognostics of Energy Conversion Plants," *International Journal of Thermodynamics*, vol. 5, no. 2, pp. 85–99, Feb. 2010.
- [16] P. J. Vlok, J. L. Coetzee, D. Banjevic, A. K. S. Jardine, and V. Makis, "Optimal Component Replacement Decisions Using Vibration Monitoring and the Proportional-Hazards Model," *The Journal of the Operational Research Society*, vol. 53, no. 2, pp. 193–202, Feb. 2002.
- [17] R. B. Randall, *Vibration-based condition monitoring: industrial, aerospace, and automotive applications*. Chichester, West Sussex, U.K. ; Hoboken, N.J.: Wiley, 2011.
- [18] J. J. Zakrajsek, D. P. Townsend, and H. J. Decker, "An Analysis of Gear Fault Detection Methods as Applied to Pitting Fatigue Failure Data," Jan. 1993.
- [19] H. J. Decker and J. J. Zakrajsek, "Comparison of Interpolation Methods as Applied to Time Synchronous Averaging," Jun. 1999.
- [20] H. J. Decker, R. F. Handschuh, and J. J. Zakrajsek, "An Enhancement to the NA4 Gear Vibration Diagnostic Parameter.," Jul. 1994.
- [21] J. J. Zakrajsek, "An Investigation of Gear Mesh Failure Prediction Techniques," Oct. 1989.
- [22] J. J. Zakrajsek, D. P. Townsend, D. G. Lewicki, H. J. Decker, and R. F. Handschuh, "Transmission Diagnostic Research at NASA Lewis Research Center.," Nov. 1995.
- [23] S. T. Lin and P. D. McFadden, "GEAR VIBRATION ANALYSIS BY B-SPLINE WAVELET-BASED LINEAR WAVELET TRANSFORM," *Mechanical Systems and Signal Processing*, vol. 11, no. 4, pp. 603–609, Jul. 1997.
- [24] Z. K. Peng and F. L. Chu, "Application of the wavelet transform in machine condition monitoring and fault diagnostics: a review with bibliography," *Mechanical Systems and Signal Processing*, vol. 18, no. 2, pp. 199–221, Mar. 2004.
- [25] P. D. McFadden and W. Wang, "ORA Report: 'Time-frequency domain analysis of vibration signals for machinery diagnostics (1) Introduction to the Wigner-Ville distribution' - uuid:f9025874-c208-4984-8935-cb3801b8a04a." [Online]. Available: <http://ora.ox.ac.uk/objects/uuid:f9025874-c208-4984-8935-cb3801b8a04a>. [Accessed: 13-Aug-2013].

- [26] W. J. Staszewski, K. Worden, and G. R. Tomlinson, "TIME-FREQUENCY ANALYSIS IN GEARBOX FAULT DETECTION USING THE WIGNER-VILLE DISTRIBUTION AND PATTERN RECOGNITION," *Mechanical Systems and Signal Processing*, vol. 11, no. 5, pp. 673–692, Sep. 1997.
- [27] X. Deng, Q. Wang, and X. Chen, "A Time-Frequency Localization Method for Singular Signal Detection Using Wavelet-Based Holder Exponent and Hilbert Transform," in *Congress on Image and Signal Processing, 2008. CISP '08*, 2008, vol. 4, pp. 266–270.
- [28] A. N. Robertson, C. R. Farrar, and H. Sohn, "Singularity detection for structural health monitoring using Holder exponents," 2003, vol. 5057, pp. 569–581.
- [29] N. B. Do, S. R. Green, and Timothy A. Schwartz, "Structural Damage Detection Using the Holder Exponent," in *The 21st IMAC Conference on Structural Dynamics*, 2003.
- [30] T. Nakamura, H. Horio, and Y. Chiba, "Local Holder exponent analysis of heart rate variability in preterm infants," *IEEE Transactions on Biomedical Engineering*, vol. 53, no. 1, pp. 83–88, 2006.
- [31] J. Antoni, "Fast computation of the kurtogram for the detection of transient faults," *Mechanical Systems and Signal Processing*, vol. 21, no. 1, pp. 108–124, Jan. 2007.
- [32] J. Antoni and R. B. Randall, "The spectral kurtosis: application to the vibratory surveillance and diagnostics of rotating machines," *Mechanical Systems and Signal Processing*, vol. 20, no. 2, pp. 308–331, Feb. 2006.
- [33] J. Antoni, "The spectral kurtosis: a useful tool for characterising non-stationary signals," *Mechanical Systems and Signal Processing*, vol. 20, no. 2, pp. 282–307, Feb. 2006.
- [34] N. Sawalhi and R. B. Randall, "Spectral kurtosis optimization for rolling element bearings," in *Proceedings of the Eighth International Symposium on Signal Processing and Its Applications*, 2005, 2005, vol. 2, pp. 839–842.
- [35] E. Bechhoefer, "A Quick Introduction to Bearing Envelope Analysis." [Online]. Available: <http://www.scribd.com/doc/110769949/A-Quick-Introduction-to-Bearing-Envelope-Analysis>. [Accessed: 12-Aug-2013].
- [36] A. Heng, S. Zhang, A. C. C. Tan, and J. Mathew, "Rotating machinery prognostics: State of the art, challenges and opportunities," *Mechanical Systems and Signal Processing*, vol. 23, no. 3, pp. 724–739, Apr. 2009.
- [37] W. Wang, P. A. Scarf, and M. A. J. Smith, "On the Application of a Model of Condition-Based Maintenance," *The Journal of the Operational Research Society*, vol. 51, no. 11, pp. 1218–1227, Nov. 2000.
- [38] J. Yan, "A prognostic algorithm for machine performance assessment and its application," *Production Planning & Control: The Management of Operations*, vol. 15, pp. 796–801, 2004.
- [39] E. B. Flynn and M. D. Todd, "A Bayesian approach to optimal sensor placement for structural health monitoring with application to active sensing," *Mechanical Systems and Signal Processing*, vol. 24, no. 4, pp. 891–903, May 2010.
- [40] Q. Liu and H. Wang, "A case study on multisensor data fusion for imbalance diagnosis of rotating machinery," *Artif. Intell. Eng. Des. Anal. Manuf.*, vol. 15, no. 3, pp. 203–210, Jun. 2001.

- [41] P. D. Welch, "The use of fast Fourier transform for the estimation of power spectra: A method based on time averaging over short, modified periodograms," *IEEE Transactions on Audio and Electroacoustics*, vol. 15, no. 2, pp. 70–73, 1967.
- [42] J. Markel, "Digital inverse filtering—a new tool for formant trajectory estimation," *IEEE Transactions on Audio and Electroacoustics*, vol. 20, no. 2, pp. 129–137, 1972.
- [43] "Mother Wavelets." [Online]. Available: <http://www.ljmu.ac.uk/GERI/98293.htm>. [Accessed: 22-Aug-2013].
- [44] F. Bonnardot, M. El Badaoui, R. B. Randall, J. Danière, and F. Guillet, "Use of the acceleration signal of a gearbox in order to perform angular resampling (with limited speed fluctuation)," *Mechanical Systems and Signal Processing*, vol. 19, no. 4, pp. 766–785, Jul. 2005.
- [45] J. R. Blough, "Adaptive Resampling—Transforming from the Time to the Angle Domain," *IMAC-XXIV: Conference & Exposition on Structural Dynamics*, 2006.
- [46] E. Bechhoefer and M. Kingsley, "A review of time synchronous average algorithms," *Annual Conference of the Prognostics and Health Management Society*, 2009.
- [47] F. Combet and L. Gelman, "An automated methodology for performing time synchronous averaging of a gearbox signal without speed sensor," *Mechanical Systems and Signal Processing*, vol. 21, no. 6, pp. 2590–2606, Aug. 2007.
- [48] K. McClintic, M. Lebold, K. Maynard, C. Byington, and R. Campbell, "Residual and difference feature analysis with transitional gearbox data," *In 54 th Meeting of the Society for Machinery Failure Prevention Technology*, 2000.
- [49] P. D. McFadden, "Interpolation techniques for time domain averaging of gear vibration," *Mechanical Systems and Signal Processing*, vol. 3, no. 1, pp. 87–97, Jan. 1989.
- [50] J. Antoni and R. B. Randall, "Unsupervised noise cancellation for vibration signals: part I—evaluation of adaptive algorithms," *Mechanical Systems and Signal Processing*, vol. 18, no. 1, pp. 89–101, Jan. 2004.
- [51] J. Antoni and R. B. Randall, "Unsupervised noise cancellation for vibration signals: part II—a novel frequency-domain algorithm," *Mechanical Systems and Signal Processing*, vol. 18, no. 1, pp. 103–117, Jan. 2004.
- [52] M. K. P. Veveçev r, "Condition Indicators for Gearbox Condition Monitoring Systems," *Acta Polytechnica*, vol. 45, pp. 35–43, 2005.
- [53] A. S. Sait and Y. I. Sharaf-Eldeen, "A Review of Gearbox Condition Monitoring Based on vibration Analysis Techniques Diagnostics and Prognostics," in *Rotating Machinery, Structural Health Monitoring, Shock and Vibration, Volume 5*, T. Proulx, Ed. Springer New York, 2011, pp. 307–324.
- [54] M. Lebold, K. McClintic, R. Campbell, C. Byington, and K. Maynard, "Review of vibration analysis methods for gearbox diagnostics and prognostics." 2000.
- [55] A. P. Bradley, "The use of the area under the ROC curve in the evaluation of machine learning algorithms," *Pattern Recognition*, vol. 30, no. 7, pp. 1145–1159, Jul. 1997.